

Hydrodynamic theory of two-dimensional incompressible polar active fluids with quenched and annealed disorder

Leiming Chen, Chiu Fan Lee, Ananyo Maitra, John Toner

▶ **To cite this version:**

Leiming Chen, Chiu Fan Lee, Ananyo Maitra, John Toner. Hydrodynamic theory of two-dimensional incompressible polar active fluids with quenched and annealed disorder. Physical Review E , 2022, 106 (4), pp.044608. 10.1103/physreve.106.044608 . hal-03889092

HAL Id: hal-03889092
https://hal.science/hal-03889092

Submitted on 7 Dec 2022

HAL is a multi-disciplinary open access archive for the deposit and dissemination of scientific research documents, whether they are published or not. The documents may come from teaching and research institutions in France or abroad, or from public or private research centers.

L'archive ouverte pluridisciplinaire **HAL**, est destinée au dépôt et à la diffusion de documents scientifiques de niveau recherche, publiés ou non, émanant des établissements d'enseignement et de recherche français ou étrangers, des laboratoires publics ou privés.

Featured in Physics

Hydrodynamic theory of two-dimensional incompressible polar active fluids with quenched and annealed disorder

Leiming Chen [1,*] Chiu Fan Lee,[2,†] Ananyo Maitra [3,‡] and John Toner [4,5,§]

[1]*School of Material Science and Physics, China University of Mining and Technology, Xuzhou Jiangsu 221116, People's Republic of China*
[2]*Department of Bioengineering, Imperial College London, South Kensington Campus, London SW7 2AZ, United Kingdom*
[3]*Laboratoire de Physique Théorique et Modélisation, CNRS UMR 8089, CY Cergy Paris Université, F-95032 Cergy-Pontoise Cedex, France*
[4]*Department of Physics and Institute of Theoretical Science, University of Oregon, Eugene, Oregon 97403, USA*
[5]*Max Planck Institute for the Physics of Complex Systems, Nöthnitzer Straße 38, 01187 Dresden, Germany*

(Received 28 May 2022; accepted 12 September 2022; published 27 October 2022)

We study the moving phase of two-dimensional (2D) incompressible polar active fluids in the presence of both quenched and annealed disorder. We show that long-range polar order persists even in this defect-ridden two-dimensional system. We obtain the large-distance, long-time scaling laws of the velocity fluctuations using three distinct dynamic renormalization group schemes. These are an uncontrolled one-loop calculation in exactly two dimensions, and two $d = (d_c - \epsilon)$ expansions to $O(\epsilon)$, obtained by two different analytic continuations of our 2D model to higher spatial dimensions: a "hard" continuation which has $d_c = \frac{7}{3}$, and a "soft" continuation with $d_c = \frac{5}{2}$. Surprisingly, the quenched and annealed parts of the velocity correlation function have the same anisotropy exponent and the relaxational and propagating parts of the dispersion relation have the same dynamic exponent in the nonlinear theory even though they are distinct in the linearized theory. This is due to anomalous hydrodynamics. Furthermore, all three renormalization schemes yield very similar values for the universal exponents, and therefore we expect the numerical values that we predict for them to be highly accurate.

DOI: 10.1103/PhysRevE.106.044608

I. INTRODUCTION

The competition between order and disorder is one of the central themes of statistical mechanics and condensed matter physics. It is well known that below a certain lower critical dimension, it is impossible to have ordered phases; i.e., disorder always wins. The "Mermin-Wagner-Hohenberg" theorem [1] proves this for equilibrium systems trying to break a continuous symmetry at finite temperature in two or fewer dimensions.

Once out of equilibrium, however, the Mermin-Wagner theorem no longer applies. It has been demonstrated for one particular class of nonequilibrium systems, namely active systems, that long-range order is possible in two dimensions even in the presence of noise [2–4]. In particular, polar self-propelled particles moving over a frictional substrate (a system often described as a "dry polar active fluid") can "flock," that is, form a state with a nonzero average velocity $\langle \mathbf{v} \rangle$, even when perturbed by noise.

The aforementioned results all describe systems in which the "noise"—that is, the random force trying to disorder the system—is "annealed," that is, time-dependent with only short ranged in time temporal correlations. Thermal "Brownian" noise is "annealed" in this sense.

In equilibrium systems, it is known that *quenched* disorder [5–8]—that is, disorder that is time-*independent*—is even more destructive of order than "annealed" thermal noise. This is because quenched noise induces much greater fluctuations than annealed noise does. Indeed, even arbitrarily small quenched disorder destroys long-range ferromagnetic and crystalline order in all spatial dimensions $d \leqslant 4$ [5–8].

It is natural, therefore, to wonder what the effect of quenched disorder on active systems is. This question has received much attention in recent years [9–19]. In particular, it has been shown [9,10] that for three-dimensional dry polar active systems with quenched disorder, long-range polar order (i.e., a nonzero average velocity $\langle \mathbf{v} \rangle$) can survive such quenched disorder. But in two dimensions, only quasi-long-range polar order (i.e., $\langle \mathbf{v} \rangle$ decaying to zero as a power of the system size) was found in [9,10,18].

In this paper, we report that it is possible to achieve true long-range order in two dimensions in dry polar active systems with quenched disorder, if those systems are incompressible. A brief summary of our key results was given in the companion paper [20].

In the following, we will first present a hydrodynamic theory of incompressible polar active fluids on a frictional substrate [21–23] with both annealed disorder (i.e., time-dependent noise arising from endogenous fluctuations due to, e.g., the errors made by a motile agent attempting to follow its neighbors [2]) and quenched disorder (caused by, e.g., static random impurities on the frictional substrate). We then study the system in the linear regime, and subsequently use three different dynamic renormalization group (DRG) schemes to

*leiming@cumt.edu.cn
†c.lee@imperial.ac.uk
‡nyomaitra07@gmail.com
§jjt@uoregon.edu

 ©2022 American Physical Society

uncover a novel universality class, whose associated scaling exponents fully characterize the scaling behavior of the system in the moving phase. Specifically, in this moving phase, these exponents characterize the fluctuations $\mathbf{u}(\mathbf{r},t)$ of the local active fluid velocity about its mean value $\langle\mathbf{v}\rangle = v_0\hat{\mathbf{x}}$, where we have defined our coordinate system so that $\hat{\mathbf{x}}$ is along the mean velocity spontaneously chosen by the system. That is, $\mathbf{u}(\mathbf{r},t) \equiv \mathbf{v}(\mathbf{r},t) - v_0\hat{\mathbf{x}}$. In particular, the overall real-space velocity autocorrelation $\langle\mathbf{u}(\mathbf{r},t)\cdot\mathbf{u}(0,\mathbf{0})\rangle$ is given by

$$\langle\mathbf{u}(\mathbf{r},t)\cdot\mathbf{u}(\mathbf{0},0)\rangle = |y|^{2\chi}\mathcal{G}_Q\left(\frac{|x|}{|y|^\zeta}\right) + |y|^{2\chi'}\mathcal{G}_A\left(\frac{|x|}{|y|^\zeta},\frac{|t|}{|y|^z}\right), \tag{1}$$

where $\mathcal{G}_{A,Q}$ are scaling functions that are each universal up to an overall multiplicative factor (a different overall multiplicative factor for each), corresponding to the annealed and quenched parts of the correlations, respectively.

One of the unusual features of our result is that the annealed part $\mathcal{G}_A(\frac{|x|}{|y|^\zeta},\frac{|t|}{|y|^z})$ of the correlations has such a simple scaling form. This is quite different from, e.g., a simple compressible fluid, in which the density fluctuations are associated with dispersionless propagating sound waves, which corresponds to a dynamic exponent $z = 1$ (i.e., distance proportional to time), while the decay of those modes is diffusive, which corresponds to a dynamic exponent $z = 2$. As we will see, a *linear* theory of our system also predicts such a "double scaling" character—i.e., propagating and diffusive parts with different dynamic exponents—but the full, nonlinear theory has the simpler, "single scaling" form given in (1). Thus, this simplicity is an unusual feature of the anomalous hydrodynamics—i.e., the fact that the hydrodynamic fluctuations of the system (and, therefore, the scaling exponents) are divergently modified from those predicted by the linearized theory, due to nonlinearities, whatever the magnitude of those nonlinearities.

Another consequence of the anomalous hydrodynamics is that the anisotropy exponent ζ takes on the same value in both $\mathcal{G}_A(\frac{|x|}{|y|^\zeta},\frac{|t|}{|y|^z})$ and $\mathcal{G}_Q(\frac{|x|}{|y|^\zeta})$ in the full, nonlinear theory. In contrast, the linear theory predicts different values of ζ's for the annealed part of the correlations $\mathcal{C}_A(\frac{|x-\gamma t|}{|y|^{\zeta_1}},\frac{|t|}{|y|^z})$ and the quenched part $\mathcal{C}_Q(\frac{|x|}{|y|^{\zeta_2}})$.

We have obtained the exponents in (1) using three different DRG schemes: an uncontrolled calculation in exactly two dimensions, and two different $\epsilon = (d_c - d)$ expansions, obtained from two different analytic continuations of our 2D model to higher spatial dimensions d. We call these continuations the "hard continuation" and "soft continuation," and they lead respectively to $d_c^{\text{hard}} = 7/3$ and $d_c^{\text{soft}} = 5/2$.

In the uncontrolled calculation in exactly two dimensions, we find

$$z = \tfrac{13}{27} \approx 0.48, \tag{2a}$$
$$\zeta = \tfrac{7}{9} \approx 0.78, \tag{2b}$$
$$\chi = -\tfrac{2}{9} \approx -0.22, \tag{2c}$$
$$\chi' = -\tfrac{19}{54} \approx -0.35. \tag{2d}$$

The fact that both χ and χ' are negative implies that the fluctuations remain finite as the system size goes to infinity. This means that the system has long-range polar order for sufficiently weak disorder. The same statement is true of the other two schemes.

In the "hard" continuation, $d_c = 7/3$, and a first order in ϵ expansion gives

$$z = \tfrac{2}{3} - \tfrac{5}{9}\epsilon + O(\epsilon^2) \approx \tfrac{13}{27} \approx 0.48, \tag{3a}$$
$$\zeta = \tfrac{2}{3} + \tfrac{1}{3}\epsilon + O(\epsilon^2) \approx \tfrac{7}{9} \approx 0.78, \tag{3b}$$
$$\chi = -\tfrac{1}{3} + \tfrac{1}{3}\epsilon + O(\epsilon^2) \approx -\tfrac{2}{9} \approx -0.22, \tag{3c}$$
$$\chi' = -\tfrac{1}{2} + \tfrac{4}{9}\epsilon + O(\epsilon^2) \approx -\tfrac{19}{54} \approx -0.35, \tag{3d}$$

with $\epsilon = 7/3 - d$ and the numerical values are evaluated to $O(\epsilon)$ for $d = 2$. Coincidentally, these results are exactly the same as the $(d = 2)$-uncontrolled-calculation results (2).

In the "soft" continuation, $d_c = 5/2$, and, defining $\tilde{\epsilon} \equiv 5/2 - d$, we find

$$z = \tfrac{2}{3} - \tfrac{8}{27}\tilde{\epsilon} + O(\tilde{\epsilon}^2), \tag{4a}$$
$$\zeta = \tfrac{2}{3} + \tfrac{4}{27}\tilde{\epsilon} + O(\tilde{\epsilon}^2), \tag{4b}$$
$$\chi = -\tfrac{1}{3} + \tfrac{4}{27}\tilde{\epsilon} + O(\tilde{\epsilon}^2), \tag{4c}$$
$$\chi' = -\tfrac{1}{2} + \tfrac{1}{9}\tilde{\epsilon} + O(\tilde{\epsilon}^2). \tag{4d}$$

For $d = 2$, $\tilde{\epsilon} = 1/2$, and the above results give

$$z \approx \tfrac{14}{27} \approx 0.52, \tag{5a}$$
$$\zeta \approx \tfrac{20}{27} \approx 0.74, \tag{5b}$$
$$\chi \approx -\tfrac{7}{27} \approx -0.26, \tag{5c}$$
$$\chi' \approx -\tfrac{4}{9} \approx -0.44, \tag{5d}$$

which are very close to the values obtained from both the uncontrolled calculation and the hard continuation.

We estimate the actual values of these scaling exponents as an equally weighted average of these three results. We can estimate the likely errors in these numerical values as the difference between these averaged results and the equal hard-continuation and uncontrolled-calculation results. This gives

$$z = 0.49 \pm 0.01, \tag{6a}$$
$$\zeta = 0.77 \pm 0.01, \tag{6b}$$
$$\chi = -0.23 \pm 0.01, \tag{6c}$$
$$\chi' = -0.37 \pm 0.02. \tag{6d}$$

Note that compared to having annealed disorder alone [21], the anisotropic exponent ζ is closer to 1, thus suggesting that the system becomes less anisotropic due to the quenched disorder.

One way to experimentally test these exponents is by measuring the equal-time velocity correlation function. This is dominated by the quenched part, and goes like

$$\langle\mathbf{u}(\mathbf{r},t)\cdot\mathbf{u}(\mathbf{0},t)\rangle \sim \begin{cases} |y|^{2\chi}, & \text{if } |y|^\zeta \gg |x|, \\ |x|^{2\chi/\zeta}, & \text{if } |y|^\zeta \ll |x|, \end{cases} \tag{7}$$

and for equal positions, the change in the correlation function with time is dominated by the annealed part:

$$\langle\mathbf{u}(\mathbf{r},t+T)\cdot\mathbf{u}(\mathbf{r},T)\rangle - \langle\mathbf{u}(\mathbf{r},T)\cdot\mathbf{u}(\mathbf{r},T)\rangle \propto |t|^{2\chi'/z}. \tag{8}$$

Our best estimate of the numerical value of $2\chi'/z$, using (6), is

$$\frac{2\chi'}{z} = -1.51 \pm 0.11. \tag{9}$$

II. HYDRODYNAMIC DESCRIPTION

We start with a hydrodynamic model of a generic 2D incompressible polar active fluid, moving on a disordered substrate, in the presence of both quenched (time-independent) and annealed (time-dependent) noise. As for incompressible passive fluids [24,25] described by the Navier-Stokes equation, the only hydrodynamic variable for our system is the velocity field $\mathbf{v}$. However, in contrast to the Navier-Stokes equation, $\mathbf{v}$ is hydrodynamic not because it is conserved—it is not, because the substrate is a momentum sink—but because it is a broken symmetry variable (more precisely, certain components of it are). Furthermore, because our nonequilibrium system breaks detailed balance, and therefore, is not constrained by Onsager symmetry, this equation contains additional terms which would have been absent both from the Navier-Stokes equation and from the equation of motion (EOM) of passive fluid films on substrates. That is, the EOM of $\mathbf{v}$ is only constrained by the spatial symmetries of our system, in particular, rotation and translation invariance. This reasoning implies that the EOM for $\mathbf{v}$ takes the form [3,4,21,22,26]

$$\begin{aligned}&\partial_t \mathbf{v} + \lambda(\mathbf{v}\cdot\nabla)\mathbf{v}\\ &\quad = -\nabla\Pi - (\mathbf{v}\cdot\nabla\Pi_1)\mathbf{v} + U(|\mathbf{v}|)\mathbf{v} + \mu_1\nabla^2\mathbf{v}\\ &\qquad + \mu_2(\mathbf{v}\cdot\nabla)^2\mathbf{v} + \mathbf{f}_Q(\mathbf{r}) + \mathbf{f}_A(\mathbf{r},t),\end{aligned} \tag{10}$$

where the "pressure" Π acts as a Lagrange multiplier to enforce the incompressibility constraint: $\nabla\cdot\mathbf{v} = 0$. The $U(|\mathbf{v}|)$ term in Eq. (10) makes the local $\mathbf{v}$ have a nonzero magnitude v_0 in the ordered phase, by the simple expedient of having $U(|\mathbf{v}|) > 0$ for $|\mathbf{v}| < v_0$, $U(|\mathbf{v}|) = 0$ for $|\mathbf{v}| = v_0$, and $U(|\mathbf{v}|) < 0$ for $|\mathbf{v}| > v_0$. Aside from this, and the assumption that $U(|\mathbf{v}|)$ is a smooth, analytic function of $|\mathbf{v}|$, we will make no assumptions about $U(|\mathbf{v}|)$. Similarly, the "anisotropic pressure" Π_1 is also a generic analytic function of $|\mathbf{v}|$. Finally, $\mathbf{f}_Q(\mathbf{r})$ and $\mathbf{f}_A(\mathbf{r},t)$ are respectively the quenched and annealed noise terms, which have zero means, and correlations:

$$\left\langle f_Q^i(\mathbf{r}) f_Q^j(\mathbf{r}')\right\rangle = 2D_Q\delta_{ij}\delta^2(\mathbf{r}-\mathbf{r}'), \tag{11a}$$

$$\left\langle f_A^i(\mathbf{r},t) f_A^j(\mathbf{r}',t')\right\rangle = 2D_A\delta_{ij}\delta^2(\mathbf{r}-\mathbf{r}')\delta(t-t'), \tag{11b}$$

where the indices i, j enumerate the spatial coordinates. Since our hydrodynamic theory focuses on time and distance scales that are long compared to those of the underlying microscopic dynamics, the temporal and spatial correlations in the noises are taken to be delta correlated. Also, the noise $\mathbf{f}_Q(\mathbf{r})$ is time-*independent*; this is what we mean by "quenched." Note that we do not assume any correlation between the annealed and quenched fluctuations as they stem from distinct origins, e.g., annealed noise may originate from the random mistakes that an active crawler makes as it moves, while the quenched noise comes from the random defects on the surface, which skew the crawler to move in a particular direction. However, studying the potential effects of correlated annealed and quenched noises is an interesting possible future project.

In the EOM (10), we have only included terms that are relevant to the universal behavior based on the DRG analysis that follows, by which we mean terms that can change the long-distance, long-time behavior of the system. This equation differs from the EOM introduced in [21] only through the presence of the quenched noise $\mathbf{f}_Q(\mathbf{r})$. As we will see, however, this quenched noise radically changes the behavior of the system.

In the moving phase, we focus on the velocity deviation field $\mathbf{u}$, from the mean flow $v_0\hat{\mathbf{x}}$: $\mathbf{u} = \mathbf{v} - v_0\hat{\mathbf{x}}$. We will expand (10) in powers of the fluctuation $\mathbf{u}$, keeping only relevant terms, by which we mean all terms, both linear and nonlinear, which control the long-distance, large-time behavior of the model. These terms do not vanish upon recursively applying the RG transformation we will describe below. Doing so, we find that the EOM governing $\mathbf{u}$ is, in Einstein component notation,

$$\begin{aligned}\partial_t u_i = &-\partial_i\Pi - \gamma\partial_x u_i - b\delta_{ix}\partial_x u_x\\ &-\alpha\left(u_x + \frac{u_y^2}{2v_0}\right)\left(\delta_{ix} + \frac{u_y}{v_0}\delta_{iy}\right) + f_Q^i + f_A^i,\end{aligned} \tag{12}$$

where $\gamma \equiv \lambda v_0$, $\alpha \equiv -v_0(\frac{dU}{d|\mathbf{v}|})_{|\mathbf{v}|=v_0}$, $b \equiv v_0^2(\frac{d\Pi_1}{d|\mathbf{v}|})_{|\mathbf{v}|=v_0}$, $\mu_\perp \equiv \mu_1$, and $\mu_x \equiv \mu_1 + \mu_2 v_0^2$. We have dropped some terms irrelevant to the long-wavelength behavior of the system from (12).

We first focus on the linear regime of the above EOM, which we expect to capture the hydrodynamic behavior over a large range of length scales if the noise is sufficiently small.

III. LINEAR REGIME

To study the system's behavior in the linear regime, we first spatiotemporally Fourier transform the linearized version of the EOM (12). The convention we use here is the following:

$$\mathbf{u}(\mathbf{q},\omega) \equiv \int_{t,\mathbf{r}} e^{i(\mathbf{q}\cdot\mathbf{r}-\omega t)}\mathbf{u}(\mathbf{r},t), \tag{13}$$

where $\int_t \equiv \int \frac{dt}{\sqrt{2\pi}}$ and $\int_{\mathbf{r}} \equiv \int \frac{d^2r}{2\pi}$. We will continue to use this shorthand notation for integration throughout the paper. We will also use the same convention in Fourier space; i.e., $\int_\omega \equiv \int \frac{d\omega}{\sqrt{2\pi}}$ and $\int_{\mathbf{q}} \equiv \int \frac{d^2q}{2\pi}$.

The linearized version of EOM (12) in Fourier space is

$$\begin{aligned}&[-i(\omega - \gamma q_x) + \Gamma(\mathbf{q})]u_i(\tilde{\mathbf{q}}) + (\alpha + ibq_x)\delta_{ix}u_x(\tilde{\mathbf{q}})\\ &\quad = -iq_i\Pi + f_Q^i + f_A^i,\end{aligned} \tag{14}$$

where we have introduced the composite vector $\tilde{\mathbf{q}} \equiv (\mathbf{q},\omega)$, and the $\mathbf{q}$-dependent damping coefficient $\Gamma(\mathbf{q}) \equiv \mu_\perp q_y^2 + \mu_x q_x^2$.

Acting on both sides with the transverse projection operator

$$P_{li}(\mathbf{q}) = \delta_{li} - \frac{q_l q_i}{q^2}, \tag{15}$$

which projects orthogonal to the spatial wave vector $\mathbf{q}$, eliminates the pressure (Π) term. Using $P_{li}u_i = u_l$, which follows from the incompressibility condition $q_x u_x + q_y u_y = 0$, setting $l = y$, and using the replacement $u_x = -\frac{q_y}{q_x}u_y$ that follows

from the same incompressibility condition gives us a simple algebraic equation for $u_y(\mathbf{q},\omega)$:

$$[G(\tilde{\mathbf{q}})]^{-1}u_y(\tilde{\mathbf{q}}) = P_{yi}\left(f_{_Q}^i + f_{_A}^i\right), \tag{16}$$

where the "propagator" $G(\tilde{\mathbf{q}})$ is as follows:

$$G(\tilde{\mathbf{q}}) \equiv \left\{-i\left[\omega - \left(\gamma + b\frac{q_y^2}{q^2}\right)q_x\right] + \left(\alpha\frac{q_y^2}{q^2} + \Gamma(\mathbf{q})\right)\right\}^{-1}. \tag{17}$$

The poles in this propagator in the complex ω plane are the eigenfrequencies of our problem. In the limit $q_y \ll q_x$, which we will show in a moment is the regime of wave vector space that dominates the fluctuations, those eigenfrequencies are given by

$$\omega(\mathbf{q}) = \gamma q_x - i\left(\mu_x q_x^2 + \alpha\frac{q_y^2}{q_x^2}\right). \tag{18}$$

These eigenfrequencies have a rather complicated multiple scaling form. That is, they cannot be written in a simple scaling form, but require the introduction of two distinct scaling functions f_{real} and $f_{\text{imaginary}}$:

$$\omega(\mathbf{q}) = |q_y|^{z_1} f_{\text{real}}\left(\frac{q_x}{|q_y|^{\zeta_1}}\right) - i|q_y|^{z_2} f_{\text{imaginary}}\left(\frac{|q_x|}{|q_y|^{\zeta_2}}\right) \tag{19}$$

with

$$f_{\text{real}}(m) = \gamma m, \tag{20}$$

whose form unfortunately makes it impossible to fix ζ_1 and z_1 for the linear problem, but does require

$$z_1 = \zeta_1, \tag{21a}$$

$$z_2 = 1, \tag{21b}$$

$$f_{\text{imaginary}}(m) = m^2(\mu_x + \alpha m^{-4}), \tag{21c}$$

$$\zeta_2 = 1/2. \tag{21d}$$

Note that, although the individual values of z_1 and ζ_1 cannot be determined, we cannot possibly have $z_1 = z_2 = 1$ and $\zeta_1 = \zeta_2 = 1/2$, since this violates (21a). Hence, we are forced to use the double scaling form (19).

We will show in Secs. V and VI that this complexity disappears in two dimensions once the effects of nonlinearities are taken into account. These nonlinear effects replace the multiple scaling form (19) with the simple scaling form

$$\omega(\mathbf{q}) = |q_y|^{z} f_{\omega}\left(\frac{q_x}{|q_y|^{\zeta}}\right), \tag{22}$$

with the unique universal exponents z and ζ given by Eqs. (3), and a single, albeit complex, scaling function f_ω.

This simplification of the eigenfrequencies carries through to all of the correlation functions as well. Indeed, *every* long-wavelength, long-time property of the system exhibits simple scaling with the single dynamic exponent z, and the single anisotropy exponent ζ, given by (3).

Solving Eq. (16) for u_y, autocorrelating the result with itself, and using our expressions (11a) and (11b) for the autocorrelations of the noises gives the autocorrelation of $u_y(\mathbf{q},\omega)$. Using $u_x = -\frac{q_y}{q_x}u_y$, which follows from the incompressibility condition, then gives the autocorrelations of $u_x(\mathbf{q},\omega)$, and the cross-correlations of $u_x(\mathbf{q},\omega)$ and $u_y(\mathbf{q},\omega)$. We find

$$\langle u_i(\tilde{\mathbf{q}})u_j(\tilde{\mathbf{q}}')\rangle = C_{_A}^{ij}(\tilde{\mathbf{q}})\delta(\omega+\omega')\delta(\mathbf{q}+\mathbf{q}') + C_{_Q}^{ij}(\tilde{\mathbf{q}})\delta(\omega)\delta(\omega')\delta(\mathbf{q}+\mathbf{q}'), \tag{23}$$

where

$$C_{_A}^{xx}(\tilde{\mathbf{q}}) = \frac{q_y^2}{q^2}C_{_A}(\tilde{\mathbf{q}}), \tag{24a}$$

$$C_{_A}^{xy}(\tilde{\mathbf{q}}) = -\frac{q_x q_y}{q^2}C_{_A}(\tilde{\mathbf{q}}) = C_{_A}^{yx}(\tilde{\mathbf{q}}), \tag{24b}$$

$$C_{_A}^{yy}(\tilde{\mathbf{q}}) = \frac{q_x^2}{q^2}C_{_A}(\tilde{\mathbf{q}}), \tag{24c}$$

$$C_{_Q}^{xx}(\tilde{\mathbf{q}}) = \frac{q_y^2}{q^2}C_{_Q}(\tilde{\mathbf{q}}), \tag{24d}$$

$$C_{_Q}^{xy}(\tilde{\mathbf{q}}) = -\frac{q_x q_y}{q^2}C_{_Q}(\tilde{\mathbf{q}}) = C_{_Q}^{yx}(\tilde{\mathbf{q}}), \tag{24e}$$

$$C_{_Q}^{yy}(\tilde{\mathbf{q}}) = \frac{q_x^2}{q^2}C_{_Q}(\tilde{\mathbf{q}}), \tag{24f}$$

with

$$C_{_A}(\tilde{\mathbf{q}}) = \frac{2D_{_A}}{\left[\omega - \left(\frac{bq_y^2}{q^2}+\gamma\right)q_x\right]^2 + \left[\frac{\alpha q_y^2}{q^2}+\Gamma(\mathbf{q})\right]^2}, \tag{25a}$$

$$C_{_Q}(\tilde{\mathbf{q}}) = \frac{4\pi D_{_Q}}{\left(\frac{bq_y^2}{q^2}+\gamma\right)^2 q_x^2 + \left[\frac{\alpha q_y^2}{q^2}+\Gamma(\mathbf{q})\right]^2}, \tag{25b}$$

and the subscripts A and Q denoting the contributions from the annealed and quenched noises, respectively.

The equal-time correlations of $\mathbf{u}$ can now be obtained by inverse Fourier transformation. We find in the hydrodynamic limit (i.e., $\mathbf{q} \to \mathbf{0}$) the annealed and quenched parts of these correlations are given by

$$\langle u_x(\mathbf{q},t)u_x(\mathbf{q}',t)\rangle_{_A} \approx \frac{D_{_A}q_y^2}{\alpha q_y^2 + \mu_x q_x^4}\delta(\mathbf{q}+\mathbf{q}'), \tag{26a}$$

$$\langle u_y(\mathbf{q},t)u_y(\mathbf{q}',t)\rangle_{_A} \approx \frac{D_{_A}q_x^2}{\alpha q_y^2 + \mu_x q_x^4}\delta(\mathbf{q}+\mathbf{q}'), \tag{26b}$$

$$\langle u_x(\mathbf{q},t)u_x(\mathbf{q}',t)\rangle_{_Q} \approx \frac{2D_{_Q}q_y^2 q^2}{\alpha^2 q_y^4 + \gamma^2 q_x^6}\delta(\mathbf{q}+\mathbf{q}'), \tag{26c}$$

$$\langle u_y(\mathbf{q},t)u_y(\mathbf{q}',t)\rangle_{_Q} \approx \frac{2D_{_Q}q_x^2 q^2}{\alpha^2 q_y^4 + \gamma^2 q_x^6}\delta(\mathbf{q}+\mathbf{q}'). \tag{26d}$$

We see that as $q \to 0$, $\langle u_x(\mathbf{q},t)u_x(\mathbf{q}',t)\rangle_{_A}$ is always finite. In contrast, $\langle u_y(\mathbf{q},t)u_y(\mathbf{q}',t)\rangle_{_A}$ diverges in the regime $q_x \gtrsim q_y^{1/2}$ as $1/q^2$. The correlations $\langle u_x(\mathbf{q},t)u_x(\mathbf{q}',t)\rangle_{_Q}$ and $\langle u_y(\mathbf{q},t)u_y(\mathbf{q}',t)\rangle_{_Q}$ diverge in the regime $q_x \gtrsim q_y^{2/3}$, where they scale as $1/q$ and $1/q^2$, respectively. Note that $q_x \gtrsim q_y^{2/3}$ covers a much larger area in $\mathbf{q}$ space than $q_x \gtrsim q_y^{1/2}$ does. In spite of these divergences, it is easy to show that the integrals of $\langle u_x(\mathbf{q},t)u_x(\mathbf{q}',t)\rangle_{_{A,Q}}$ and $\langle u_y(\mathbf{q},t)u_y(\mathbf{q}',t)\rangle_{_{A,Q}}$ over $\mathbf{q}$ and $\mathbf{q}'$ both converge in the infrared, which implies that the corresponding real-space fluctuations remain finite in the infinite system size limit. This demonstrates that long-range

polar order persists in these systems, at least according to this linear theory.

These observations imply that (i) the u_y fluctuations dominate in the hydrodynamic limit, which is not a surprise since u_y is the "Goldstone mode," (ii) the quenched fluctuations dominate, again in the hydrodynamic limit, (iii) the long-range polar order is robust against the quenched disorder, and (iv) the quenched and annealed anisotropy exponents $\zeta_{\text{quenched}} = 2/3$ and $\zeta_{\text{annealed}} = 1/2$, respectively. All of these conclusions except the last continue to hold even when the nonlinearities are taken into account, as we will show in the next section.

Note that it is the term $\gamma^2 q_x^6$ appearing in the denominator in (26d) that stabilizes long-range order in the presence of quenched disorder. If that term were absent—as it is in equilibrium "divergence-free magnets" (that is, magnets subject to the constraint $\nabla \cdot \mathbf{M} = 0$, where $\mathbf{M}$ is the magnetization), whose hydrodynamic properties in the presence of annealed noise are equivalent to incompressible flocks [21]—its place would be taken by $\mu_x^2 q_x^8$. Such a strong divergence of angular fluctuations for $q_y = 0$ would destroy long-range, and even *quasi*-long-range polar order, which is exactly what happens in equilibrium divergence-free magnets with quenched disorder.

The physical mechanism of this stabilization of order is suggested by the origin of the $\gamma^2 q_x^6$ term in the correlation functions: the propagation term $\gamma(\partial_x \mathbf{u})$ in the EOM (12). This term causes fluctuations along $\hat{\mathbf{x}}$ to propagate with speed γ. Thus, in a frame of reference comoving with the fluctuations, the quenched disorder looks time-dependent, and, so, more like annealed disorder. Indeed, for $q_y = 0$ both $\langle u_y(\mathbf{q}, t) u_y(\mathbf{q}', t)\rangle_Q$ and $\langle u_y(\mathbf{q}, t) u_y(\mathbf{q}', t)\rangle_A$ scale in the same way as $\mathbf{q} \to \mathbf{0}$: both are $\propto 1/q_x^2$. This "annealization" effect reduces the quenched fluctuations. Nevertheless, the quenched disorder is not completely "annealized" as overall the quenched fluctuations are still larger than the annealed.

Now we turn to the general real-space $\mathbf{u}$-$\mathbf{u}$ correlation function $\langle \mathbf{u}(\mathbf{r}, t) \cdot \mathbf{u}(\mathbf{0}, 0)\rangle$, which is the inverse Fourier transform of $\langle \mathbf{u}(\tilde{\mathbf{q}}) \cdot \mathbf{u}(\tilde{\mathbf{q}}')\rangle$:

$$\begin{aligned}\langle \mathbf{u}(\mathbf{r}, t) \cdot \mathbf{u}(\mathbf{0}, 0)\rangle &= \int_{\omega,\omega',\mathbf{q},\mathbf{q}'} \langle \mathbf{u}(\tilde{\mathbf{q}}) \cdot \mathbf{u}(\tilde{\mathbf{q}}')\rangle\, e^{i(\mathbf{q}\cdot\mathbf{r} - \omega t)} \\ &= C_A(\mathbf{r}, t) + C_Q(\mathbf{r}),\end{aligned} \tag{27}$$

where

$$C_A(\mathbf{r}, t) = \int_{\omega,\mathbf{q}} \frac{2D_A e^{i(\mathbf{q}\cdot\mathbf{r} - \omega t)}}{(\omega - \gamma q_x)^2 + \left(\frac{\alpha q_y^2}{q_x^2} + \mu_x q_x^2\right)^2}, \tag{28a}$$

$$C_Q(\mathbf{r}) = \int_{\mathbf{q}} \frac{2D_Q q_x^4}{\alpha q_y^4 + \gamma^2 q_x^6} e^{i\mathbf{q}\cdot\mathbf{r}}. \tag{28b}$$

In the above expressions, we have simplified the denominators inside the integrals by keeping only the dominant terms [see (24)] in the limit $q_y \ll q_x$, which we have shown is the regime of wave vector space that dominates the fluctuations.

The scaling behavior of $C_A(\mathbf{r}, t)$ and $C_Q(\mathbf{r})$ can now be worked out by changing the variables of integration: We first rewrite $C_A(\mathbf{r}, t)$ as

$$\begin{aligned}C_A(\mathbf{r}, t) = \int_{\delta\omega,\mathbf{q}} &\left[\frac{2D_A}{(\delta\omega)^2 + \left(\frac{\alpha q_y^2}{q_x^2} + \mu_x q_x^2\right)^2}\right] \\ &\times e^{-i[\delta\omega t - q_x(x - \gamma t) - q_y y]},\end{aligned} \tag{29}$$

where $\delta\omega \equiv \omega - \gamma q_x$, and then introduce the new variables Ω and $\mathbf{Q}$ as follows:

$$q_x = \frac{Q_x}{|y|^{\frac{1}{2}}}, \quad q_y = \frac{Q_y}{|y|}, \quad \delta\omega = \frac{\Omega}{|y|}. \tag{30}$$

Now, rewriting the integral in (29) in terms of Ω and $\mathbf{Q}$, we get

$$C_A(\mathbf{r}, t) = |y|^{-\frac{1}{2}} \mathcal{C}_A\left(\frac{|x - \gamma t|}{|y|^{\frac{1}{2}}}, \frac{|t|}{|y|}\right), \tag{31}$$

where

$$\begin{aligned}\mathcal{C}_A\left(\frac{|x - \gamma t|}{|y|^{\frac{1}{2}}}, \frac{|t|}{|y|}\right) \equiv \int_{\Omega,\mathbf{Q}} &\left[\frac{2D_A}{\Omega^2 + \left(\frac{\alpha Q_y^2}{Q_x^2} + \mu_x Q_x^2\right)^2}\right] \\ &\exp\left[-i\left(\frac{\Omega t}{|y|} - Q_y - \frac{Q_x(x - \gamma t)}{|y|^{\frac{1}{2}}}\right)\right].\end{aligned} \tag{32}$$

Likewise changing variables of integration on $C_Q(\mathbf{r})$ we get

$$C_Q(\mathbf{r}) = |y|^{-\frac{1}{3}} \mathcal{C}_Q\left(\frac{|x|}{|y|^{\frac{2}{3}}}\right), \tag{33}$$

where

$$\mathcal{C}_Q\left(\frac{|x|}{|y|^{\frac{2}{3}}}\right) \equiv \int_{\mathbf{Q}} \left(\frac{2D_Q Q_x^4}{\alpha^2 Q_y^4 + \gamma^2 Q_x^6}\right) e^{i\left(Q_y + \frac{|x| Q_x}{|y|^{\frac{2}{3}}}\right)}. \tag{34}$$

Finally, the overall correlation of $\langle \mathbf{u}(\mathbf{r}, t) \cdot \mathbf{u}(\mathbf{0}, 0)\rangle$ is given by

$$|y|^{-\frac{1}{3}} \mathcal{C}_Q\left(\frac{|x|}{|y|^{\frac{2}{3}}}\right) + |y|^{-\frac{1}{2}} \mathcal{C}_A\left(\frac{|x - \gamma t|}{|y|^{\frac{1}{2}}}, \frac{|t|}{|y|}\right). \tag{35}$$

Therefore, the linear theory recovers a form similar to (1), with the quenched and the annealed anisotropy exponent given by $\zeta_{\text{quenched}} = 2/3$ and $\zeta_{\text{annealed}} = 1/2$, respectively, the quenched and annealed roughness exponents given by $\chi = -1/6$ and $\chi' = -1/4$, respectively, and the dynamic exponent $z = 1$. We will now show that these exponents are modified by the nonlinearities in the EOM, and in particular, the two anisotropy exponents become equal.

IV. NONLINEAR REGIME AND DRG ANALYSIS

We turn now to the full EOM of $\mathbf{u}$ (12). Fourier transforming this, and acting on both sides with the transverse projection operator $P_{li}(\mathbf{q})$ (15), we obtain

$$\begin{aligned}-i\omega u_y = P_{yx}(\mathbf{q}) \mathcal{F}_{\tilde{\mathbf{q}}} &\left[-\alpha\left(u_x + \frac{u_y^2}{2}\right)\right] \\ &+ \mathcal{F}_{\tilde{\mathbf{q}}}\Big[-\gamma \partial_x u_y + \mu_x \partial_x^2 u_y - \lambda u_y \partial_y u_y \\ &- \alpha\left(u_x + \frac{u_y^2}{2}\right) u_y + f_A^y + f_Q^y\Big],\end{aligned} \tag{36}$$

where $\mathcal{F}_{\tilde{\mathbf{q}}}$ represents the $\tilde{\mathbf{q}}$th Fourier component. In writing this equation, we have rescaled the fields ($\mathbf{u} \to \mathbf{u}v_0$) and the noise terms ($\mathbf{f}_{A,Q} \to \mathbf{f}_{A,Q}v_0$) to eliminate the v_0's. We have also neglected many terms which are irrelevant due to the fact that the dominant regime of wave vector is $q_y \ll q_x$, as we discovered in our treatment of the linear theory. We will assume, and verify *a posteriori*, that this continues to hold true for the nonlinear theory.

First, this assumption implies that the noise terms $P_{yx}f^x_{A,Q}$ are irrelevant in comparison to $P_{yy}f^y_{A,Q}$. Second, due to the incompressibility constraint, $P_{yx}\partial_x u_x$ is as relevant as $P_{yx}\partial_y u_y$, and the latter, again due to the anisotropic scaling, is less relevant than $P_{yy}\partial_x u_y$. Therefore, $P_{yx}\partial_x u_x$ is also irrelevant in comparison to $P_{yy}\partial_x u_y$. Similarly, $P_{yy}\partial_y^2 u_y$ is irrelevant in comparison to $P_{yy}\partial_x^2 u_y$. Naively $P_{yy}\partial_x^2 u_y$ is also irrelevant in comparison to $P_{yy}\partial_x u_y$. However, because $P_{yy}\partial_x u_y$ only leads to propagation, not damping, we need to keep the $P_{yy}\partial_x^2 u_y$ term. This is very similar to keeping the viscous term in the dynamics of a simple fluid, even though it is formally less relevant than the pressure term, since the pressure only leads to sound *propagation*, while it is the viscosity which controls sound *damping*.

Finally, in the limit of interest $q_y \ll q_x$, we can approximate $P_{yy}(\mathbf{q}) \approx 1$.

To evaluate the importance of the nonlinear terms in (36), we first power count (which can be thought of as a zeroth order renormalization group analysis). We rescale time, lengths, and fields as

$$t \to te^{z\ell}, \quad x \to xe^{\zeta\ell}, \quad y \to ye^{\ell}, \tag{37a}$$

$$u_y \to u_y e^{\ell\chi}, \quad u_x \to u_x e^{(\chi+\zeta-1)\ell}, \tag{37b}$$

and keep the form of the resultant EOM unchanged by absorbing the rescaling factors into the coefficients. Specifically, the coefficients of the linear terms $P_{yx}u_x$, $\partial_x u_y$, and the noise strength are rescaled respectively as

$$\alpha \to \alpha e^{(z+2\zeta-2)\ell}, \quad \gamma \to \gamma e^{(z-\zeta)\ell}, \quad \mu_x \to \mu_x e^{(z-2\zeta)\ell}, \tag{38a}$$

$$D_A \to D_A e^{(z-2\chi-\zeta-1)\ell}, \quad D_Q \to D_Q e^{(2z-2\chi-\zeta-1)\ell}, \tag{38b}$$

and the coefficients of the nonlinear terms $P_{yx}u_y^2$, $u_y\partial_y u_y$, $u_x u_y$, and u_y^3 as

$$\frac{\alpha}{2} \to \frac{\alpha}{2} e^{(z+\chi+\zeta-1)\ell}, \quad \lambda \to \lambda\, e^{(z+\chi-1)\ell}, \tag{39a}$$

$$\alpha \to \alpha\, e^{(z+\chi+\zeta-1)\ell}, \quad \frac{\alpha}{2} \to \frac{\alpha}{2} e^{(z+2\chi)\ell}. \tag{39b}$$

We choose z, ζ, and χ to fix α, γ, and D_Q, which control the size of the dominant fluctuations (i.e., those coming from the quenched noise). Note that we need not keep μ_x fixed, since it only affects the subdominant, annealed part of the fluctuations.

This choice leads to the following values of the scaling exponents:

$$z = \tfrac{2}{3}, \quad \zeta = \tfrac{2}{3}, \quad \chi = -\tfrac{1}{6}. \tag{40}$$

Note that, as expected, these values of ζ and χ are identical to those for the quenched part of the velocity correlations obtained from our linear theory [e.g., see (35)]. Technically, the z we get here is the dynamic exponent for the *quenched* correlations, which, however, are purely static. As a result, its value is different from $z = 1$, which is the dynamic exponent for the annealed part of the correlations in (35).

Substituting these values into (39), we find the coefficients of the nonlinear terms $P_{yx}u_y^2$, $u_x u_y$, and u_y^3 all diverge as $\ell \to \infty$; specifically

$$\alpha \to \alpha\, e^{\ell/6}, \quad \frac{\alpha}{2} \to \frac{\alpha}{2} e^{\ell/3}, \tag{41a}$$

which implies these nonlinear terms are *relevant* in the hydrodynamic limit, while λ vanishes, which implies $u_y\partial_y u_y$ is *irrelevant* and hence can be neglected.

We will deal with the relevant nonlinearities using the DRG approach of Refs. [24,25]. This begins by formally "solving" the hydrodynamic EOM (36) for u_y by Fourier transforming in space *and time* to get

$$u_y(\tilde{\mathbf{q}}) = G(\tilde{\mathbf{q}})\Big[f^y_Q(\tilde{\mathbf{q}}) + f^y_A(\tilde{\mathbf{q}}) - \Big(\frac{\alpha}{2}\Big)P_{yx}(\mathbf{q}) \times \int_{\tilde{\mathbf{k}}} u_y(\tilde{\mathbf{k}})u_y(\tilde{\mathbf{q}}-\tilde{\mathbf{k}}) - \alpha\int_{\tilde{\mathbf{k}}} u_x(\tilde{\mathbf{q}}-\tilde{\mathbf{k}})u_y(\tilde{\mathbf{k}}) - \Big(\frac{\alpha}{2}\Big)\int_{\tilde{\mathbf{k}},\tilde{\mathbf{k}}'} u_y(\tilde{\mathbf{q}}-\tilde{\mathbf{k}}-\tilde{\mathbf{k}}')u_y(\tilde{\mathbf{k}})u_y(\tilde{\mathbf{k}}')\Big], \tag{42}$$

where $G(\tilde{\mathbf{q}})$ is given by (17), and we have defined $\int_{\tilde{\mathbf{k}}} \equiv \int d\Omega d^2k/(\sqrt{2\pi})^3$. In the limits of small $\mathbf{q}$ and $q_y \ll q_x$, $G(\tilde{\mathbf{q}})$ can be simplified to

$$G(\tilde{\mathbf{q}}) \equiv \left[-i(\omega - \gamma q_x) + \left(\alpha\frac{q_y^2}{q^2} + \mu_x q_x^2\right)\right]^{-1}. \tag{43}$$

To "regularize" our theory, we must introduce a short-distance (i.e., large wave vector) cutoff. We do so by restricting the wave vectors in (42) to lie within a Brillouin zone whose shape is a strip, infinite in the q_x direction, and of width 2Λ in the q_y direction. That is, our allowed wave vectors $\mathbf{q}$ lie in the range $-\infty < q_x < \infty$, $-\Lambda < q_y < \Lambda$, where Λ is the ultraviolet cutoff.

Next we decompose $u_y(\tilde{\mathbf{q}})$ into "slow" components $u_y^<(\tilde{\mathbf{q}})$ and "fast" components $u_y^>(\tilde{\mathbf{q}})$, where $u_y^<(\tilde{\mathbf{q}})$ is supported in the wave vector space $-\infty < q_x < \infty$, $|q_y| < \Lambda e^{-d\ell}$, and $u_y^>$ in the "momentum shell" $-\infty < q_x < \infty$, $\Lambda e^{-d\ell} < |q_y| < \Lambda$, where $d\ell \ll 1$ is an arbitrary rescaling factor. We likewise decompose the noises $f^y_{A,Q}$ into fast and slow components $f^{y>}_{A,Q}(\tilde{\mathbf{q}})$ and $f^{y<}_{A,Q}(\tilde{\mathbf{q}})$, respectively. Next we solve (42) iteratively for $u_y^>(\tilde{\mathbf{q}})$ in terms of $u_y^<(\tilde{\mathbf{q}})$ and the noises $f^{y>}_{A,Q}(\tilde{\mathbf{q}})$. We then substitute the solution into the EOM (36) for $u_y^<(\tilde{\mathbf{q}})$, and average over the short wavelength noises $f^{y<}_{A,Q}(\tilde{\mathbf{q}})$. This renormalizes the various coefficients in the EOM for $u_y^<(\tilde{\mathbf{q}})$. Following this averaging step, we perform a rescaling step in which we rescale time, lengths, and fields

$$t \to te^{zd\ell}, \quad x \to xe^{\zeta d\ell}, \quad y \to ye^{d\ell}, \tag{44a}$$

$$u_y \to u_y e^{\chi d\ell}, \quad u_x \to u_x e^{(\chi+\zeta-1)d\ell}, \tag{44b}$$

to bring the cutoff back to Λ. Upon repeating this process recursively with the definition $\ell = nd\ell$, where n is the number of iterations of this renormalization process, we obtain a set of recursion relations. The values of the parameters after these n steps are denoted as $\alpha(\ell)$, etc., with ℓ treated as a continuous

variable. This enables us to write the recursion relations as differential equations.

In obtaining the recursion relations we also make use of an important symmetry property: due to the rotation invariance of the hydrodynamic EOM, all the "α"s in that equation should remain equal upon renormalization and we choose values of χ and ζ that ensure this; i.e.,

$$\chi = \zeta - 1. \tag{45}$$

With this, the recursion relations can be written exactly as

$$\frac{d\ln\alpha}{d\ell} = z + 2\zeta - 2 + \eta_\alpha, \tag{46a}$$

$$\frac{d\ln\gamma}{d\ell} = z - \zeta + \eta_\gamma, \tag{46b}$$

$$\frac{d\ln\mu_x}{d\ell} = z - 2\zeta + \eta_\mu, \tag{46c}$$

$$\frac{d\ln D_{\mathcal{Q}}}{d\ell} = 2z - 3\zeta + 1 + \eta_{\mathcal{Q}}, \tag{46d}$$

$$\frac{d\ln D_A}{d\ell} = z - 3\zeta + 1 + \eta_A, \tag{46e}$$

where $\eta_{\alpha,\gamma,\mu,\mathcal{Q},A}$ denote the corrections arising from averaging the nonlinear terms in the EOM over the short wavelength noises. We calculate $\eta_{\alpha,\gamma,\mu,\mathcal{Q},A}$ perturbatively using three different schemes. These are an uncontrolled one-loop calculation in exactly $d = 2$, an $\epsilon = 7/3 - d$ expansion to $O(\epsilon)$, and an $\tilde{\epsilon} = 5/2 - d$ expansion to $O(\tilde{\epsilon})$. The details of these calculations are given in Appendix A. We now describe DRG analysis for each of these three schemes in turn.

A. Uncontrolled calculation in exactly $d = 2$

We first present the DRG for the one-loop uncontrolled calculation in exactly $d = 2$. The reason we refer to this calculation as "uncontrolled" is that, in contrast to the ϵ expansions we will describe in the next two sections, which become asymptotically exact as we approach the critical dimension [i.e., in the limit ϵ (or $\tilde{\epsilon}$) $\to 0$], this uncontrolled calculation has no such limit in which it becomes exact, since the dimension of our system (i.e., 2) differs always from the critical dimension by an amount of order 1.

The detailed calculation of the graphical corrections for this scheme is presented in Appendix A, and obtains, to one-loop order,

$$\eta_\alpha = -\tfrac{1}{27} g^{(\mathrm{unc})}, \tag{47a}$$

$$\eta_\gamma = \tfrac{8}{27} g^{(\mathrm{unc})}, \tag{47b}$$

$$\eta_{\mathcal{Q}} = \tfrac{10}{27} g^{(\mathrm{unc})}, \tag{47c}$$

$$\eta_A = \tfrac{16}{27} g^{(\mathrm{unc})}, \tag{47d}$$

$$\eta_\mu = g_\mu^{(\mathrm{unc})} + \tfrac{2}{27} g^{(\mathrm{unc})}, \tag{47e}$$

where the two dimensionless couplings are given by

$$g^{(\mathrm{unc})} = \frac{D_{\mathcal{Q}}}{\pi} |\gamma|^{-\frac{7}{3}} \alpha^{\frac{1}{3}} \Lambda^{-\frac{1}{3}}, \tag{48a}$$

$$g_\mu^{(\mathrm{unc})} \propto D_{\mathcal{Q}} |\gamma|^{-1} \mu_x^{-1} \Lambda^{-1}. \tag{48b}$$

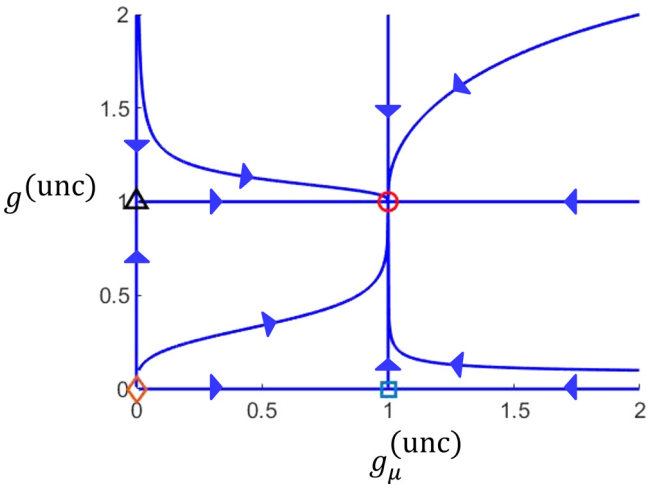


FIG. 1. Renormalization group flows in $d = 2$ in the plane of $g^{(\mathrm{unc})}$ and $g_\mu^{(\mathrm{unc})}$ (50). There are three unstable fixed points (indicated by the triangle, square, and diamond symbols), and one stable fixed point at $(g^{(\mathrm{unc})}, g_\mu^{(\mathrm{unc})}) = (1, 1)$ (indicated by the red circle), which is our focus here.

In writing these expressions (47) for the graphical corrections, we have ignored all corrections to all parameters from the annealed noise strength D_A other than D_A itself; that is, we have set $D_A = 0$ for all corrections except that to D_A itself. And even that correction is evaluated only to linear order in D_A. This will be justified *a posteriori* by showing that the effective coupling $g_A^{(\mathrm{unc})}$ associated with the annealed noise (which we will calculate below) flows to zero under the DRG transformation.

Because of this, it is possible to show, to all orders in perturbation theory, that η_α, η_γ, and $\eta_{\mathcal{Q}}$ all depend only on the coupling $g^{(\mathrm{unc})}$ defined in (48a) at the fixed point. This observation, together with the fact that $g^{(\mathrm{unc})}$ flows to a nonzero stable fixed point, which we will show below, implies an exact relation, which does not depend on perturbation theory, between the graphical corrections $\eta_{\gamma,\alpha,\mathcal{Q}}$. Since η_μ also depends on $g_\mu^{(\mathrm{unc})}$, which we will show also flows to a nonzero stable fixed point, we further obtain a second exact relation which is again independent of the perturbation theory.

Using the definitions of $g^{(\mathrm{unc})}$ and $g_\mu^{(\mathrm{unc})}$ and recursion relations (46), we can construct the following formally exact recursion relations:

$$\frac{d\ln g^{(\mathrm{unc})}}{d\ell} = \frac{1}{3} - \frac{7}{3}\eta_\gamma + \frac{1}{3}\eta_\alpha + \eta_{\mathcal{Q}}, \tag{49a}$$

$$\frac{d\ln g_\mu^{(\mathrm{unc})}}{d\ell} = 1 - \eta_\gamma - \eta_\mu + \eta_{\mathcal{Q}}. \tag{49b}$$

Next, inserting (47) into (49) we get two closed recursion relations for $g^{(\mathrm{unc})}$ and $g_\mu^{(\mathrm{unc})}$:

$$\frac{dg^{(\mathrm{unc})}}{d\ell} = \frac{1}{3}(1 - g^{(\mathrm{unc})})g^{(\mathrm{unc})}, \tag{50a}$$

$$\frac{dg_\mu^{(\mathrm{unc})}}{d\ell} = \left(1 - g_\mu^{(\mathrm{unc})}\right)g_\mu^{(\mathrm{unc})}. \tag{50b}$$

The associated DRG flow diagram is depicted in Fig. 1, which shows that the flows have one stable fixed point and three

unstable fixed points in the $g^{(\mathrm{unc})}$-$g_\mu^{(\mathrm{unc})}$ plane. The stable fixed point, which generically describes the universal behavior of the system, is at

$$g^{(\mathrm{unc})*} = g_\mu^{(\mathrm{unc})*} = 1. \tag{51}$$

At this nonzero stable fixed point, $dg^{(\mathrm{unc})}/d\ell$ and $dg_\mu^{(\mathrm{unc})}/d\ell$ are both 0; Eqs. (49) imply two exact relations between the η's:

$$7\eta_\gamma - 3\eta_Q - 1 = \eta_\alpha, \tag{52a}$$

$$1 - \eta_\gamma + \eta_Q = \eta_\mu. \tag{52b}$$

To get quantitative results for η's, we insert (51) into (47a)–(47d), which gives

$$\eta_\alpha = -\tfrac{1}{27}, \tag{53a}$$

$$\eta_\gamma = \tfrac{8}{27}, \tag{53b}$$

$$\eta_Q = \tfrac{10}{27}, \tag{53c}$$

$$\eta_A = \tfrac{16}{27}. \tag{53d}$$

Inserting (53b) and (53c) into the exact relation (52b), we get

$$\eta_\mu = \tfrac{29}{27}. \tag{54}$$

We will choose the scaling exponents χ, ζ, and z to keep the coefficients γ, α, and D_Q fixed under renormalization. We will show in Sec. V that, as usual in the DRG [24,25], this choice makes these values of χ, ζ, and z those that appear in the scaling laws (1). Since these coefficients determine the coupling coefficient $g^{(\mathrm{unc})}$, which goes to a nonzero constant at the fixed point, keeping any two of these coefficients fixed automatically fixes the remaining one. For instance, by keeping α and γ fixed [i.e., setting the right-hand side of (46a) and (46b) to be zero], we get

$$\zeta = \frac{2 + \eta_\gamma - \eta_\alpha}{3}, \quad z = \frac{2 - 2\eta_\gamma - \eta_\alpha}{3}. \tag{55}$$

Inserting (55) into (45), we obtain χ:

$$\chi = \frac{-1 + \eta_\gamma - \eta_\alpha}{3}. \tag{56}$$

The exponent χ' is also derived in Sec. V. Here we only quote the result:

$$\chi' = \frac{\eta_A - \eta_\gamma - 1}{2}. \tag{57}$$

Using the values (53a)–(53d) of the η's, we then obtain the exponents' values explicitly:

$$z = \tfrac{13}{27}, \tag{58a}$$

$$\zeta = \tfrac{7}{9}, \tag{58b}$$

$$\chi = -\tfrac{2}{9}, \tag{58c}$$

$$\chi' = -\tfrac{19}{54}. \tag{58d}$$

Coincidentally, these scaling exponents will turn out to be exactly equal to those obtained by the $\epsilon = (7/3 - d)$ expansion in the "hard" continuation approach to be discussed next, when ϵ is taken to be $1/3$.

The above analysis ignored most of the graphical corrections induced by the annealed noise. The only such correction we included was in the correction η_A to the annealed noise variance D_A itself, and even for that correction, we left out one-loop corrections that involve two annealed noises. In Appendix B, we show that those two annealed noise corrections to D_A itself are controlled by the "annealed coupling coefficient"

$$g_A^{(\mathrm{unc})} \propto \frac{\alpha^{1/4} D_A}{\mu_x^{5/4} \Lambda^{\frac{1}{2}}}. \tag{59}$$

Corrections to all other coefficients, such as α, stemming from the annealed noise, are also controlled by the same coupling coefficient.

We will now show that $g_A^{(\mathrm{unc})}$ flows to zero at the fixed point we have just found, thereby justifying our neglect of the graphical corrections arising from the annealed noise. From its definition (59) and the recursion relations (46), we can derive the formally exact recursion relations for $g_A^{(\mathrm{unc})}$:

$$\begin{aligned}\frac{d \ln g_A^{(\mathrm{unc})}}{d\ell} &= \frac{1}{4}\frac{d \ln \alpha}{d\ell} + \frac{d \ln D_A}{d\ell} - \frac{5}{4}\frac{d \ln \mu_x}{d\ell} \\ &= \frac{1}{2} + \frac{(\eta_\alpha + 4\eta_A - 5\eta_\mu)}{4}.\end{aligned} \tag{60}$$

Inserting (53a), (53d), and (54) into (60) gives

$$\frac{d \ln g_A^{(\mathrm{unc})}}{d\ell} = -\frac{7}{27}. \tag{61}$$

Since this eigenvalue is less than zero, we can conclude that the annealed noise is irrelevant at the quenched fixed point. This justifies our neglect of corrections coming from the annealed noise in (47).

B. "Hard" continuation

In this section, we will obtain DRG recursion relations using an ϵ-expansion method. This presents a problem since the model we described is defined precisely in two dimensions. We circumvent this issue by only analytically continuing the integrals in Fourier space required for the averaging over the large wave number modes in the nonlinear terms, and making the trivial (but important) changes in the power counting on the rescaling step of the DRG. In this section, we generalize our calculation to dimensions $d > 2$ by treating the "soft" direction (x direction) as one-dimensional, while treating the other spatial component y (the "hard" direction) as $(d-1)$-dimensional. That is, we replace $y \to \mathbf{r}_h$, and, in Fourier space, $q_y \to \mathbf{q}_h$. In particular, the integrals of Fourier variables become $\int_{\mathbf{q}} \equiv \int d\Omega d^{d-1} q_h dq_x/(\sqrt{2\pi})^{d+1}$. Of course, this extension also changes the recursion relations for D_Q and D_A from (46d) and (46e), since these explicitly depend on the dimensionality d. For clarity, we rewrite all the recursion relations again:

$$\frac{d \ln \alpha}{d\ell} = z + 2\zeta - 2 + \eta_\alpha, \tag{62a}$$

$$\frac{d \ln \gamma}{d\ell} = z - \zeta + \eta_\gamma, \tag{62b}$$

$$\frac{d\ln\mu_x}{d\ell} = z - 2\zeta + \eta_\mu, \tag{62c}$$

$$\frac{d\ln D_Q}{d\ell} = 2z - 3\zeta + 3 - d + \eta_Q, \tag{62d}$$

$$\frac{d\ln D_A}{d\ell} = z - 3\zeta + 3 - d + \eta_A. \tag{62e}$$

Note the power counting of $D_{Q,A}$ is changed due to the fact that we are not in $d = 2$.

The η's for this hard-continuation ϵ expansion are calculated in Appendix A and, to one-loop order, are identical to our uncontrolled-calculation results (47), i.e.,

$$\eta_\alpha = -\tfrac{1}{27}g^{(\mathrm{hard})}, \quad \eta_\gamma = \tfrac{8}{27}g^{(\mathrm{hard})}, \tag{63a}$$

$$\eta_Q = \tfrac{10}{27}g^{(\mathrm{hard})}, \quad \eta_A = \tfrac{16}{27}g^{(\mathrm{hard})}, \tag{63b}$$

$$\eta_\mu = g_\mu^{(\mathrm{hard})} + \tfrac{2}{27}g^{(\mathrm{hard})}. \tag{63c}$$

The only difference between these graphical corrections and those of the uncontrolled calculation is the generalization of the dimensionless couplings $g^{(\mathrm{unc})}$ and $g_\mu^{(\mathrm{unc})}$ to higher dimensions. These new dimensionless couplings $g^{(\mathrm{hard})}$ and $g_\mu^{(\mathrm{hard})}$ are given by

$$g^{(\mathrm{hard})} \equiv \frac{S_{d-1}}{(2\pi)^{d-1}}|\gamma|^{-\frac{7}{3}}\alpha^{\frac{1}{3}}\Lambda^{\frac{3d-7}{3}}D_Q, \tag{64a}$$

$$g_\mu^{(\mathrm{hard})} \propto |\gamma|^{-1}\mu_x^{-1}D_Q\Lambda^{d-3}. \tag{64b}$$

In writing (63), we have, as in the uncontrolled calculation, ignored all corrections to any parameters from the annealed noise strength D_A other than D_A itself; that is, we have set $D_A = 0$ for all corrections except that to D_A itself. And even that correction is evaluated only to linear order in D_A. This will again be justified *a posteriori* by showing that the effective coupling $g_A^{(\mathrm{hard})}$ associated with the annealed noise actually flows to zero under the DRG transformation. As in the last section, we can construct an exact relation between the graphical corrections $\eta_{\gamma,\alpha,Q}$. Using the definition of $g^{(\mathrm{hard})}$ (64a) and (62) we construct a formally exact recursion relation for $g^{(\mathrm{hard})}$:

$$\frac{d\ln g^{(\mathrm{hard})}}{d\ell} = \left[\frac{1}{3}(7-3d) - \frac{7}{3}\eta_\gamma + \frac{1}{3}\eta_\alpha + \eta_Q\right]. \tag{65}$$

At the fixed point, since $\frac{dg^{(\mathrm{hard})}}{d\ell} = 0$, Eq. (65) clearly implies that either $g^{(\mathrm{hard})} = 0$ or

$$7 - 3d - 7\eta_\gamma + \eta_\alpha + 3\eta_Q = 0. \tag{66}$$

It is easy to see by inspection that the $g^{(\mathrm{hard})} = 0$ fixed point is unstable (with eigenvalue $7/3 - d$) for $d < 7/3$, and, hence, in the physical case $d = 2$. Therefore, in $d = 2$, and formally in all spatial dimensions $d < 7/3$, the graphical corrections η_γ, η_α, and η_Q must obey (66) exactly, at the nonzero stable fixed point, as expected from our previous calculation in the uncontrolled-calculation scheme (52a).

Likewise, we can construct a formally exact recursion relation for $g_\mu^{(\mathrm{hard})}$:

$$\frac{d\ln g_\mu^{(\mathrm{hard})}}{d\ell} = 3 - d - \eta_\gamma - \eta_\mu + \eta_Q. \tag{67}$$

Reasoning as we just did for $g^{(\mathrm{hard})}$, this recursion relation implies that the $g_\mu^{(\mathrm{hard})} = 0$ fixed point is unstable for any $d < 3$. Hence, in all $d < 3$ and, in particular, in the physical case $d = 2$, we obtain a second exact relation since $\frac{dg_\mu^{(\mathrm{hard})}}{d\ell} = 0$ at the nonzero stable fixed point:

$$3 - d + \eta_Q - \eta_\gamma - \eta_\mu = 0. \tag{68}$$

Note that this reduces to (52b) for $d = 2$.

Subtracting 1/3 of Eq. (66) from (68), we obtain an exact relation between η_μ, η_γ, and η_α:

$$\eta_\mu = \frac{2 + 4\eta_\gamma - \eta_\alpha}{3}, \tag{69}$$

which will prove useful later.

To proceed further and obtain quantitative predictions for the exponents, we use the perturbation theory results (63) for the graphical corrections in the recursion relations (65) and (67). This gives

$$\frac{dg^{(\mathrm{hard})}}{d\ell} = \frac{1}{3}(7 - 3d - g^{(\mathrm{hard})})g^{(\mathrm{hard})}, \tag{70a}$$

$$\frac{dg_\mu^{(\mathrm{hard})}}{d\ell} = \left(3 - d - g_\mu^{(\mathrm{hard})}\right)g_\mu^{(\mathrm{hard})}. \tag{70b}$$

The associated DRG flow diagram for $d = 2$ is identical to that in the uncontrolled calculation, as shown in Fig. 1, which shows that the flows have one stable fixed point and three unstable fixed points. The stable fixed point, which generically describes the universal behavior of the system, is at

$$g^{(\mathrm{hard})*} = 3\epsilon + O(\epsilon^2), \tag{71a}$$

where $\epsilon = 7/3 - d$. Inserting the definition of ϵ in (70b), we can also obtain an expression for the stable fixed point of $g_\mu^{(\mathrm{hard})}$ for $d < 7/3$:

$$g_\mu^{(\mathrm{hard})*} = \tfrac{2}{3} + \epsilon. \tag{72}$$

Note that, unlike our result (71) for $g^{(\mathrm{hard})*}$, this result is not, strictly speaking, asymptotically valid in the limit of small ϵ. This is because this value of $g_\mu^{(\mathrm{hard})*}$ does not become small for $\epsilon \ll 1$; hence, there is no formal justification for dropping terms higher order in $g_\mu^{(\mathrm{hard})}$ from the recursion relation for $g_\mu^{(\mathrm{hard})}$. However, this is not a problem, since our results for all of the other η's (except η_μ) are asymptotically correct in the limit $\epsilon \ll 1$. We can therefore obtain quantitatively valid results for $\epsilon \ll 1$ for those other η's, and then use the exact scaling relation (69) to determine η_μ.

Inserting this result for the fixed point value of the dimensionless coupling $g^{(\mathrm{hard})}$ into our earlier expressions (63a) and (63b) for the graphical corrections $\eta_{\alpha,\gamma,Q,A}$ gives their fixed point values explicitly as a functions of ϵ:

$$\eta_\alpha = -\frac{\epsilon}{9}, \quad \eta_\gamma = \frac{8\epsilon}{9}, \tag{73a}$$

$$\eta_Q = \frac{10\epsilon}{9}, \quad \eta_A = \frac{16\epsilon}{9}. \tag{73b}$$

Inserting these into the exact relation (69) gives our ϵ-expansion result for η_μ:

$$\eta_\mu = \frac{2}{3} + \frac{11\epsilon}{9}. \tag{74}$$

The $O(\epsilon^2)$ corrections can in principle be obtained through higher-loop calculations. We have not attempted this formidable calculation, because we expect our one-loop DRG results to be very quantitatively accurate. This is because, in $d = 2, \epsilon = 1/3$, which is extremely small for ϵ expansions.

As in the last section, we have ignored the graphical corrections induced by the annealed noise, which are controlled by the coupling coefficient $g_A^{(\mathrm{hard})}$. We show in Appendix B that, for this hard continuation, this coupling is given by

$$g_A^{(\mathrm{hard})} \propto \frac{\alpha^{1/4} D_A}{\mu_x^{5/4} \Lambda^{\frac{5}{2}-d}}. \tag{75}$$

As we did for the uncontrolled approximation, here too we can justify our neglect of the corrections arising from the annealed noise by demonstrating that the coupling $g_A^{(\mathrm{hard})}$ just defined is irrelevant in the dimension of physical interest $d = 2$.

We do this by using the definition (75) and the recursion relations (62) to derive the formally exact recursion relation for $g_A^{(\mathrm{hard})}$:

$$\frac{d \ln g_A^{(\mathrm{hard})}}{d\ell} = \frac{5}{2} - d + \frac{(\eta_\alpha + 4\eta_A - 5\eta_\mu)}{4}. \tag{76}$$

Inserting the fixed point values of η's (73), (74) into (76) gives

$$\frac{d \ln g_A^{(\mathrm{hard})}}{d\ell} = \frac{59 - 33d}{27}, \tag{77}$$

where we have inserted $\epsilon = \frac{7}{3} - d$.

Since the eigenvalue $\frac{59-33d}{27}$ is less than zero both near the critical dimension $d = 7/3$, where it is $-\frac{2}{3}$, and in $d = 2$, where it is $-\frac{7}{27}$, we can conclude that the annealed noise is irrelevant at the quenched fixed point. This justifies our neglect of the corrections to the η's coming from the annealed noise in (63).

Finally, to obtain the scaling exponents, we substitute the fixed point values of the η's (73) into Eqs. (55), (56), and (57). This gives

$$z = \tfrac{2}{3} - \tfrac{5}{9}\epsilon + O(\epsilon^2), \tag{78a}$$
$$\zeta = \tfrac{2}{3} + \tfrac{1}{3}\epsilon + O(\epsilon^2), \tag{78b}$$
$$\chi = -\tfrac{1}{3} + \tfrac{1}{3}\epsilon + O(\epsilon^2), \tag{78c}$$
$$\chi' = -\tfrac{1}{2} + \tfrac{4}{9}\epsilon + O(\epsilon^2). \tag{78d}$$

C. "Soft" continuation

In this section we obtain the DRG recursion relations using a "soft" continuation to higher dimensions. In this approach, we treat the "hard" direction y as one-dimensional, while the "soft" direction x is extended to $(d-1)$ dimensions. In practice, this means we will simply replace q_x in Fourier space with a $(d-1)$-dimensional vector $\mathbf{q}_s$ orthogonal to the y direction.

As in the last section, this modifies the form of the recursion relations for D_Q and D_A. Rewriting the full set of recursion relations for completeness, we have

$$\frac{d \ln \alpha}{d\ell} = z + 2\zeta - 2 + \eta_\alpha, \tag{79a}$$
$$\frac{d \ln \gamma}{d\ell} = z - \zeta + \eta_\gamma, \tag{79b}$$
$$\frac{d \ln \mu_x}{d\ell} = z - 2\zeta + \eta_\mu, \tag{79c}$$
$$\frac{d \ln D_Q}{d\ell} = 2z - (d+1)\zeta + 1 + \eta_Q, \tag{79d}$$
$$\frac{d \ln D_A}{d\ell} = z - (d+1)\zeta + 1 + \eta_A. \tag{79e}$$

The η's for the soft continuation are obtained in Appendix A and are

$$\eta_\alpha = 0, \tag{80a}$$
$$\eta_\gamma = \tfrac{2}{3} g^{(\mathrm{soft})}, \tag{80b}$$
$$\eta_Q = \tfrac{2}{3} g^{(\mathrm{soft})}, \tag{80c}$$
$$\eta_A = g^{(\mathrm{soft})}, \tag{80d}$$
$$\eta_\mu = g_\mu^{(\mathrm{soft})} + \tfrac{1}{6} g^{(\mathrm{soft})}, \tag{80e}$$

where the two dimensionless couplings are given by

$$g^{(\mathrm{soft})} \equiv \frac{S_{d-1} D_Q}{\sqrt{2}(2\pi)^{d-1}} |\gamma|^{-(\frac{d+5}{3})} \alpha^{(\frac{d-1}{3})} \Lambda^{(\frac{2d-5}{3})}, \tag{81a}$$
$$g_\mu^{(\mathrm{soft})} \propto D_Q \mu_x^{-1} \alpha^{(\frac{d-2}{3})} |\gamma|^{-(\frac{d+1}{3})} \Lambda^{(\frac{2d-7}{3})}. \tag{81b}$$

Inserting (80a)–(80c) into (79a), (79b), and (79d) and using the definitions of $g^{(\mathrm{soft})}$ and $g_\mu^{(\mathrm{soft})}$ (81), we get two closed recursion relations for $g^{(\mathrm{soft})}$ and $g_\mu^{(\mathrm{soft})}$:

$$\frac{d \ln g^{(\mathrm{soft})}}{d\ell} = \left(\frac{5-2d}{3}\right) - \left(\frac{2d+4}{9}\right) g^{(\mathrm{soft})}, \tag{82a}$$
$$\frac{d \ln g_\mu^{(\mathrm{soft})}}{d\ell} = \left(\frac{7-2d}{3}\right) + \left(\frac{5-4d}{18}\right) g^{(\mathrm{soft})} - g_\mu^{(\mathrm{soft})}. \tag{82b}$$

As in the uncontrolled calculation and the hard-continuation scheme, the trivial $g^{(\mathrm{soft})} = 0$ and $g_\mu^{(\mathrm{soft})} = 0$ fixed points are obviously unstable at the physically relevant dimension $d = 2$. In fact, here the $g^{(\mathrm{soft})} = 0$ fixed point is unstable for all $d < 5/2$, and the $g_\mu^{(\mathrm{soft})} = 0$ fixed point is unstable for all $d < 7/2$. Below $d = 5/2$, the stable fixed point which generically describes hydrodynamics of the system is at

$$g^{(\mathrm{soft})*} = \tfrac{2}{3}\tilde{\epsilon} + O(\tilde{\epsilon}^2), \tag{83}$$

where $\tilde{\epsilon} = 5/2 - d$. We can now insert the fixed point value of $g^{(\mathrm{soft})}$ (83) into (82b) to obtain the fixed point value of $g_\mu^{(\mathrm{soft})}$ for $d < 5/2$:

$$g_\mu^{(\mathrm{soft})*} = \tfrac{2}{3} + \tfrac{13}{27}\tilde{\epsilon}. \tag{84}$$

As for the hard continuation, unlike our result (83) for $g^{(\mathrm{soft})*}$, this result is not, strictly speaking, asymptotically valid in the limit of small $\tilde{\epsilon}$. This is because this value of $g_\mu^{(\mathrm{soft})*}$ does not become small for $\tilde{\epsilon} \ll 1$; hence, there is no formal justification for dropping terms higher order in $g_\mu^{(\mathrm{soft})}$ from the recursion relation for $g_\mu^{(\mathrm{soft})}$. However, again, this is not a problem, since

our results for all of the other η's (except η_μ) are exact to linear order in $\tilde{\epsilon} \ll 1$. We can therefore obtain quantitatively valid results for $\tilde{\epsilon} \ll 1$ for those other η's, and then use the exact scaling relation (85b), which we will derive below, to determine η_μ.

Again, the fact that both $g^{(\mathrm{soft})}$ and $g_\mu^{(\mathrm{soft})}$ flow to a nonzero stable fixed point for $d < 5/2$ implies a pair of exact relations between η's:

$$\left(\frac{5-2d}{3}\right) + \eta_Q - \left(\frac{d+5}{3}\right)\eta_\gamma + \left(\frac{d-1}{3}\right)\eta_\alpha = 0, \tag{85a}$$

$$\eta_\mu - \left(\frac{7-2d}{3}\right) - \left(\frac{d-2}{3}\right)\eta_\alpha + \left(\frac{d+1}{3}\right)\eta_\gamma - \eta_Q = 0. \tag{85b}$$

Inserting (83) into (80a)–(80d) yields

$$\eta_\alpha = 0, \tag{86a}$$

$$\eta_\gamma = \tfrac{4}{9}\tilde{\epsilon} + O(\tilde{\epsilon}^2), \tag{86b}$$

$$\eta_Q = \tfrac{4}{9}\tilde{\epsilon} + O(\tilde{\epsilon}^2), \tag{86c}$$

$$\eta_A = \tfrac{2}{3}\tilde{\epsilon} + O(\tilde{\epsilon}^2). \tag{86d}$$

Then inserting (86a), (86b), and (86c) into the exact relation (85b), we get

$$\eta_\mu = \tfrac{2}{3} + \tfrac{16}{27}\tilde{\epsilon} + O(\tilde{\epsilon}^2). \tag{87}$$

Using these values in Eqs. (55), (56), and (57) yields the $O(\tilde{\epsilon})$ values for the scaling exponents:

$$z = \tfrac{2}{3} - \tfrac{8}{27}\tilde{\epsilon} + O(\tilde{\epsilon}^2), \tag{88a}$$

$$\zeta = \tfrac{2}{3} + \tfrac{4}{27}\tilde{\epsilon} + O(\tilde{\epsilon}^2), \tag{88b}$$

$$\chi = -\tfrac{1}{3} + \tfrac{4}{27}\tilde{\epsilon} + O(\tilde{\epsilon}^2), \tag{88c}$$

$$\chi' = -\tfrac{1}{2} + \tfrac{1}{9}\tilde{\epsilon} + O(\tilde{\epsilon}^2). \tag{88d}$$

It is easy to check that the numerical values of these exponents in $d = 2$ to $O(\tilde{\epsilon} = \frac{1}{2})$ are very close to those obtained in the uncontrolled calculation and the hard continuation.

As in the other two schemes, we have ignored the graphical corrections induced by the annealed fluctuations. We will now show that these graphical corrections are also irrelevant in the soft-continuation scheme. In Appendix B, we show that these graphical corrections are controlled by the dimensionless coupling

$$g_A^{(\mathrm{soft})} \propto D_A \alpha^{\frac{(d-1)}{4}} \mu_x^{-\frac{(d+3)}{4}} \Lambda^{\frac{d-3}{2}}. \tag{89}$$

Using (89) and (79) we get the recursion relation for $g_A^{(\mathrm{soft})}$ at the fixed point controlled by the quenched fluctuations:

$$\frac{d \ln g_A^{(\mathrm{soft})}}{d\ell} = -\frac{2}{3} + \frac{14}{27}\tilde{\epsilon} + O(\tilde{\epsilon}^2). \tag{90}$$

This eigenvalue is $-\frac{11}{27}$ in $d = 2$ to $O(\tilde{\epsilon} = \frac{1}{2})$, which is less than 0, and thus again shows the irrelevance of graphical corrections coming from the annealed noises.

An equally weighted average of the values of the exponents obtained using the three schemes described above yields the values listed in (6).

V. SCALING BEHAVIOR

Now we utilize the DRG to calculate the real time–real space correlation functions $\langle \mathbf{u}(\mathbf{r}, t) \cdot \mathbf{u}(\mathbf{0}, 0)\rangle$. Let us first focus on the quenched part $C_Q(\mathbf{r}) \equiv \langle \mathbf{u}(\mathbf{r}, t) \cdot \mathbf{u}(\mathbf{0}, 0)\rangle_Q$ [see (28b)], which is purely static. Keeping track of the rescalings done on each step of the DRG enables us to relate the correlation functions in the renormalized theory to those in the original (unrenormalized) model. This relation, known as a "trajectory integral matching" formula, reads, for the real-space correlations [27],

$$C_Q(\alpha_0, \gamma_0, D_{Q,0}, \mathbf{r}) = e^{2\chi\ell} C_Q[\alpha(\ell), \gamma(\ell), D_Q(\ell), |x|e^{-\zeta\ell}, |y|e^{-\ell}]. \tag{91}$$

We have explicitly displayed the renormalized parameters α, γ, and D_Q because they are the parameters that determine $C_Q(\mathbf{r})$, as we saw in the linear theory. In (91) the subscript "0" denotes the bare values of the parameters. Note that $C_Q(\mathbf{r})$ only depends on the absolute values of x and y.

Let us now choose the exponents z, ζ, and χ, to be the values given by (55) and (56), which keep α, γ, and D_Q fixed, and also choose $\ell = \ln(\Lambda|y|)$. Equation (91) can then be rewritten as

$$C_Q(\alpha_0, \gamma_0, D_{Q0}, \mathbf{r}) = |y|^{2\chi} \mathcal{G}_Q\left(\frac{|x|}{|y|^\zeta}\right), \tag{92}$$

where

$$\mathcal{G}_Q\left(\frac{|x|}{|y|^\zeta}\right) \equiv \Lambda^{2\chi} C_Q\left[\alpha_0, \gamma_0, D_{Q0}, \frac{|x|}{(|y|\Lambda)^\zeta}, \frac{1}{\Lambda}\right]. \tag{93}$$

We have found the quenched part of the correlation function shown in (1). Now we turn to the annealed part of the correlations, for which there is a relation similar to (91):

$$C_A(\alpha_0, \mu_{x0}, D_{A0}, \mathbf{r}, t) = e^{2\chi\ell} C_A[\alpha(\ell), \mu_x(\ell), D_A(\ell), |x|e^{-\zeta\ell}, |y|e^{-\ell}, |t|e^{-z\ell}], \tag{94}$$

where $C_A(\mathbf{r}, t) \equiv \langle \mathbf{u}(\mathbf{r}, t) \cdot \mathbf{u}(\mathbf{0}, 0)\rangle_A$ [see (28a)], whose value is determined by α, μ, and D_A, as we saw in the linear theory.

Next we make the same choice of ζ, z, χ, and ℓ as we did in deriving the quenched part of the correlations. In addition to α, γ, and D_Q this choice also fixes μ_x due to the exact scaling relation (52b), or equivalently (68) or (85a). The three exact scaling relations become identical in $d = 2$.

On the other hand, with our choice of the rescaling exponents, $D_A(\ell)$ is *not* fixed. Instead, it is straightforward to show that, in all three of our approaches,

$$\frac{d \ln D_A}{d\ell} - \frac{d \ln D_Q}{d\ell} = \eta_A - \eta_Q - z. \tag{95}$$

With our choice of exponents, $\frac{d \ln D_Q}{d\ell} = 0$, so we have

$$\frac{d \ln D_A}{d\ell} = \eta_A - \eta_Q - z, \tag{96}$$

which we can immediately solve for the renormalized annealed noise strength $D_A(\ell)$:

$$D_A(\ell) = D_{A0} \exp[(\eta_A - \eta_Q - z)\ell]. \tag{97}$$

We can therefore rewrite (94) as

$$C_A(\alpha_0, \mu_{x0}, D_{A0}, \mathbf{r}, t) = e^{2\chi\ell} C_A[\alpha_0, \mu_{x0}, D_A(\ell), |x|e^{-\zeta\ell}, |y|e^{-\ell}, |t|e^{-z\ell}], \quad (98)$$

with $D_A(\ell)$ given by (97).

To proceed, we recall the result from the linear theory that C_A is proportional to D_A. The linear theory should be valid on the right-hand side of (98) if we choose ℓ so that the y argument of C_A on that side is of order a microscopic length (i.e., Λ^{-1}, where Λ is the ultraviolet cutoff). That is, we will choose

$$\ell = \ell^*(y) = \ln(\Lambda|y|) \quad (99)$$

again. Doing so, and using the fact that, with this choice of ℓ, the linear theory works, and making further use of the fact that, in the linear theory, the annealed correlation function is proportional to D_A, we have

$$C_A(\alpha_0, \mu_{x0}, D_{A0}, \mathbf{r}, t) = (|y|\Lambda)^{2\chi} D_A(\ell^*(y)) \Theta\left(\frac{|x|}{|y|^\zeta}, \frac{|t|}{|y|^z}\right), \quad (100)$$

where we have defined

$$\Theta\left(\frac{|x|}{|y|^\zeta}, \frac{|t|}{|y|^z}\right) \equiv \frac{C_A\left(\alpha_0, \mu_{x0}, D_A(\ell^*), \frac{|x|}{(|y|\Lambda)^\zeta}, \frac{1}{\Lambda}, \frac{|t|}{(|y|\Lambda)^z}\right)}{D_A(\ell_*)}. \quad (101)$$

Note that Θ is actually independent of $D_A(\ell^*)$, since we have canceled off its linear dependence on $D_A(\ell^*)$. Indeed, Θ depends only on the ratios $\frac{|x|}{|y|^\zeta}$ and $\frac{|t|}{|y|^z}$, since α_0, μ_{x0}, and Λ are constants.

Inserting our result (97) for $D_A(\ell)$ into (100), and evaluating it at $\ell^*(y)$, gives

$$C_A(\alpha_0, \mu_{x0}, D_{A0}, \mathbf{r}, t) = |y|^{2\chi'} \mathcal{G}_A\left(\frac{|x|}{|y|^\zeta}, \frac{|t|}{|y|^z}\right), \quad (102)$$

where

$$\mathcal{G}_A\left(\frac{|x|}{|y|^\zeta}, \frac{|t|}{|y|^z}\right) \equiv \Lambda^{2\chi'} D_{A0} \Theta\left(\frac{|x|}{|y|^\zeta}, \frac{|t|}{|y|^z}\right) \quad (103)$$

and

$$\chi' = \chi + \tfrac{1}{2}(\eta_A - \eta_Q - z). \quad (104)$$

Insert (55) and (56) into (104) and use the exact scaling relation (52a) to eliminate η_Q. This leads to

$$\chi' = \frac{\eta_A - \eta_\gamma - 1}{2}, \quad (105)$$

which is the value of χ' that we quoted in (57).

Alternatively, the correlations can be derived by performing the inverse Fourier transform of the correlation function obtained in the linear theory (24), albeit now with wavenumber-dependent coefficients due to the renormalization. The Fourier transformed correlations are also of interest in their own right. Again using trajectory matching, we have

$$\langle u_y(\tilde{\mathbf{q}}) u_y(\tilde{\mathbf{q}}')\rangle = e^{2(d-1+z+\zeta+\chi)\ell} \langle u'_y(e^\ell q_x, e^{\zeta\ell} q_y, e^{z\ell}\omega) u'_y \times (e^\ell q'_x, e^{\zeta\ell} q'_y, e^{z\ell}\omega')\rangle, \quad (106)$$

where $u_y(\tilde{\mathbf{q}})$ and $u'_y(e^\ell q_x, e^{\zeta\ell} q_y, e^{z\ell}\omega)$ represent the velocity field before and after rescaling, respectively.

Since the nonlinear corrections become more important as we go to longer wavelengths (i.e., smaller $\mathbf{q}$), it conversely follows that we can best approximate the right-hand side of (106) using the linear theory if we make $(e^\ell q_x, e^{\zeta\ell} q_y)$ on the right-hand side as large as possible. We will therefore choose ℓ so that this rescaled momentum lies near the Brillouin zone (BZ) boundary. This allows us to evaluate the correlation function on the right-hand side of Eq. (106) using the linear theory (24). To determine the value ℓ^* of ℓ that is sufficiently near the BZ boundary to allow this, we use the criterion

$$\gamma^2 |q_x|^6 + \alpha^2 |q_y|^4 = \alpha^2 \Lambda^4. \quad (107)$$

Our motivation for this choice is that it makes the denominator of the quenched part of the u_y-u_y correlation function given in Eq. (26d) as large as its smallest value on the BZ boundary. For the rescaled momentum to satisfy this condition, we must have

$$\gamma^2(\ell^*)(|q_x|e^{\zeta\ell^*})^6 + \alpha^2(\ell^*)(|q_y|e^{\ell^*})^4 = \alpha^2(\ell^*)\Lambda^4, \quad (108)$$

where the ℓ^* dependencies of $\alpha(\ell^*)$ and $\gamma(\ell^*)$ are obtained by solving the recursion relations (62a) and (62b), respectively. These are most easily solved by choosing the rescaling exponents z and ζ to keep γ and α fixed at their bare values. (This leads to the values of z and ζ quoted in (55).) Making this choice and dividing (108) by α^2 gives

$$a^2(|q_x|e^{\zeta\ell^*})^6 + (|q_y|e^{\ell^*})^4 = \Lambda^4, \quad (109)$$

where we have defined the microscopic length $a \equiv \frac{\gamma_0}{\alpha_0}$.

We will seek a scaling solution for e^{ℓ^*} of (109) of the form

$$e^{\ell^*} = \frac{\Lambda}{|q_y|} f_1\left(\frac{|q_x|/\Lambda'}{(|q_y|/\Lambda)^\zeta}\right), \quad (110)$$

where $\Lambda' \equiv \Lambda^{\frac{2}{3}} a^{-\frac{1}{3}}$, and ζ is given by (55).

Inserting this scaling ansatz (110) into our condition (109) gives

$$\left(\frac{a^2\Lambda^{6\zeta}|q_x|^6}{|q_y|^{6\zeta}}\right)\left[f_1\left(\frac{|q_x|/\Lambda'}{(|q_y|/\Lambda)^\zeta}\right)\right]^{6\zeta} + \Lambda^4\left[f_1\left(\frac{|q_x|/\Lambda'}{(|q_y|/\Lambda)^\zeta}\right)\right]^4 = \Lambda^4. \quad (111)$$

Dividing both sides of this expression by Λ^4 and reorganizing a bit yields

$$\left(\frac{a^2\Lambda^{6\zeta-4}|q_x|^6}{|q_y|^{6\zeta}}\right)\left[f_1\left(\frac{|q_x|/\Lambda'}{(|q_y|/\Lambda)^\zeta}\right)\right]^{6\zeta} + \left[f_1\left(\frac{|q_x|/\Lambda'}{(|q_y|/\Lambda)^\zeta}\right)\right]^4 = 1. \quad (112)$$

The coefficient of $[f_1(\frac{|q_x|/\Lambda'}{(|q_y|/\Lambda)^\zeta})]^{6\zeta}$ in this expression can be reexpressed as

$$\left(\frac{a^2\Lambda^{6\zeta-4}|q_x|^6}{|q_y|^{6\zeta}}\right) = \left(\frac{a^{1/3}\Lambda^{\zeta-2/3}|q_x|}{|q_y|^\zeta}\right)^6 = \left(\frac{a^{1/3}\Lambda^{-2/3}|q_x|}{(|q_y|/\Lambda)^\zeta}\right)^6 = \left(\frac{|q_x|/\Lambda'}{(|q_y|/\Lambda)^\zeta}\right)^6 = w^6, \tag{113}$$

where we have defined the argument of the scaling function f_1 in our ansatz (110) to be w; i.e.,

$$w \equiv \left(\frac{|q_x|/\Lambda'}{(|q_y|/\Lambda)^\zeta}\right). \tag{114}$$

Thus, our condition on the scaling function f_1 can be rewritten as

$$w^6[f_1(w)]^{6\zeta} + [f_1(w)]^4 = 1. \tag{115}$$

Since this condition only involves the scaling argument w, defined by (114), and the scaling function $f_1(w)$, which also only depends on w, it is clear that our ansatz has worked, and that the scaling function $f_1(w)$ is determined by the solution of (115). That solution is easily seen to have the following limiting behaviors:

$$f_1(x) = \begin{cases} 1, & x \ll 1, \\ x^{-\frac{1}{\zeta}}, & x \gg 1. \end{cases} \tag{116}$$

Inserting (110) into our expression (106) for the correlation function in Fourier space, and evaluating the correlation function on the right-hand side using the linear theory (23), we obtain the velocity correlation function in momentum space:

$$\begin{aligned}\langle u_y(\tilde{\mathbf{q}})u_y(\tilde{\mathbf{q}}')\rangle &= \left[\frac{2D_{A0}e^{\eta_A \ell^*}\delta(\omega+\omega')\delta(\mathbf{q}+\mathbf{q}')}{\left(\omega-\gamma_0 e^{\eta_\gamma \ell^*}q_x\right)^2 + \left(\frac{\alpha_0 e^{\eta_\alpha \ell^*}q_y^2}{q_x^2} + \mu_{x0}e^{\eta_\mu \ell^*}q_x^2\right)^2} + \frac{4\pi D_{Q0}e^{\eta_Q \ell^*}q_x^4\delta(\omega)\delta(\omega')\delta(\mathbf{q}+\mathbf{q}')}{(\alpha_0 e^{\eta_\alpha \ell^*})^2 q_y^4 + (\gamma_0 e^{\eta_\gamma \ell^*})^2 q_x^6}\right] \\ &= \left[\frac{2D_A(\mathbf{q})\delta(\omega+\omega')\delta(\mathbf{q}+\mathbf{q}')}{[\omega-\gamma(\mathbf{q})q_x]^2 + \left[\frac{\alpha(\mathbf{q})q_y^2}{q_x^2} + \mu_x(\mathbf{q})q_x^2\right]^2} + \frac{4\pi D_Q(\mathbf{q})q_x^4\delta(\omega)\delta(\omega')\delta(\mathbf{q}+\mathbf{q}')}{\alpha^2(\mathbf{q})q_y^4 + \gamma^2(\mathbf{q})q_x^6}\right],\end{aligned} \tag{117}$$

where

$$\gamma(\mathbf{q}) = \gamma_0|q_y|^{-\eta_\gamma} f_\gamma\left(\frac{|q_x|}{|q_y|^\zeta}\right), \tag{118a}$$

$$\alpha(\mathbf{q}) = \alpha_0|q_y|^{-\eta_\alpha} f_\alpha\left(\frac{|q_x|}{|q_y|^\zeta}\right), \tag{118b}$$

$$\mu_x(\mathbf{q}) = \mu_{x0}|q_y|^{-\eta_\mu} f_\mu\left(\frac{|q_x|}{|q_y|^\zeta}\right), \tag{118c}$$

$$D_{A,Q}(\mathbf{q}) = D_{A0,Q0}|q_y|^{-\eta_{A,Q}} f_{A,Q}\left(\frac{|q_x|}{|q_y|^\zeta}\right), \tag{118d}$$

and

$$f_{\gamma,\alpha,\mu,A,Q}\left(\frac{|q_x|}{|q_y|^\zeta}\right) \equiv \Lambda^{\eta_{\gamma,\alpha,\mu,A\cdot Q}}\left[f_1\left(\frac{|q_x|/\Lambda'}{(|q_y|/\Lambda)^\zeta}\right)\right]^{\eta_{\gamma,\alpha,\mu,A,Q}}. \tag{119}$$

The subscript "0" denotes the bare value of the coefficient.

We Fourier transform the momentum-space correlation function to obtain the real-space one. But first it is convenient to write $\langle u_y(\tilde{\mathbf{q}})u_y(\tilde{\mathbf{q}}')\rangle$ in a compact form:

$$\langle u_y(\tilde{\mathbf{q}})u_y(\tilde{\mathbf{q}}')\rangle = \left[|q_y|^{-(2z+\eta_A)}F_A\left(\frac{q_x}{|q_y|^\zeta}, \frac{\omega}{|q_y|^z}\right)\delta(\omega+\omega') + |q_y|^{-(4-4\zeta+\eta_Q-2\eta_\alpha)}F_Q\left(\frac{q_x}{|q_y|^\zeta}\right)\delta(\omega)\delta(\omega')\right]\delta(\mathbf{q}+\mathbf{q}'), \tag{120}$$

where

$$F_A\left(\frac{q_x}{|q_y|^\zeta}, \frac{\omega}{|q_y|^z}\right) \equiv \frac{2D_{A0}f_A\left(\frac{|q_x|}{|q_y|^\zeta}\right)}{\left[\frac{\omega}{|q_y|^z} - \gamma_0\frac{q_x}{|q_y|^\zeta}f_\gamma\left(\frac{|q_x|}{|q_y|^\zeta}\right)\right]^2 + \left[\frac{\alpha_0 f_\alpha\left(\frac{|q_x|}{|q_y|^\zeta}\right)}{(|q_x|/|q_y|^\zeta)^2} + \mu_{x0}\left(\frac{|q_x|}{|q_y|^\zeta}\right)^2 f_\mu\left(\frac{|q_x|}{|q_y|^\zeta}\right)\right]^2}, \tag{121a}$$

$$F_Q\left(\frac{|q_x|}{|q_y|^\zeta}\right) \equiv \frac{4\pi D_{Q0}\left(\frac{|q_x|}{|q_y|^\zeta}\right)^4 f_Q\left(\frac{|q_x|}{|q_y|^\zeta}\right)\delta(\mathbf{q}+\mathbf{q}')}{\left[\gamma_0\left(\frac{|q_x|}{|q_y|^\zeta}\right)^3 f_\gamma\left(\frac{|q_x|}{|q_y|^\zeta}\right)\right]^2 + \left[\alpha_0 f_\alpha\left(\frac{|q_x|}{|q_y|^\zeta}\right)\right]^2}. \tag{121b}$$

In deriving (120) we have used the exact relations (52).

We will next calculate the annealed part of the real-space correlation functions. Using the scaling form (120) we get

$$\langle u_y(\mathbf{r},t)u_y(\mathbf{0},0)\rangle_A = \int_{\omega,\omega',\mathbf{q},\mathbf{q}'} |q_y|^{-(2z+\eta_A)} F_A\left(\frac{q_x}{|q_y|^\zeta}, \frac{\omega}{|q_y|^z}\right)\delta(\omega+\omega')\delta(\mathbf{q}+\mathbf{q}')e^{-i(\omega t-\mathbf{q}\cdot\mathbf{r})}. \tag{122}$$

Changing variables of integration,

$$q_y = \frac{Q_y}{|y|}, \quad q_x = \frac{Q_x}{|y|^\zeta}, \quad \omega = \frac{\Omega}{|y|^z}, \tag{123}$$

we write (122) as

$$\langle u_y(\mathbf{r},t)u_y(\mathbf{0},0)\rangle_A = |y|^{2\chi'}\mathcal{G}_A\left(\frac{|x|}{|y|^\zeta}, \frac{|t|}{|y|^z}\right), \tag{124}$$

where

$$\chi' = \frac{1}{2}(z-\zeta+\eta_A-1), \tag{125}$$

$$\mathcal{G}_A\left(\frac{|x|}{|y|^\zeta}, \frac{|t|}{|y|^z}\right) \equiv \frac{1}{(2\pi)^{3/2}}\int_{\Omega,\mathbf{Q}} |Q_y|^{-(2z+\eta_A)} F_A\left(\frac{Q_x}{|Q_y|^\zeta}, \frac{\Omega}{|Q_y|^z}\right)e^{-i\left(\frac{t\Omega}{|y|^z}-\frac{xQ_x}{|y|^\zeta}-\frac{yQ_y}{|y|}\right)}, \tag{126}$$

and the values of ζ, z, and χ are again given by (55) and (56). Inserting (55) into (125) leads to (57) again.

The quenched part of the correlation is obtained in essentially the same way, and the result is

$$\langle u_y(\mathbf{r},t)u_y(\mathbf{0},0)\rangle_Q = |y|^{2\chi}\mathcal{G}_Q\left(\frac{|x|}{|y|^\zeta}\right), \tag{127}$$

$$\mathcal{G}_Q\left(\frac{|x|}{|y|^\zeta}\right) \equiv \frac{1}{2\pi}\int_{\mathbf{Q}} |Q_y|^{-(4-4\zeta+\eta_Q-2\eta_\alpha)} F_Q\left(\frac{|Q_x|}{|Q_y|^\zeta}\right)e^{i\left(\frac{yQ_y}{|y|}+\frac{xQ_x}{|y|^\zeta}\right)}, \tag{128}$$

where the values of ζ and χ are again given by (55) and (56). In deriving (127) we have used the exact relation (52b).

Here, we have focused exclusively on the u_y-u_y correlation. This is sufficient to calculate $\langle \mathbf{u}(\mathbf{r},t)\cdot\mathbf{u}(\mathbf{0},0)\rangle$, since the u_x correlations—related to the u_y-u_y correlation by the incompressibility constraint—are much smaller than the u_y-u_y correlations in the dominant regime of wave vector $q_x \sim |q_y|^\zeta \gg |q_y|$ and can therefore be ignored.

VI. EQUALIZATION OF THE EXPONENTS z AND ζ

As we discovered in Sec. III, the linear theory leads to two different dynamic exponents $z_{1,2}$, and two different anisotropy exponents $\zeta_{1,2}$ for the annealed fluctuations, as defined by the expression

$$\omega(\vec{q}) = |q_y|^{z_1} f_{\text{real}}\left(\frac{q_x}{|q_y|^{\zeta_1}}\right) - i|q_y|^{z_2} f_{\text{imaginary}}\left(\frac{|q_x|}{|q_y|^{\zeta_2}}\right). \tag{129}$$

Furthermore, the anisotropy exponent ζ_2 differs from that for the quenched fluctuations. However, the DRG analysis presented in Sec. IV identified a unique ζ and z. The reason for this is that once nonlinearities are taken into account, all three anisotropy exponents, and both z's, become equal. We will demonstrate this explicitly in this section and discuss how this equalization comes about as a function of dimensionality. This is analogous to the situation in smectics. The linear hydrodynamic theory of smectics-A predicts a "second sound" mode [28], which has the dispersion relation

$$\omega = \pm c_2(\phi)q - i\nu(\phi)q^2, \tag{130}$$

where ϕ is the angle between the wave vector and the layer normal, $c_2(\phi)$ is a direction-dependent sound speed, and $\nu(\phi)$ a direction-dependent viscosity. This has different z's for the real and the imaginary part: $z=1$ for the real part, and $z=2$ for the imaginary part.

However, in three dimensions, once nonlinearities are taken into account, one finds [29]

$$\omega = \pm c_2(\phi)q - i\nu_{\text{renorm}}(q,\phi)q^2, \tag{131}$$

with

$$\nu_{\text{renorm}}(q,\phi) = \frac{f(\phi)}{q}, \tag{132}$$

which, when inserted into (133), gives

$$\omega = \pm c_2(\phi)q - if(\phi)q, \tag{133}$$

which has the same value of z (namely, $z=1$) for both the real and the imaginary part.

How does the smectic go from having two z's that differ by an amount of $O(1)$ in high dimensions (where linear theory works), to equality in $d=3$? This is because ν becomes anomalous in a higher dimension than c_2; the critical dimension for ν is [29] $d_c^\nu = 5$, while the critical dimension for c_2 (which is proportional to $\sqrt{B}$, where B is the smectic layer compression modulus) is [30] $d_c^{c_2} = 3$. And it is between these two critical dimensions that z_2 continuously evolves from $z_2 = 2$ to $z_2 = 1$. In general spatial dimensions between $d=5$ and $d=3$,

$$\nu_{\text{renorm}}(q,\theta) \propto q^{(d-5)/2}, \tag{134}$$

which, when inserted into (133), gives

$$\mathrm{Im}(\omega) \propto q^{(d-1)/2}, \tag{135}$$

which implies

$$z_2 = \frac{d-1}{2}. \tag{136}$$

This interpolates continuously between the linear value $z_2 = 2$ and the $d = 3$ nonlinear value $z = 1$ as one lowers the dimension from 5 to 3.

We now show that an analogous variation of μ_x, which plays the role of viscosity in our model, in dimensions higher than the critical dimension of our model is responsible for the equalization of the exponents. However, unlike the smectic, the incompressible flock model we have described here is strictly only valid in two dimensions. Nevertheless, we formally analytically continue the model, as in Sec. IV, to higher dimension to understand how the multiple z and ζ linear scaling behavior reduces to one with a unique z and ζ once nonlinearities are accounted for. Of course, we can use either hard continuation or soft continuation for this examination. Here, we choose to use the former. The critical dimension of the incompressible flock with the hard continuation extension is 7/3. We first demonstrate that for $d < 7/3$, there is indeed a unique z and ζ and then show that this comes about because μ_x starts changing from its linear value for $d < 3$. An analogous argument can be constructed for soft continuation as well, where there is a unique z and ζ for $d < 5/2$ which comes about because μ_x starts changing from its linear value for $d < 7/2$, but we will not present it here.

A. Incompressible flocks in $d < 7/3$ (hard continuation)

We begin by recalling that the result of the DRG analysis is that all linearized expressions become valid for the nonlinear problem provided that we replace all of the constant phenomenological parameters γ, α, μ_x, and $D_{A,Q}$ with the wave-vector-dependent renormalized quantities $\gamma(\mathbf{q})$, $\alpha(\mathbf{q})$, $\mu_x(\mathbf{q})$, and $D_{A,Q}(\mathbf{q})$ given by Eqs. (118). Doing this with our expression (129) for the eigenfrequencies gives

$$\begin{aligned}\omega(\mathbf{q}) &= \gamma(\mathbf{q})q_x - i\left(\mu_x(\mathbf{q})q_x^2 + \alpha(\mathbf{q})\frac{|\mathbf{q}_h|^2}{q_x^2}\right)\\ &= \gamma_0|\mathbf{q}_h|^{-\eta_\gamma} f_\gamma\left(\frac{|q_x|}{|\mathbf{q}_h|^\zeta}\right)q_x - i\left\{\mu_{x0}|\mathbf{q}_h|^{-\eta_\mu} f_\mu\left(\frac{|q_x|}{|\mathbf{q}_h|^\zeta}\right)q_x^2 + \alpha_0|\mathbf{q}_h|^{-\eta_\alpha} f_\alpha\left(\frac{|q_x|}{|\mathbf{q}_h|^\zeta}\right)\frac{|\mathbf{q}_h|^2}{|q_x|^2}\right\},\end{aligned} \tag{137}$$

where we have extended the y direction to be $(d-1)$-dimensional and replaced q_y with $\mathbf{q}_h$. The real part of this can be written

$$\mathrm{Re}(\omega) = \gamma_0|\mathbf{q}_h|^{-\eta_\gamma} f_\gamma\left(\frac{|q_x|}{|\mathbf{q}_h|^\zeta}\right)q_x = \gamma_0|\mathbf{q}_h|^{z_1}\frac{q_x}{|\mathbf{q}_h|^{z_1+\eta_\gamma}} f_\gamma\left(\frac{|q_x|}{|\mathbf{q}_h|^\zeta}\right), \tag{138}$$

where the second equality is true for any value of z_1. However, if we choose z_1 such that

$$z_1 + \eta_\gamma = \zeta, \tag{139}$$

then the factor $\frac{q_x}{|\mathbf{q}_h|^{z_1+\eta_\gamma}} = \frac{q_x}{|\mathbf{q}_h|^\zeta}$, and the entire factor $\frac{q_x}{|\mathbf{q}_h|^{z_1+\eta_\gamma}} f_\gamma(\frac{|q_x|}{|\mathbf{q}_h|^\zeta}) = \frac{q_x}{|\mathbf{q}_h|^\zeta} f_\gamma(\frac{|q_x|}{|\mathbf{q}_h|^\zeta})$, which is obviously a function only of the scaling ratio $\frac{q_x}{|\mathbf{q}_h|^\zeta}$. Hence, we can define a new scaling function

$$f_{\mathrm{real}}(m) \equiv \gamma_0 m f_\gamma(m), \tag{140}$$

and rewrite Eq. (138) as

$$\mathrm{Re}(\omega) = |\mathbf{q}_h|^{z_1} f_{\mathrm{real}}\left(\frac{q_x}{|\mathbf{q}_h|^{\zeta_1}}\right), \tag{141}$$

with $\zeta_1 = \zeta$, provided that (139) is satisfied. Using our earlier expression (55) for ζ in terms of η_α and η_γ, and solving (139) for z_1, we find

$$z_1 = \zeta - \eta_\gamma = \frac{2 + \eta_\gamma - \eta_\alpha}{3} - \eta_\gamma = z, \tag{142}$$

where in the last equality we have used the result (55) for z found earlier.

Thus we have established that the real part of ω can be written in the form

$$\mathrm{Re}[\omega(\mathbf{q})] = |\mathbf{q}_h|^z f_{\mathrm{real}}\left(\frac{q_x}{|\mathbf{q}_h|^\zeta}\right) \tag{143}$$

with z and ζ the exponents we found in our DRG analysis of Sec. IV, whose values are given by (55).

We will now show that the imaginary part of ω can also be written in this scaling form, with its dynamic and anisotropy exponents z_2 and ζ_2, respectively, also being given by $z_2 = z$ and $\zeta_2 = \zeta$.

The proof is quite straightforward. The imaginary part of $\omega(\mathbf{q})$ can, by factoring out $|\mathbf{q}_h|^z$ and reorganizing (137) a bit, be rewritten as

$$\begin{aligned}\mathrm{Im}[\omega(\mathbf{q})] = -|\mathbf{q}_h|^z\Bigg\{&\mu_{x0}q_x^2|\mathbf{q}_h|^{-\eta_\mu - z} f_\mu\left(\frac{|q_x|}{|\mathbf{q}_h|^\zeta}\right)\\ &+\alpha_0\left(\frac{|\mathbf{q}_h|^{2-\eta_\alpha - z}}{q_x^2}\right) f_\alpha\left(\frac{|q_x|}{|\mathbf{q}_h|^\zeta}\right)\Bigg\}.\end{aligned} \tag{144}$$

Using the relation (55) between z, ζ, and $\eta_{\alpha,\gamma}$, and the exact scaling relation (69) between η_μ and $\eta_{\alpha,\gamma}$, we see that

$$\begin{aligned}\eta_\mu + z &= \left(\frac{2 + 4\eta_\gamma - \eta_\alpha}{3}\right) + \left(\frac{2 - 2\eta_\gamma - \eta_\alpha}{3}\right)\\ &= \frac{4 + 2\eta_\gamma - 2\eta_\alpha}{3} = 2\zeta,\end{aligned} \tag{145a}$$

$$2 - z - \eta_\alpha = 2 - \frac{2 - 2\eta_\gamma - \eta_\alpha}{3} - \eta_\alpha$$
$$= \frac{4 + 2\eta_\gamma - 2\eta_\alpha}{3} = 2\zeta. \tag{145b}$$

With these results in hand, we can rewrite (144) as

$$\mathrm{Im}[\omega(\mathbf{q})] = -|\mathbf{q}_h|^z \left\{ \left(\frac{q_x}{|\mathbf{q}_h|^\zeta} \right)^2 \mu_{x0} f_\mu \left(\frac{|q_x|}{|\mathbf{q}_h|^\zeta} \right) + \left(\frac{|\mathbf{q}_h|^\zeta}{q_x} \right)^2 \alpha_0 f_\alpha \left(\frac{|q_x|}{|\mathbf{q}_h|^\zeta} \right) \right\} \tag{146a}$$
$$= |\mathbf{q}_h|^z f_{\mathrm{Im}} \left(\frac{|q_x|}{|\mathbf{q}_h|^\zeta} \right), \tag{146b}$$

where we have defined

$$f_{\mathrm{Im}}(m) \equiv m^2 f_\mu(m) \mu_{x0} + m^{-2} f_\alpha(m) \alpha_0. \tag{147}$$

So there *is* only one z and ζ for this problem in the nonlinear theory, despite the fact that there are two ζ's and z's for the linear theory.

B. Incompressible flocks for $7/3 < d < 3$ (hard continuation)

The reader might reasonably wonder how we get from the linear result, with its different values of z and ζ for the real and imaginary parts of ω, to this result in the nonlinear theory of a single z and a single ζ for both parts. The answer is that, as we come down in dimension from $d = 3$ to $d = 7/3$, the exponents z_2 and ζ_2 for the imaginary part of ω evolve continuously from their linear values of $z_{2\mathrm{lin}} = 1$ and $\zeta_{2\mathrm{lin}} = 1/2$ to become equal to the values $z_{1\mathrm{lin}} = \zeta_{1\mathrm{lin}} = 2/3$ in $d = 7/3$. At this point, z_2 locks onto z_1, and ζ_2 locks onto ζ_1 as the dimension is lowered.

To see this, first note, as is clear from the recursion relation (70b) for $g_\mu^{(\mathrm{hard})}$, that μ_x becomes anomalous not in $d = 7/3$, as α and γ do, but, rather, in $d = 3$. For $7/3 < d < 3$, the nonlinear coupling $g^{(\mathrm{hard})}$ flows to zero, so the scaling relation (66), which was derived by assuming that $g^{(\mathrm{hard})}$ renormalized to a nonzero fixed point value, no longer holds. However, because μ_x grows upon renormalization if its bare value is small (again, as shown by the recursion relation (70b), its fixed point value must be nonzero. Hence, the exact scaling relation (68) does hold, even for $7/3 < d < 3$. Furthermore, because $g^{(\mathrm{hard})} \to 0$ upon renormalization for $7/3 < d < 3$, the exponents $\eta_{\alpha,\gamma,\varrho} = 0$ for $7/3 < d < 3$. Hence, the scaling relation (68) implies that

$$\eta_\mu = 3 - d \tag{148}$$

while $\eta_{\alpha,\gamma,\varrho} = 0$.

Hence we can write

$$\omega(\mathbf{q}) = \gamma_0 q_x - i \left(\mu_x(\mathbf{q}) q_x^2 + \alpha_0 \frac{|\mathbf{q}_h|^2}{q_x^2} \right) \tag{149}$$

with

$$\mu_x(\mathbf{q}) = \mu_{x0} |\mathbf{q}_h|^{d-3} f_\mu \left(\frac{|q_x|}{|\mathbf{q}_h|^{\zeta_2}} \right), \tag{150}$$

where the anisotropy exponent ζ_2 remains to be determined.

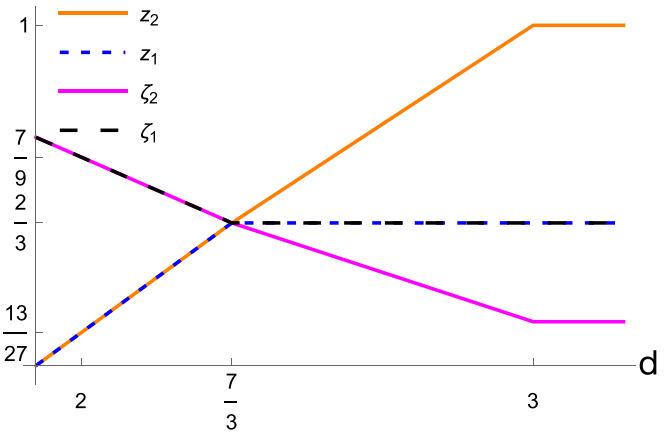


FIG. 2. Plot of the exponents $z_{1,2}$ and $\zeta_{1,2}$ versus dimension in the hard continuation to $O(\epsilon = \frac{7}{3} - d)$. The exponents z_2 and ζ_2 become anomalous (i.e., depart from the values $z_2 = 1$ and $\zeta_2 = 2/3$ below $d = 3$). The two z's and the two ζ's lock onto equality below $d = 7/3$. At $d = 7/3$, $z_{1,2} = \zeta_{1,2} = \frac{2}{3}$; at $d = 2$, $z_{1,2} = \frac{13}{27}$, $\zeta_{1,2} = \frac{7}{9}$. There are small slope discontinuities in $z_2(d)$ and $\zeta_2(d)$ at $d = 7/3$; the slope of z_2 changes from $1/2$ to $5/9$, while that of ζ_2 changes from $-1/4$ to $-1/3$. Both changes are so small as to be invisible to the naked eye, but are present in this plot.

We can do so by factoring $|\mathbf{q}_h|^{z_2}$ out of the imaginary part of ω in (149):

$$\mathrm{Im}[\omega(\mathbf{q})] = -|\mathbf{q}_h|^{z_2} \left[\mu_{x0} q_x^2 |\mathbf{q}_h|^{d-3-z_2} f_\mu \left(\frac{|q_x|}{|\mathbf{q}_h|^{\zeta_2}} \right) + \alpha_0 \frac{|\mathbf{q}_h|^{2-z_2}}{q_x^2} \right], \tag{151}$$

where z_2 also remains to be determined. We can do so by requiring that (151) take the form

$$\mathrm{Im}[\omega(\mathbf{q})] = |\mathbf{q}_h|^{z_2} f_{\mathrm{Im}} \left(\frac{|q_x|}{|\mathbf{q}_h|^{\zeta_2}} \right). \tag{152}$$

Comparing this with (151), we see that to make these two forms equal, we must have

$$d - 3 - z_2 = -2\zeta_2 \tag{153}$$

and

$$2 - z_2 = 2\zeta_2. \tag{154}$$

The simultaneous solution of these two equations is trivially found to be

$$\zeta_2 = \frac{5 - d}{4}, \quad z_2 = \frac{d - 1}{2}. \tag{155}$$

Note that, as d is decreased between 3 and $7/3$, this smoothly interpolates between the values in the linearized theory for the annealed anisotropy and dynamic exponents $\zeta_2 = \frac{1}{2}$ and $z_2 = 1$ in $d = 3$, and the values $\zeta_2 = z_2 = 2/3$ in $d = 7/3$. Once we go below $d = 7/3$, the analysis given earlier in this section applies, so the quenched and annealed anisotropy exponents remain locked together, and both evolve away from the value in the linearized theory, as described by the $7/3 - \epsilon$ expansion. The exponents $z_{1,2}$ and $\zeta_{1,2}$ are plotted as functions of dimension in Fig. 2.

VII. SUMMARY AND OUTLOOK

In this article, we have examined the effects of quenched disorder on the moving phase of an incompressible polar active fluid in 2D. We show that, surprisingly, the polarized phase retains long-range order in 2D even in the presence of quenched disorder. This is all the more surprising since the closest equilibrium analogs of our system, which are equilibrium magnets constrained to have a divergenceless magnetization, whose long-time, large-scale properties are exactly equivalent to incompressible flocks [21] in the presence of only annealed disorder, are much more susceptible to quenched disorder and do not form an ordered phase in 2D.

We have also characterized the hydrodynamic properties of the polarized phase, uncovering a novel universality class and calculating the exponents using three distinct DRG analyses. Since the values obtained from all three methods are very close to each other, we expect them to be quantitatively accurate. Our results should be readily testable in agent-based simulations. Further, since quenched disorder is inevitable in all experiments, our results may also be relevant for interpreting experiments on motile cell layers.

Looking ahead, our work suggests that novel physics may also emerge from the incompressibility constraint in active polar suspensions, which are a two-component (swimmers and solvent) system that is only incompressible as a whole.

ACKNOWLEDGMENTS

L.C. acknowledges support by the National Science Foundation of China (under Grant No. 11874420). J.T. thanks the Max Planck Institute for the Physics of Complex Systems, Dresden, Germany, for their support through a Martin Gutzwiller Fellowship during this period. L.C. also thanks the MPI-PKS, where the early stage of this work was performed, for their support. A.M. was supported by a TALENT fellowship awarded by the CY Cergy Paris Université.

APPENDIX A: CALCULATING THE GRAPHICAL CORRECTIONS TO THE VARIOUS COEFFICIENTS

In this Appendix, we explicitly calculate the corrections to the various coefficients in the EOM for u_y upon averaging over the short-distance fluctuations.

The hydrodynamic EOM, retaining only relevant terms, that we will analyze using DRG is the following:

$$\partial_t u_y(\mathbf{q}) = P_{yx}(\mathbf{q})\mathcal{F}_{\mathbf{q}}\left[-\alpha\left(u_x + \frac{u_y^2}{2}\right)\right] + \mathcal{F}_{\mathbf{q}}\left[-\gamma\,\partial_x u_y + \mu_x\partial_x^2 u_y - \alpha\left(u_x + \frac{u_y^2}{2}\right)u_y + f_A^y + f_Q^y\right], \tag{A1}$$

which can be rewritten as

$$u_y(\tilde{\mathbf{q}}) = G(\tilde{\mathbf{q}})\left[f_A^y(\tilde{\mathbf{q}}) + f_Q^y(\tilde{\mathbf{q}}) + \left(\frac{\alpha}{2}\right)P_{yx}(\mathbf{q})\int_{\tilde{\mathbf{k}}} u_y(\tilde{\mathbf{k}})u_y(\tilde{\mathbf{q}}-\tilde{\mathbf{k}}) - \alpha\int_{\tilde{\mathbf{k}}} u_y(\tilde{\mathbf{k}})u_x(\tilde{\mathbf{q}}-\tilde{\mathbf{k}}) - \left(\frac{\alpha}{2}\right)\int_{\tilde{\mathbf{k}},\tilde{\mathbf{k}}'} u_y(\tilde{\mathbf{k}})u_y(\tilde{\mathbf{k}}')u_y(\tilde{\mathbf{q}}-\tilde{\mathbf{k}}-\tilde{\mathbf{k}}')\right] \tag{A2}$$

with the bare propagator

$$G(\tilde{\mathbf{q}}) = \left[-i(\omega-\gamma q_x) + \left(\alpha\frac{q_y^2}{q^2} + \mu_x q_x^2\right)\right]^{-1} = \frac{i(\omega-\gamma q_x) + \left(\alpha\frac{q_y^2}{q^2} + \mu_x q_x^2\right)}{(\omega-\gamma q_x)^2 + \left(\alpha\frac{q_y^2}{q^2} + \mu_x q_x^2\right)^2}. \tag{A3}$$

We remind the reader that the bare correlation functions (i.e., those of the linear theory) are given by

$$\langle u_i(\tilde{\mathbf{q}})u_j(\tilde{\mathbf{q}}')\rangle = C_A^{ij}(\tilde{\mathbf{q}})\delta(\omega+\omega')\delta(\mathbf{q}+\mathbf{q}') + C_Q^{ij}(\tilde{\mathbf{q}})\delta(\omega)\delta(\omega')\delta(\mathbf{q}+\mathbf{q}'), \tag{A4}$$

where

$$C_A^{xx}(\tilde{\mathbf{q}}) = \frac{q_y^2}{q^2}C_A(\tilde{\mathbf{q}}), \tag{A5a}$$

$$C_A^{xy}(\tilde{\mathbf{q}}) = -\frac{q_x q_y}{q^2}C_A(\tilde{\mathbf{q}}) = C_A^{yx}(\tilde{\mathbf{q}}), \tag{A5b}$$

$$C_A^{yy}(\tilde{\mathbf{q}}) = \frac{q_x^2}{q^2}C_A(\tilde{\mathbf{q}}), \tag{A5c}$$

$$C_Q^{xx}(\tilde{\mathbf{q}}) = \frac{q_y^2}{q^2}C_Q(\tilde{\mathbf{q}}), \tag{A5d}$$

$$C_Q^{xy}(\tilde{\mathbf{q}}) = -\frac{q_x q_y}{q^2}C_Q(\tilde{\mathbf{q}}) = C_Q^{yx}(\tilde{\mathbf{q}}), \tag{A5e}$$

$$C_Q^{yy}(\tilde{\mathbf{q}}) = \frac{q_x^2}{q^2}C_Q(\tilde{\mathbf{q}}), \tag{A5f}$$

with

$$C_Q(\tilde{\mathbf{q}}) = \frac{4\pi D_Q q_x^4}{\gamma^2 q_x^6 + \alpha^2 q_y^4}, \qquad C_A(\tilde{\mathbf{q}}) = \frac{2D_A}{(\omega-\gamma q_x)^2 + \left(\alpha\frac{q_y^2}{q^2} + \mu_x q_x^2\right)^2}. \tag{A6}$$

Here the subscripts A and Q denote the contributions from the annealed and quenched noises, respectively.

Note that we can think of (A2) as a closed equation for $u_y(\tilde{\mathbf{q}})$ with $u_x(\tilde{\mathbf{q}})$ simply a shorthand notation for $-\frac{q_y}{q_x}u_y(\tilde{\mathbf{q}})$, which follows from the incompressibility condition.

As usual (see, e.g., [24,25]), our formal solution (A2) can be represented by Feynman graphs, as illustrated in Fig. 3. The

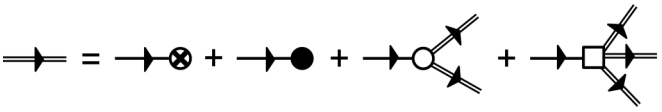


FIG. 3. Feynman diagram representation of the formal solution (A2) of (A1). The circle with an interior cross represents the quenched noise, while the solid circle represents the annealed noise. The meaning of the various other elements in this figure are given in Fig. 4.

definition of the various pictorial elements in this diagram are given in Fig. 4.

The most useful way to derive the DRG recursion relations for the various parameters is to divide EOM (A2) by $G(\tilde{\mathbf{q}})$, which gives

$$G^{-1}(\tilde{\mathbf{q}})u_y(\tilde{\mathbf{q}}) = \Big[f_A^y(\tilde{\mathbf{q}}) + f_Q^y(\tilde{\mathbf{q}}) + \Big(\frac{\alpha}{2}\Big)P_{yx}(\mathbf{q}) \times \int_{\tilde{\mathbf{k}}} u_y(\tilde{\mathbf{k}})u_y(\tilde{\mathbf{q}}-\tilde{\mathbf{k}}) - \alpha\int_{\tilde{\mathbf{k}}} u_y(\tilde{\mathbf{k}})u_x(\tilde{\mathbf{q}}-\tilde{\mathbf{k}}) - \Big(\frac{\alpha}{2}\Big)\int_{\tilde{\mathbf{k}},\tilde{\mathbf{k}}'} u_y(\tilde{\mathbf{k}})u_y(\tilde{\mathbf{k}}')u_y(\tilde{\mathbf{q}}-\tilde{\mathbf{k}}-\tilde{\mathbf{k}}')\Big]. \tag{A7}$$

Graphically, this amounts to "amputating" the leftmost leg of each of the Feynman diagrams in Fig. 3, which gives Fig. 5.

Now we decompose $u_y(\tilde{\mathbf{q}})$ into "slow" components $u_y^<(\tilde{\mathbf{q}})$ and "fast" components $u_y^>(\tilde{\mathbf{q}})$, where $u_y^<(\tilde{\mathbf{q}})$ is supported in the wave vector space $|q_x| < \infty$, $|q_y| < \Lambda e^{-d\ell}$, and $u_y^>(\tilde{\mathbf{q}})$ in the "momentum shell" $|q_x| < \infty$, $\Lambda e^{-d\ell} < |q_y| < \Lambda$, where Λ is the ultraviolet cutoff, and $d\ell \ll 1$ is an arbitrary rescaling factor. We likewise decompose the noises $f_{A,Q}^y$ into fast and slow components $f_{A,Q}^{y>}$ and $f_{A,Q}^{y<}$, respectively.

The Feynman graphs are useful for the next step, which is to solve (A2) perturbatively for $u_y^>(\tilde{\mathbf{q}})$ in terms of $u_y^<(\tilde{\mathbf{q}})$ and the noises $f_{A,Q}^{y>}$. This perturbative solution can be represented by the graphs shown in Fig. 6.

We next substitute this solution into the EOM (A7) for $u_y^<(\tilde{\mathbf{q}})$, that is, the EOM represented in Fig. 5, with the field on the left-hand side taken to be $u_y^<(\tilde{\mathbf{q}})$. This leads to the series of graphs shown in Fig. 7.

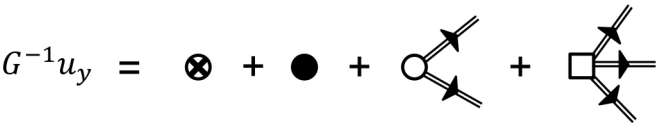


FIG. 5. Feynman diagram representation of the EOM (A7). This amounts to "amputating" the leftmost leg of each of the Feynman diagrams in Fig. 3.

Once this is done, one can see at once that the graphs like Figs. 7(c), 7(d), and 7(e), for which the incoming momentum $\mathbf{q}$ on the left is in the long-wavelength (small $\mathbf{q}$) interior with every line ending in a short-wavelength noise $f_{A,Q}^{y>}(\tilde{\mathbf{q}})$, can be thought of as an extra contribution to the long-wavelength noises $f_{A,Q}^{y<}(\tilde{\mathbf{q}})$. Their correlations, therefore, are renormalizations of the noise correlations, represented by the Feynman graphs shown in Figs. 8 and 9.

Next, we must average over the short-wavelength noises $f_{A,Q}^{y<}(\tilde{\mathbf{q}})$. Since the averages of two noises are only nonzero if their wave vectors and frequencies are equal and opposite, we represent this averaging by connecting lines that end in noises. The result is components of the graphs shown in Figs. 4(d) and 4(e), which simply represent the correlation functions.

Performing this connection for the graphs in Fig. 7 yields the graphs in Fig. 10.

Note that these graphs are *linear* in the slow fields $u_y^<(\tilde{\mathbf{q}})$, as can be seen by the fact that they have precisely one external line coming off to the right. The terms they represent can therefore be pulled over to the left-hand side of the equation schematically represented by Fig. 7, and absorbed into renormalizations of the inverse propagator $G^{-1}(\tilde{\mathbf{q}})$. From the form of $G^{-1}(\tilde{\mathbf{q}})$, we see that the part of such correction terms proportional to $iq_xu_y(\tilde{\mathbf{q}})$ can be absorbed into renormalizations of the linear coefficient γ. Likewise, terms proportional to $(\frac{q_y}{q_x})^2u_y(\tilde{\mathbf{q}})$ renormalize α, and those proportional to $q_x^2u_y(\tilde{\mathbf{q}})$ renormalize μ_x. This is how we will obtain the graphical corrections to those parameters.

This averaging process also generates graphs which are quadratic and cubic in the slow fields $u_y^<(\tilde{\mathbf{q}})$. This leads to the renormalization of the coefficients of the quadratic and cubic terms. However, as argued in the main text, these coefficients are locked to the coefficient α of the linear term $(\frac{q_y}{q_x})^2u_y(\tilde{\mathbf{q}})$, or equivalently, $(\frac{q_y}{q_x})u_x(\tilde{\mathbf{q}})$. This is because the EOM is

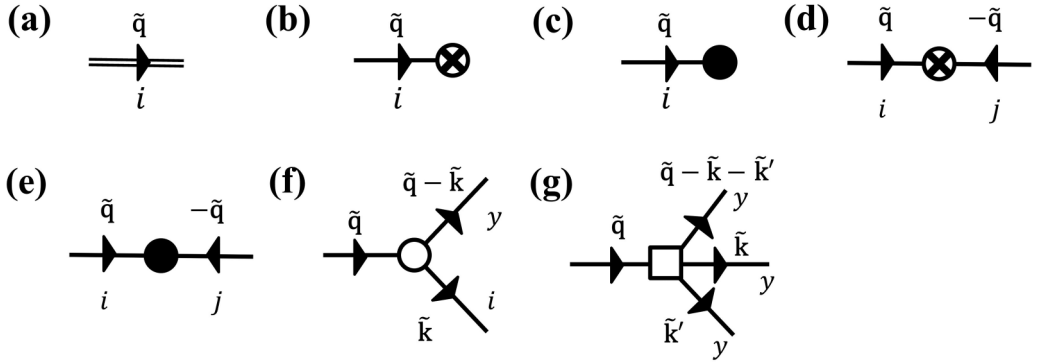


FIG. 4. Definitions of the elements in the Feynman diagrams: (a) $= u_i(\tilde{\mathbf{q}})$, (b) $= \frac{q_y(1-2\delta_{ix})}{q_i}G(\tilde{\mathbf{q}})f_Q^i(\tilde{\mathbf{q}})$, (c) $= \frac{q_y(1-2\delta_{ix})}{q_i}G(\tilde{\mathbf{q}})f_A^i(\tilde{\mathbf{q}})$, (d) $= C_Q^{ij}(\tilde{\mathbf{q}})\delta(\omega)$, (e) $= C_A^{ij}(\tilde{\mathbf{q}})$, (f) the circle $= -\alpha(1-\frac{1}{2}\delta_{yi})[\delta_{xi}+P_{yx}(\mathbf{q})\delta_{yi}]$, (g) the square $= -\alpha/2$.

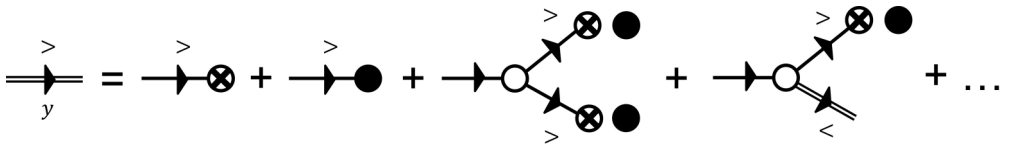


FIG. 6. A diagrammatic expansion of the "fast" component of $u_y(\tilde{\mathbf{q}})$ after partitioning $u_y(\tilde{\mathbf{q}})$ into "slow" components $u_y^<(\tilde{\mathbf{q}})$ and "fast" components $u_y^>(\tilde{\mathbf{q}})$.

rotation-invariant, and this symmetry must be preserved under the DRG transformation. In particular, this means the graphical corrections to these coefficients are all equal to each other. Therefore, in this problem we only need to consider the (one-loop) graphs renormalizing the linear terms and the noise, which does not involve the cubic vertex (i.e., the square-shaped knot) at all.

Unusually, in this problem we find that there is one additional correction, which we have not yet described, that affects the renormalization of all the parameters. This arises from the fact that the inverse propagator $G^{-1}(\tilde{\mathbf{q}})$ also gets a contribution from the graphs proportional to $-i\omega$. That is, on the right-hand side of Fig. 7, we also get contributions proportional to $-i\omega u_y$. As a result, our final expression for the renormalized EOM for the slow modes $u_y^<(\tilde{\mathbf{q}})$ in Fourier space takes the form

$$\Big(-i\omega(1+\eta_\omega d\ell) - i\gamma\big(1+\eta_\gamma^{\rm direct} d\ell\big)q_x + \alpha\big(1+\eta_\alpha^{\rm direct} d\ell\big)\frac{q_y^2}{q^2} + \mu_x\big(1+\eta_\mu^{\rm direct} d\ell\big)q_x^2\Big)u_y^<(\tilde{\mathbf{q}}) = f_Q^{yR} + f_A^{yR} + \mathrm{NL}\{u_y^<(\tilde{\mathbf{q}})\}, \tag{A8}$$

where $\gamma\eta_\gamma^{\rm direct} d\ell$, $\alpha\eta_\alpha^{\rm direct} d\ell$, and $\mu_x\eta_\mu^{\rm direct} d\ell$ represent the "direct" corrections to γ, α, and μ_x calculated as described above, and $-i\omega\eta_\omega d\ell$ likewise represents the correction to the inverse propagator proportional to $-i\omega$ described above. The renormalized noises $f_{Q,A}^{yR}$ are calculated as described above.

The expression $\mathrm{NL}\{u_y^<(\tilde{\mathbf{q}})\}$ represents the terms nonlinear in the slow fields $u_y^<(\tilde{\mathbf{q}})$; as in the original EOM, these will couple $u_y^<(\tilde{\mathbf{q}})$ to the $u_y^<(\tilde{\mathbf{k}})$'s at all $\tilde{\mathbf{k}}$ in the (slightly smaller) Brillouin zone.

The coefficient of $-i\omega$ in the original EOM was 1. To make our renormalized EOM look as much like the original as possible, and to avoid having to introduce yet another parameter into our EOM (namely, a coefficient of the $-i\omega$ term that is not unity, but a free parameter that can also renormalize), we simply divide the EOM (A8) by the factor $1+\eta_\omega d\ell$, which gives, in the limit $d\ell \ll 1$ in which we are working,

$$\Big(-i\omega - i\gamma(1+\eta_\gamma d\ell)q_x + \alpha(1+\eta_\alpha d\ell)\frac{q_y^2}{q^2} + \mu_x(1+\eta_\mu d\ell)q_x^2\Big)u_y^<(\tilde{\mathbf{q}}) = \big(f_Q^{yR} + f_A^{yR} + \mathrm{NL}\{u_y^<(\tilde{\mathbf{q}})\}\big)(1-\eta_\omega d\ell), \tag{A9}$$

with

$$\eta_\gamma = \eta_\gamma^{\rm direct} - \eta_\omega, \quad \eta_\alpha = \eta_\alpha^{\rm direct} - \eta_\omega, \quad \eta_\mu = \eta_\mu^{\rm direct} - \eta_\omega. \tag{A10}$$

The η_γ, η_α, and η_μ defined above are those quoted in the main text, which give the graphical corrections to the renormalizations of γ, α, and μ_x. Indeed, defining the renormalized values γ^R, α^R, and μ_x^R to be the coefficients of the appropriate terms in the renormalized EOM (A9), we have

$$\gamma^R = \gamma(1+\eta_\gamma d\ell), \quad \alpha^R = \alpha(1+\eta_\alpha d\ell), \quad \mu_x^R = \mu_x(1+\eta_\mu d\ell). \tag{A11}$$

Combining these graphical corrections with the effect of the rescalings leads to the recursion relations presented in the main text.

Defining the effective fully renormalized noises $f_{Q,A}^{yF}$ on the right-hand side of this equation via

$$f_{Q,A}^{yF} \equiv f_{Q,A}^{yR}(1-\eta_\omega d\ell), \tag{A12}$$

we see that these acquire an extra factor of $(1+\eta_\omega d\ell)$ in addition to their corrections coming from the graphs in Figs. 8 and 9. Hence, their *correlations* pick up (for small $d\ell$) an extra

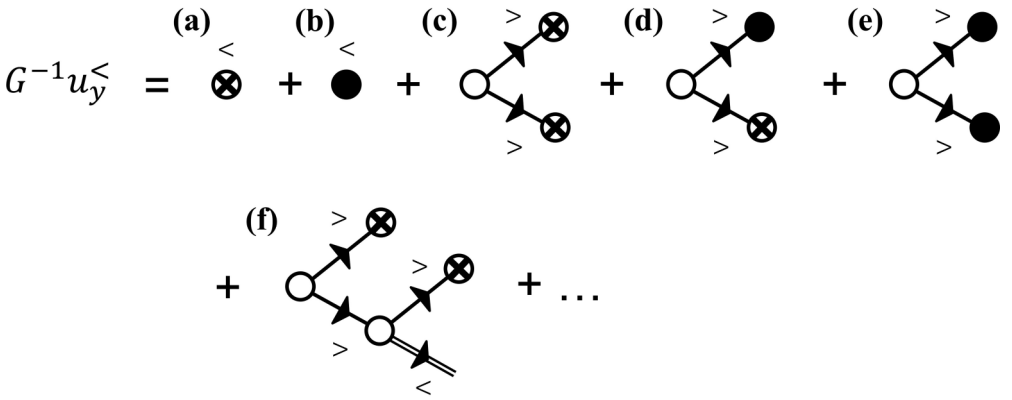


FIG. 7. A diagrammatic expansion of $G^{-1}(\tilde{\mathbf{q}})u_y^<(\tilde{\mathbf{q}})$ after partitioning $u_y(\tilde{\mathbf{q}})$ into "slow" components $u_y^<(\tilde{\mathbf{q}})$ and "fast" components $u_y^>(\tilde{\mathbf{q}})$.

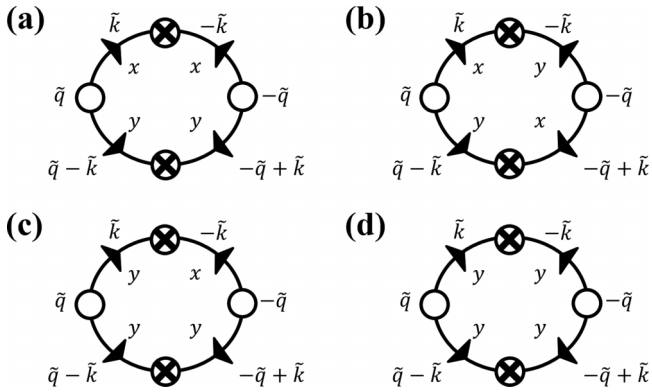


FIG. 8. The graphical representations of the correction to D_Q.

factor of $(1-2\eta_\omega d\ell)$ (note the "2"), in addition to the direct graphical correction from Figs. 8 and 9, whose calculation we described above. That is,

$$\left\langle f_Q^{yF}(\mathbf{r}) f_Q^{yF}(\mathbf{r}')\right\rangle = 2D_Q^R \delta^2(\mathbf{r}-\mathbf{r}'), \tag{A13a}$$

$$\left\langle f_A^{yF}(\mathbf{r},t) f_A^{yF}(\mathbf{r}',t')\right\rangle = 2D_A^R \delta^2(\mathbf{r}-\mathbf{r}')\delta(t-t'), \tag{A13b}$$

where the renormalized noise strengths are given by

$$D_Q^R = \left(1+\left(\eta_Q^{\text{direct}} - 2\eta_\omega\right)d\ell\right)D_Q \equiv (1+\eta_Q d\ell)D_Q, \tag{A14a}$$

$$D_A^R = \left(1+\left(\eta_A^{\text{direct}} - 2\eta_\omega\right)d\ell\right)D_A \equiv (1+\eta_A d\ell)D_A, \tag{A14b}$$

where we have defined

$$\eta_Q \equiv \eta_Q^{\text{direct}} - 2\eta_\omega, \quad \eta_A \equiv \eta_A^{\text{direct}} - 2\eta_\omega. \tag{A15}$$

These $\eta_{Q,A}$ are those used in the main text.

Having set up the logic of our approach to the perturbative portion of the DRG, all that remains is to actually do the hard work of evaluating the graphs. We will do so now.

1. Quenched noise (D_Q) renormalization

The graphs in Fig. 8 renormalize the correlations of the quenched noise f_Q^y. For graphs (a) and (b) we set the wave vector $\mathbf{q}$ inside the loop integral to zero to keep only the relevant contributions to the noise correlations. These two graphs thus give identical results, and the sum of them gives a contribution to the correlations of the quenched noise:

$$\begin{aligned}&\delta\left[\left\langle f_Q^y(\mathbf{q},\omega) f_Q^y(-\mathbf{q},-\omega)\right\rangle\right]\\ &= 2\alpha^2 \int_> \frac{d^2k}{(2\pi)^2}\frac{d\Omega}{2\pi}\frac{k_y^2}{k_x^2} C_Q(\tilde{\mathbf{k}}) C_Q(-\tilde{\mathbf{k}})\delta(\Omega)\delta(\omega-\Omega)\\ &= 16\pi\alpha^2 D_Q^2 \int_> \frac{d^2k}{(2\pi)^2}\frac{k_x^6 k_y^2}{\left(\gamma^2 k_x^6 + \alpha^2 k_y^4\right)^2}\\ &= 16\pi\alpha^2 D_Q^2 \delta(\omega) I_1,\end{aligned} \tag{A16}$$

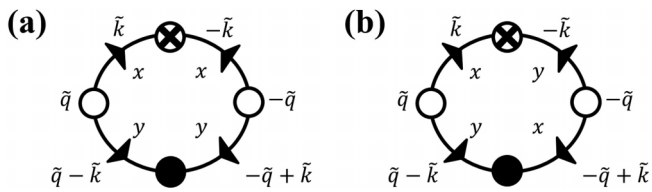


FIG. 9. Two particular graphical corrections to D_A. They correspond to the graphs (a) and (b) in Fig. 8 but with one of the quenched noise averages replaced by the annealed noise average.

where we have defined the integral

$$I_1 \equiv \int_> \frac{d^2k}{(2\pi)^2}\frac{k_y^2 k_x^6}{\left(\gamma^2 k_x^6 + \alpha^2 k_y^4\right)^2}, \tag{A17}$$

which is calculated in Appendix C 1.

Since $\langle f_Q^y(\mathbf{q},\omega) f_Q^y(-\mathbf{q},-\omega)\rangle = 4\pi D_Q \delta(\omega)$, (A16) implies a correction to the quenched noise strength D_Q:

$$\delta D_Q = 4\alpha^2 D_Q^2 I_1. \tag{A18}$$

Graph (c) has a prefactor of $q_x^3 q_y/q^4$ and graph (d) has a prefactor of $q_x^2 q_y^2/q^4$. Since in the dominant wave vector regime $q_y \ll q_x$, these prefactors $\ll 1$ and therefore, these graphs contribute corrections that are subdominant to the one in (A18).

Inserting the values of I_1 in (A18) for the three different perturbation schemes, we get

$$\text{uncontrolled } d=2: \quad \delta D_Q^{\frac{1}{2}} d\ell = \tfrac{2}{9} g^{(\text{unc})} D_Q d\ell, \tag{A19a}$$

$$\text{hard continuation:} \quad \delta D_Q = \tfrac{2}{9} g^{(\text{hard})} D_Q d\ell, \tag{A19b}$$

$$\text{soft continuation:} \quad \delta D_Q = \tfrac{1}{3} g^{(\text{soft})} D_Q d\ell, \tag{A19c}$$

where $g^{(\text{unc})} = \frac{D_Q}{\pi}|\gamma|^{-\frac{7}{3}}\alpha^{\frac{1}{3}}\Lambda^{-\frac{1}{3}}$, $g^{(\text{hard})} = \frac{S_{d-1}}{(2\pi)^{d-1}}|\gamma|^{-\frac{7}{3}}\alpha^{\frac{1}{3}}\Lambda^{\frac{3d-7}{3}} D_Q$, and $g^{(\text{soft})} = \frac{S_{d-1} D_Q}{\sqrt{2}(2\pi)^{d-1}}|\gamma|^{-(\frac{d+5}{3})}\alpha^{(\frac{d-1}{3})}\Lambda^{(\frac{2d-5}{3})}$ as defined in the main text.

The results (A19a), (A19b), and (A19c) imply a contribution to the exponent η_Q, which we call η_Q^{direct} [see (A14b) for its definition]:

$$\text{uncontrolled } d=2: \quad \eta_Q^{\text{direct}} = \tfrac{2}{9} g^{(\text{unc})}, \tag{A20a}$$

$$\text{hard continuation:} \quad \eta_Q^{\text{direct}} = \tfrac{2}{9} g^{(\text{hard})}, \tag{A20b}$$

$$\text{soft continuation:} \quad \eta_Q^{\text{direct}} = \tfrac{1}{3} g^{(\text{soft})}. \tag{A20c}$$

2. Annealed noise (D_A) renormalization

Like the correction to D_Q, the graphical corrections to D_A consist of the first two diagrams in Fig. 8, albeit with one of the quenched noise averages in each (indicated by a crossed circle) replaced by the annealed noise average (indicated by a black circle). Hence there are four diagrams in total, two of which are shown in Fig. 9; the other two are simple permutations of these.

Again setting $\mathbf{q}$ to zero inside the loop integrals, the contributions of all four diagrams are identical. The sum of them gives a contribution to the correlations of the annealed

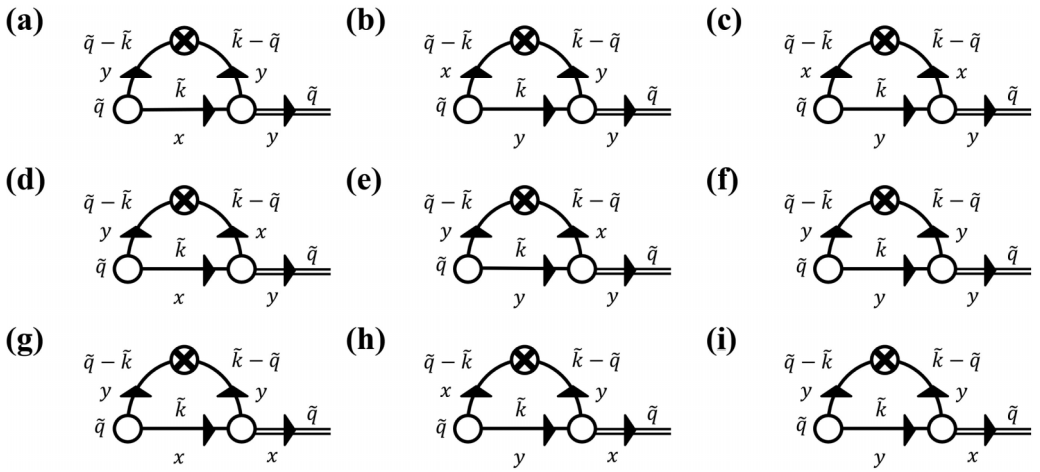


FIG. 10. The graphical representations of potential corrections to $G^{-1}(\tilde{\mathbf{q}})u_y(\tilde{\mathbf{q}})$.

noise:

$$\begin{aligned}
&\delta\left[\left\langle f_A^y(\mathbf{q},\omega)f_A^y(-\mathbf{q},-\omega)\right\rangle\right] \\
&= 4\alpha^2\int_> \frac{d^2k}{(2\pi)^2}\left(\frac{k_y}{k_x}\right)^2\left[\frac{2D_A}{\gamma^2k_x^2+\left(\alpha\frac{k_y^2}{k^2}+\mu_x k_x^2\right)^2}\right] \\
&\quad\times\left(\frac{2D_Q k_x^4}{\gamma^2k_x^6+\alpha^2k_y^4}\right) \\
&\approx 16\alpha^2 D_Q D_A\int_> \frac{d^2k}{(2\pi)^2}\,\frac{k_x^6k_y^2}{\left(\gamma^2k_x^6+\alpha^2k_y^4\right)^2} \\
&= 16\alpha^2 D_Q D_A I_1. \qquad \text{(A21)}
\end{aligned}$$

Since $\langle f_A^y(\mathbf{q},\omega)f_A^y(-\mathbf{q},-\omega)\rangle_A = 2D_A$, (A21) implies a correction to the annealed noise strength D_A:

$$\delta D_A = 8\alpha^2 D_Q D_A I_1. \qquad \text{(A22)}$$

Again, using the values of I_1 for the various schemes yields

$$\text{uncontrolled } d=2:\ \delta D_A = \tfrac{4}{9}g^{(\mathrm{unc})}D_A d\ell, \qquad \text{(A23a)}$$

$$\text{hard continuation:}\ \delta D_A = \tfrac{4}{9}g^{(\mathrm{hard})}D_A d\ell, \qquad \text{(A23b)}$$

$$\text{soft continuation:}\ \delta D_A = \tfrac{2}{3}g^{(\mathrm{soft})}D_A d\ell. \qquad \text{(A23c)}$$

These imply

$$\text{uncontrolled } d=2:\ \eta_A^{\mathrm{direct}} = \tfrac{4}{9}g^{(\mathrm{unc})}, \qquad \text{(A24a)}$$

$$\text{hard continuation:}\ \eta_A^{\mathrm{direct}} = \tfrac{4}{9}g^{(\mathrm{hard})}, \qquad \text{(A24b)}$$

$$\text{soft continuation:}\ \eta_A^{\mathrm{direct}} = \tfrac{2}{3}g^{(\mathrm{soft})}. \qquad \text{(A24c)}$$

3. Renormalization of γ

To look for renormalizations of γ, we seek graphs in Fig. 10 which have the prefactor iq_x and one outgoing $u_y(\tilde{\mathbf{q}})$ leg. Since graphs (e) and (f) both have q_y in the prefactor, and (g) to (i) all have outgoing leg $u_x(\tilde{\mathbf{q}})$, none of them can contribute to the renormalization of γ. This leaves us with graphs (a) to (d) in Fig. 10 to analyze.

Graph (a) represents a contribution to the right-hand side of the EOM (A7):

$$\begin{aligned}
&2\times(-\alpha)\times\left(-\frac{\alpha}{2}\right)u_y(\tilde{\mathbf{q}})\int_>\frac{d^2k}{(2\pi)^2}\frac{d\Omega}{2\pi}\left(-\frac{k_y}{k_x}\right)G(\tilde{\mathbf{k}})P_{yx}(\mathbf{k})C_Q(\mathbf{q}-\mathbf{k})\delta(\omega-\Omega) \\
&= \alpha^2 u_y(\tilde{\mathbf{q}})\int_>\frac{d^2k}{(2\pi)^2}\left[\frac{1}{-i(\omega-\gamma k_x)+\alpha\frac{k_y^2}{k^2}}\right]\left[\frac{2D_Q(q_x-k_x)^4}{\gamma^2(q_x-k_x)^6+\alpha^2(q_y-k_y)^4}\right]\left(\frac{k_y}{k_x}\right)^2. \qquad \text{(A25)}
\end{aligned}$$

Graph (b) represents a contribution to the right-hand side of the EOM (A7):

$$\begin{aligned}
&2\times(-\alpha)\times\left(-\frac{\alpha}{2}\right)u_y(\tilde{\mathbf{q}})\int_>\frac{d^2k}{(2\pi)^2}\frac{d\Omega}{2\pi}\left(-\frac{q_y-k_y}{q_x-k_x}\right)G(\tilde{\mathbf{k}})P_{yx}(\mathbf{k})C_Q(\mathbf{q}-\mathbf{k})\delta(\omega-\Omega) \\
&= \alpha^2 u_y(\tilde{\mathbf{q}})\int_>\frac{d^2k}{(2\pi)^2}\left[\frac{1}{-i(\omega-\gamma k_x)+\alpha\frac{k_y^2}{k^2}}\right]\left[\frac{2D_Q(q_x-k_x)^4}{\gamma^2(q_x-k_x)^6+\alpha^2(q_y-k_y)^4}\right]\left(\frac{k_y}{k_x}\right)\left(\frac{q_y-k_y}{q_x-k_x}\right). \qquad \text{(A26)}
\end{aligned}$$

Graph (c) represents a contribution to the right-hand side of the EOM (A7):

$$2\times(-\alpha)\times\left(-\frac{\alpha}{2}\right)u_y(\tilde{\mathbf{q}})\int_>\frac{d^2k}{(2\pi)^2}\frac{d\Omega}{2\pi}\left(\frac{q_y-k_y}{q_x-k_x}\right)^2 G(\tilde{\mathbf{k}})C_Q(\mathbf{q}-\mathbf{k})\delta(\omega-\Omega)$$

$$=\alpha^2u_y(\tilde{\mathbf{q}})\int_>\frac{d^2k}{(2\pi)^2}\left[\frac{1}{-i(\omega-\gamma k_x)+\alpha\frac{k_y^2}{k^2}}\right]\left[\frac{2D_Q(q_x-k_x)^4}{\gamma^2(q_x-k_x)^6+\alpha^2(q_y-k_y)^4}\right]\left(\frac{q_y-k_y}{q_x-k_x}\right)^2. \tag{A27}$$

Graph (d) represents a contribution to the right-hand side of the EOM (A7):

$$2\times(-\alpha)\times\left(-\frac{\alpha}{2}\right)u_y(\tilde{\mathbf{q}})\int_>\frac{d^2k}{(2\pi)^2}\frac{d\Omega}{2\pi}\left(-\frac{k_y-q_y}{k_x-q_x}\right)G(\tilde{\mathbf{k}})\left(-\frac{k_y}{k_x}\right)C_Q(\mathbf{q}-\mathbf{k})\delta(\omega-\Omega)$$

$$=\alpha^2u_y(\tilde{\mathbf{q}})\int_>\frac{d^2k}{(2\pi)^2}\left[\frac{1}{-i(\omega-\gamma k_x)+\alpha\frac{k_y^2}{k^2}}\right]\left[\frac{2D_Q(q_x-k_x)^4}{\gamma^2(q_x-k_x)^6+\alpha^2(q_y-k_y)^4}\right]\left(\frac{k_y}{k_x}\right)\left(\frac{q_y-k_y}{q_x-k_x}\right), \tag{A28}$$

which is the same as that of graph (b).

The integrands in the above formulas are functions of ω and q and thus can be expanded in powers of ω and $\mathbf{q}$. It is easy to check that the zeroth order terms do not vanish. In fact, they lead to a contribution proportional to u_y without any derivatives, which appears to be more relevant than all other existing linear terms in (A7). However, the generation of this new term comes from the renormalization of the mean velocity. It can be canceled off if u_x is boosted by a constant, which corresponds to the correction to the mean velocity. In what follows, we will ignore this trivial correction, and focus on the contributions linear in ω and q. Contributions higher order in $\mathbf{q}$ and ω lead only to irrelevant contributions, and will therefore also be dropped.

We will deal with the linear order piece in ω in the next section, which in fact leads a general renormalization of the temporal derivative of u_y in (A7). Here, we will focus on the linear order piece in q by expanding the integrands to linear order in q while setting ω to 0.

Specifically, the linear order piece in q_x of (A25) is

$$iq_xu_y(\tilde{\mathbf{q}})\left[8\gamma\alpha^2D_Q\int_>\frac{d^2k}{(2\pi)^2}\frac{k_y^2k_x^6}{\left(\gamma^2k_x^6+\alpha^2k_y^4\right)^2}-12\gamma^3\alpha^2D_Q\int_>\frac{d^2k}{(2\pi)^2}\frac{k_y^2k_x^{12}}{\left(\gamma^2k_x^6+\alpha^2k_y^4\right)^3}\right]$$

$$=iq_xu_y(\tilde{\mathbf{q}})(8\gamma\alpha^2D_QI_1-12\gamma^3\alpha^2D_QI_2), \tag{A29}$$

where I_2 is calculated in Appendix (C 2).

The linear order piece in q_x of (A26) is

$$iq_xu_y(\tilde{\mathbf{q}})\left[6\gamma\alpha^2D_Q\int_>\frac{d^2k}{(2\pi)^2}\frac{k_y^2k_x^6}{\left(\gamma^2k_x^6+\alpha^2k_y^4\right)^2}-12\gamma^3\alpha^2D_Q\int_>\frac{d^2k}{(2\pi)^2}\frac{k_y^2k_x^{12}}{\left(\gamma^2k_x^6+\alpha^2k_y^4\right)^3}\right]$$

$$=iq_xu_y(\tilde{\mathbf{q}})(6\gamma\alpha^2D_QI_1-12\gamma^3\alpha^2D_QI_2). \tag{A30}$$

The linear order piece in q_x of (A27) is

$$iq_xu_y(\tilde{\mathbf{q}})\left[4\gamma\alpha^2D_Q\int_>\frac{d^2k}{(2\pi)^2}\frac{k_y^2k_x^6}{\left(\gamma^2k_x^6+\alpha^2k_y^4\right)^2}-12\gamma^3\alpha^2D_Q\int_>\frac{d^2k}{(2\pi)^2}\frac{k_y^2k_x^{12}}{\left(\gamma^2k_x^6+\alpha^2k_y^4\right)^3}\right]$$

$$=iq_xu_y(\tilde{\mathbf{q}})(4\gamma\alpha^2D_QI_1-12\gamma^3\alpha^2D_QI_2). \tag{A31}$$

The linear order piece in q_x of (A28) is the same as that of (A26).

In summary, the sum of contributions linear both in q_x and $u_y(\tilde{\mathbf{q}})$ to the right-hand side of (A7) is

$$iq_xu_y(\tilde{\mathbf{q}})(24\gamma\alpha^2D_QI_1-48\gamma^3\alpha^2D_QI_2). \tag{A32}$$

Pulling this piece to the left-hand side of (A7), we find the following correction to γ:

$$\delta\gamma=-24\gamma\alpha^2D_QI_1+48\gamma^3\alpha^2D_QI_2. \tag{A33}$$

Inserting the values of I_1 and I_2 for the various schemes, we obtain

$$\text{uncontrolled } d=2:\ \delta\gamma=\tfrac{2}{9}g^{(\mathrm{unc})}\gamma d\ell, \tag{A34a}$$

$$\text{hard continuation:}\ \delta\gamma=\tfrac{2}{9}g^{(\mathrm{hard})}\gamma d\ell, \tag{A34b}$$

$$\text{soft continuation:}\ \delta\gamma=\tfrac{1}{2}g^{(\mathrm{soft})}\gamma d\ell. \tag{A34c}$$

Again, this implies

$$\text{uncontrolled } d=2:\ \eta_\gamma^{\mathrm{direct}}=\tfrac{2}{9}g^{(\mathrm{unc})}, \tag{A35a}$$

$$\text{hard continuation:}\quad \eta_\gamma^{\text{direct}} = \tfrac{2}{9} g^{(\text{hard})}, \tag{A35b}$$

$$\text{soft continuation:}\quad \eta_\gamma^{\text{direct}} = \tfrac{1}{2} g^{(\text{soft})}. \tag{A35c}$$

4. Renormalization of the temporal derivative

Here we seek one-loop contributions to $-i\omega u_y(\tilde{\mathbf{q}})$, which amounts to finding graphs in Fig. 10 which have a prefactor $i\omega$ and one outgoing $u_y(\tilde{\mathbf{q}})$ leg. Since graphs (e) to (i) either have q_y in the prefactor or have an outgoing $u_x(\mathbf{q})$ leg, none of them can generate contributions to $-i\omega u_y(\tilde{\mathbf{q}})$. Therefore, only graphs (a) to (d) can. The contribution of these graphs to the right-hand side of (A7) has been given in Appendix (A 3). To find the linear order piece in ω, we expand the integrands in (A25)–(A28) to linear order in ω and set $q = 0$. Once this is done, all four graphs become equal. The sum of them gives the following contribution to the right-hand side of (A7):

$$\begin{aligned}
&4\alpha^2 i\omega u_y(\tilde{\mathbf{q}}) \int_> \frac{d^2k}{(2\pi)^2} \left[\frac{k^4}{\left(i\gamma k_x^3 + \alpha k_y^2\right)^2}\right]\left(\frac{2D_\varrho k_x^4}{\gamma^2 k_x^6 + \alpha^2 k_y^4}\right)\left(\frac{k_y}{k_x}\right)^2 \\
&= 4\alpha^2 i\omega u_y(\tilde{\mathbf{q}}) \int_> \frac{d^2k}{(2\pi)^2} \frac{2D_\varrho k_x^2 k_y^2 k^4 \left(\alpha k_y^2 - i\gamma k_x^3\right)^2}{\left(\gamma^2 k_x^6 + \alpha^2 k_y^4\right)^3} \\
&= 4\alpha^2 i\omega P_{yy}(\mathbf{q}) u_y(\tilde{\mathbf{q}}) \int_> \frac{d^2k}{(2\pi)^2} \frac{2D_\varrho k_x^2 k_y^2 k^4 \left(\alpha^2 k_y^4 - \gamma^2 k_x^6\right)}{\left(\gamma^2 k_x^6 + \alpha^2 k_y^4\right)^3} \\
&\approx 8D_\varrho \alpha^2 i\omega u_y(\tilde{\mathbf{q}}) \left[\alpha^2 \int_> \frac{d^2k}{(2\pi)^2} \frac{k_x^6 k_y^6}{\left(\gamma^2 k_x^6 + \alpha^2 k_y^4\right)^3} - \gamma^2 \int_> \frac{d^2k}{(2\pi)^2} \frac{k_x^{12} k_y^2}{\left(\gamma^2 k_x^6 + \alpha^2 k_y^4\right)^3}\right] \\
&= 8D_\varrho \alpha^2 i\omega u_y(\tilde{\mathbf{q}})(\alpha^2 I_3 - \gamma^2 I_2),
\end{aligned} \tag{A36}$$

where $I_{2,3}$ are calculated in Appendices (C 2) and (C 3), respectively.

Pulling this piece to the left-hand side of (A7) and inserting the values of $I_{2,3}$ for the various schemes, we get the following contribution to $-i\omega u_y(\tilde{\mathbf{q}})$:

$$\text{uncontrolled } d = 2:\quad \delta[-i\omega u_y(\tilde{\mathbf{q}})] = -\tfrac{2}{27} g^{(\text{unc})} d\ell [-i\omega u_y(\tilde{\mathbf{q}})], \tag{A37a}$$

$$\text{hard continuation:}\quad \delta[-i\omega u_y(\tilde{\mathbf{q}})] = -\tfrac{2}{27} g^{(\text{hard})} d\ell [-i\omega u_y(\tilde{\mathbf{q}})], \tag{A37b}$$

$$\text{soft continuation:}\quad \delta[-i\omega u_y(\tilde{\mathbf{q}})] = -\tfrac{1}{6} g^{(\text{soft})} d\ell [-i\omega u_y(\tilde{\mathbf{q}})]. \tag{A37c}$$

This implies

$$\text{uncontrolled } d = 2:\quad \eta_\omega = -\tfrac{2}{27} g^{(\text{unc})}, \tag{A38a}$$

$$\text{hard continuation:}\quad \eta_\omega = -\tfrac{2}{27} g^{(\text{hard})}, \tag{A38b}$$

$$\text{soft continuation:}\quad \eta_\omega = -\tfrac{1}{6} g^{(\text{soft})}. \tag{A38c}$$

5. Renormalization of α

Here we seek one-loop contributions to $\frac{q_y^2}{q^2} u_y(\tilde{\mathbf{q}})$ or $\frac{q_x q_y}{q^2} u_x(\tilde{\mathbf{q}})$, where the latter is equivalent to the former by the incompressibility condition $u_x(\tilde{\mathbf{q}}) = -\frac{q_y}{q_x} u_y(\tilde{\mathbf{q}})$. Therefore, we look for graphs in Fig. 10 which either have the prefactor $\frac{q_y^2}{q^2}$ with an outgoing leg $u_y(\tilde{\mathbf{q}})$ or have the prefactor $\frac{q_x q_y}{q^2}$ with the outgoing leg $u_x(\tilde{\mathbf{q}})$.

Graphs (a) to (d), (g), and (h) have neither the prefactor $\frac{q_x q_y}{q^2}$ nor q_y^2/q^2, and graphs (e) and (f) do have the prefactor $q_x q_y/q^2$ but with the outgoing leg $u_y(\tilde{\mathbf{q}})$. Hence these graphs cannot renormalize α. The only contributing graph is therefore graph (i), which has exactly the prefactor $q_x q_y/q^2$ and the outgoing leg $u_x(\tilde{\mathbf{q}})$. This graph gives the following contribution to the right-hand side of (A7):

$$\begin{aligned}
&2 \times \left(-\frac{\alpha}{2}\right) \times (-\alpha) P_{yx}(\tilde{\mathbf{q}}) u_x(\tilde{\mathbf{q}}) \\
&\quad \times \int_> \frac{d^2k}{(2\pi)^2} \frac{d\Omega}{2\pi} G(\tilde{\mathbf{k}}) C_\varrho(\mathbf{q} - \mathbf{k}) \delta(\omega - \Omega) \\
&= \alpha^2 \frac{q_y^2}{q^2} u_y(\tilde{\mathbf{q}}) \int_> \frac{d^2k}{(2\pi)^2} \frac{d\Omega}{2\pi} \left[\frac{1}{-i(\omega - \gamma k_x) + \alpha \frac{k_y^2}{k^2}}\right] \\
&\quad \times \left[\frac{4\pi D_\varrho (q_x - k_x)^4 \delta(\omega - \Omega)}{\gamma^2 (q_x - k_x)^6 + \alpha^2 (q_y - k_y)^4}\right] \\
&= \alpha^2 \frac{q_y^2}{q^2} u_y(\tilde{\mathbf{q}}) \int_> \frac{d^2k}{(2\pi)^2} \left[\frac{1}{-i(\omega - \gamma k_x) + \alpha \frac{k_y^2}{k^2}}\right] \\
&\quad \times \left[\frac{2D_\varrho (q_x - k_x)^4}{\gamma^2 (q_x - k_x)^6 + \alpha^2 (q_y - k_y)^4}\right],
\end{aligned} \tag{A39}$$

where in the first equality we have used the incompressibility condition $u_x(\tilde{\mathbf{q}}) = -\frac{q_y}{q_x} u_y(\tilde{\mathbf{q}})$. To keep only the relevant contributions we set $\omega = 0$, $q = 0$ in the integrand, which leads to

$$\begin{aligned}
&\alpha^2 \frac{q_y^2}{q^2} u_y(\tilde{\mathbf{q}}) \int_> \frac{d^2k}{(2\pi)^2} \frac{2D_\varrho k^2 k_x^4}{\left(i\gamma k_x^3 + \alpha k_y^2\right)\left(\gamma^2 k_x^6 + \alpha^2 k_y^4\right)} \\
&= 2\alpha^2 D_\varrho \frac{q_y^2}{q^2} u_y(\tilde{\mathbf{q}}) \int_> \frac{d^2k}{(2\pi)^2} \frac{\left(-i\gamma k_x^3 + \alpha k_y^2\right) k^2 k_x^4}{\left(\gamma^2 k_x^6 + \alpha^2 k_y^4\right)^2}
\end{aligned}$$

$$= 2\alpha^3 D_Q \frac{q_y^2}{q^2} u_y(\tilde{\mathbf{q}}) \int_> \frac{d^2k}{(2\pi)^2} \frac{k^2 k_y^2 k_x^4}{\left(\gamma^2 k_x^6 + \alpha^2 k_y^4\right)^2}$$

$$\approx 2\alpha^3 D_Q \frac{q_y^2}{q^2} u_y(\tilde{\mathbf{q}}) \int_> \frac{d^2k}{(2\pi)^2} \frac{k_y^2 k_x^6}{\left(\gamma^2 k_x^6 + \alpha^2 k_y^4\right)^2}$$

$$= 2\alpha^3 D_Q I_1 \frac{q_y^2}{q^2} u_y(\tilde{\mathbf{q}}), \tag{A40}$$

where in the second equality we have neglected the imaginary part since it vanishes after the integration, and in the "$\approx$" we have only kept the dominant part (that is, the "k_x^2" component of "k^2").

Pulling this to the left-hand side of (A7) and using the explicit value for I_1 for the various schemes, we get the following correction to α:

$$\text{uncontrolled } d = 2: \ \delta\alpha = -\tfrac{1}{9} g^{(\text{unc})} \alpha d\ell, \tag{A41a}$$

$$\text{hard continuation: } \delta\alpha = -\tfrac{1}{9} g^{(\text{hard})} \alpha d\ell, \tag{A41b}$$

$$\text{soft continuation: } \delta\alpha = -\tfrac{1}{6} g^{(\text{soft})} \alpha d\ell. \tag{A41c}$$

This implies

$$\text{uncontrolled } d = 2: \ \eta_\alpha^{\text{direct}} = -\tfrac{1}{9} g^{(\text{unc})}, \tag{A42a}$$

$$\text{hard continuation: } \eta_\alpha^{\text{direct}} = -\tfrac{1}{9} g^{(\text{hard})}, \tag{A42b}$$

$$\text{soft continuation: } \eta_\alpha^{\text{direct}} = -\tfrac{1}{6} g^{(\text{soft})}. \tag{A42c}$$

6. Renormalization of μ_x

The one-loop graphical correction to μ_x can also be derived from the graphs in Fig. 10. However, our purpose here is not to get the exact result. We only need to know the dependence of η_μ^{direct} on γ, α, and D_Q, because that is sufficient for us to derive an exact relation between $\eta_{\mu,\gamma,\alpha,Q}$ at the DRG fixed point, which allows us to determine η_μ through $\eta_{\gamma,\alpha,Q}$. Therefore, for this purpose we only need to analyze one of the first four graphs in Fig. 10, for instance, graph (a). This graph represents a contribution to the right-hand side of (A7) given by (A25). Now we seek a term proportional to $q_x^2 u_y(\tilde{\mathbf{q}})$. It is the easiest that we expand the denominator of the integrand to $O(q_x^2)$ and set $\omega = 0$ and $\mathbf{q} = \mathbf{0}$ in the numerator. Doing this and focusing on the q_x^2 piece we get

$$\alpha^2 q_x^2 u_y(\tilde{\mathbf{q}}) \int_> \frac{d^2k}{(2\pi)^2} \left(\frac{k^2}{i\gamma k_x^3 + \alpha k_y^2}\right)\left(\frac{12 D_Q k_x^2}{\gamma^2 k_x^6 + \alpha^2 k_y^4}\right)\left(\frac{k_y}{k_x}\right)^2. \tag{A43}$$

By rationalizing the numerator, the imaginary part of (A43) will vanish during the integration since it is odd in k_x. So we are left with

$$\alpha^2 q_x^2 u_y(\tilde{\mathbf{q}}) \int_> \frac{d^2k}{(2\pi)^2} \frac{12\alpha D_Q k^2 k_y^4}{\left(\gamma^2 k_x^6 + \alpha^2 k_y^4\right)^2} \approx 12\alpha^3 D_Q q_x^2 u_y(\tilde{\mathbf{q}}) I_4, \tag{A44}$$

where

$$I_4 \equiv \int_> \frac{d^2k}{(2\pi)^2} \frac{k_x^2 k_y^4}{\left(\gamma^2 k_x^6 + \alpha^2 k_y^4\right)^2}, \tag{A45}$$

and in the "$\approx$" we have kept only the most diverging piece by approximating k^2 as k_x^2. The quantity I_4 is calculated in Appendix (C 4). Inserting the value of I_4 for the various schemes into (A44), we get

$$\text{uncontrolled } d = 2: \ \left(\frac{D_Q}{\pi|\gamma|}\Lambda^{-1} d\ell\right) q_x^2 u_y(\tilde{\mathbf{q}}), \tag{A46a}$$

$$\text{hard continuation: } \left[\frac{S_{d-1}}{(2\pi)^{d-1}} \frac{D_Q}{|\gamma|} \Lambda^{d-3} d\ell\right] q_x^2 u_y(\tilde{\mathbf{q}}), \tag{A46b}$$

$$\text{soft continuation: } \left[\frac{5\pi}{3\sin\left(\frac{5\pi}{12}\right)} \frac{S_{d-1}}{(2\pi)^d} D_Q \alpha^{\frac{d-2}{3}} |\gamma|^{-\frac{d+1}{3}} d\ell\right] \times q_x^2 u_y(\tilde{\mathbf{q}}). \tag{A46c}$$

Based on the result from graph (a), we conclude that the total one-loop graphical contributions to μ_x can be written as

$$\text{uncontrolled } d = 2: \ \delta\mu_x = \left(g_\mu^{(\text{unc})} d\ell\right)\mu_x, \tag{A47a}$$

$$\text{hard continuation: } \delta\mu_x = \left(g_\mu^{(\text{hard})} d\ell\right)\mu_x, \tag{A47b}$$

$$\text{soft continuation: } \delta\mu_x = \left(g_\mu^{(\text{soft})} d\ell\right)\mu_x, \tag{A47c}$$

where

$$g_\mu^{(\text{unc})} \propto D_Q |\gamma|^{-1} \mu_x^{-1} \Lambda^{-1}, \tag{A48a}$$

$$g_\mu^{(\text{hard})} \propto |\gamma|^{-1} \mu_x^{-1} D_Q \Lambda^{d-3}, \tag{A48b}$$

$$g_\mu^{(\text{soft})} \propto D_Q \mu_x^{-1} \alpha^{\frac{d-2}{3}} |\gamma|^{-\frac{d+1}{3}} \Lambda^{\frac{2d-7}{3}}. \tag{A48c}$$

This implies

$$\text{uncontrolled } d = 2: \ \eta_\mu^{\text{direct}} = g_\mu^{(\text{unc})}, \tag{A49a}$$

$$\text{hard continuation: } \eta_\mu^{\text{direct}} = g_\mu^{(\text{hard})}, \tag{A49b}$$

$$\text{soft continuation: } \eta_\mu^{\text{direct}} = g_\mu^{(\text{soft})}. \tag{A49c}$$

7. Putting it all together

Inserting (A20), (A24), (A35), (A38), (A42), (A49) into (A10) and (A15), we obtain $\eta_{\gamma,\alpha,\mu,Q,A}$ to one-loop order for the three schemes, as quoted in the main text. Specifically, for the uncontrolled calculation in $d = 2$,

$$\eta_\gamma = \tfrac{8}{27} g^{(\text{unc})}, \eta_\alpha = -\tfrac{1}{27} g^{(\text{unc})}, \eta_\mu = g_\mu^{(\text{unc})} + \tfrac{2}{27} g^{(\text{unc})},$$
$$\eta_Q = \tfrac{10}{27} g^{(\text{unc})}, \eta_A = \tfrac{16}{27} g^{(\text{unc})}; \tag{A50}$$

for the hard continuation,

$$\eta_\gamma = \tfrac{8}{27} g^{(\text{hard})}, \eta_\alpha = -\tfrac{1}{27} g^{(\text{hard})}, \eta_\mu = g_\mu^{(\text{hard})} + \tfrac{2}{27} g^{(\text{hard})},$$
$$\eta_Q = \tfrac{10}{27} g^{(\text{hard})}, \eta_A = \tfrac{16}{27} g^{(\text{hard})}; \tag{A51}$$

for the soft continuation,

$$\eta_\gamma = \tfrac{2}{3} g^{(\text{soft})}, \eta_\alpha = 0, \eta_\mu = g_\mu^{(\text{soft})} + \tfrac{1}{6} g^{(\text{soft})},$$
$$\eta_Q = \tfrac{2}{3} g^{(\text{soft})}, \eta_A = g^{(\text{soft})}. \tag{A52}$$

APPENDIX B: DERIVATION OF THE ANNEALED COUPLINGS

In this section we derive the dimensionless coupling g_A associated with the renormalization coming purely from the

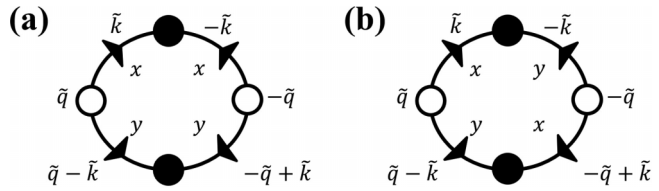


FIG. 11. Two particular graphical corrections to D_A purely from the annealed fluctuations. They correspond to the graphs (a) and (b) in Fig. 8 but with both the quenched noise averages replaced by the annealed noise averages.

annealed fluctuations. We do this by calculating the purely D_A-dependent contributions to any of the one-loop graphical corrections to D_A, α, and μ_x (all of these give the same expression for g_A). Here we choose to calculate the one-loop graphical correction to D_A. The Feynman diagrams for this calculation are given in Fig. 11, which are essentially the same as those in Fig. 8, albeit with both the quenched noise averages (indicated by crossed circles) replaced by the annealed noise averages (indicated by black circles). Setting $\tilde{\mathbf{q}} = \tilde{0}$ inside the loops, the sum of two graphs represents the following contribution to the correlations of the annealed noise:

$$\delta\left[\left\langle f_A^y(\mathbf{q},\omega) f_A^y(-\mathbf{q},\omega)\right\rangle\right] = 2\alpha^2 \int_> \frac{d^2k}{(2\pi)^2} \int \frac{d\Omega}{2\pi} C_A^{xx}(\tilde{\mathbf{k}}) C_A^{yy}(\tilde{\mathbf{k}}), \tag{B1}$$

which implies a correction to the noise strength D_A:

$$\delta D_A = \alpha^2 \int_> \frac{d^2k}{(2\pi)^2} \int \frac{d\Omega}{2\pi} C_A^{xx}(\tilde{\mathbf{k}}) C_A^{yy}(\tilde{\mathbf{k}}). \tag{B2}$$

Inserting Eqs. (A5) for the annealed correlation functions we obtain

$$\delta D_A = 4\alpha^2 D_A^2 \int_> \frac{d^2k}{(2\pi)^2} \int \frac{d\Omega}{2\pi} \frac{k_y^2}{k_x^2} \times \left(\frac{1}{(\Omega - \gamma k_x)^2 + \left[\frac{\alpha k_y^2}{k^2} + \mu_x k_x^2\right]^2} \right)^2. \tag{B3}$$

Shifting frequency from Ω to Ω' defined by

$$\Omega' \equiv \Omega - \gamma k_x \tag{B4}$$

shows that γ drops out, and leaves a simple integral over the shifted Ω'. Doing that integral gives, up to $O(1)$ multiplicative factors,

$$\delta D_A = \alpha^2 D_A^2 \int_> \frac{d^2k}{(2\pi)^2} \frac{k_y^2}{k_x^2} \left(\frac{1}{\alpha \frac{k_y^2}{k^2} + \mu_x k_x^2} \right)^3 \times O(1) = \alpha^2 D_A^2 \int_> \frac{dk_y}{2\pi} k_y^2 \int_{-\infty}^{\infty} \frac{dk_x}{2\pi} \frac{k_x^4}{\left(\alpha k_y^2 + \mu_x k_x^4\right)^3} \times O(1). \tag{B5}$$

We can pull the α, μ_x, and k_y dependence of the integral over k_x out by the simple rescaling of the variable of integration from k_x to Q_x via

$$k_x \equiv \left(\frac{\alpha}{\mu_x}\right)^{\frac{1}{4}} \sqrt{|k_y|} Q_x, \tag{B6}$$

which gives

$$\delta D_A = \frac{\alpha^{1/4} D_A^2}{\mu_x^{\frac{5}{4}}} \int_> \frac{dk_y}{2\pi} k_y^{-\frac{3}{2}} \times O(1) = \left[\alpha^{1/4} D_A / (\mu_x^{5/4} \Lambda^{\frac{1}{2}})\right] D_A d\ell \times O(1) \equiv g_A^{(\mathrm{unc})} D_A d\ell, \tag{B7}$$

where we have defined, up to $O(1)$ multiplicative factors,

$$g_A^{(\mathrm{unc})} \propto \alpha^{1/4} D_A / \left(\mu_x^{5/4} \Lambda^{\frac{1}{2}}\right), \tag{B8}$$

and the $O(1)$ factor also includes

$$\int_{-\infty}^{\infty} \frac{dQ_x}{2\pi} \frac{Q_x^4}{\left(1 + Q_x^4\right)^3} = \frac{5\sqrt{2}}{128}. \tag{B9}$$

This confirms our claim in the main text that the corrections to D_A coming purely from D_A itself are proportional to $g_A^{(\mathrm{unc})}$ as defined in (B8). Hence, our demonstration in the main text that $g_A^{(\mathrm{unc})}$ flows to zero upon renormalization at our fixed point shows that the purely annealed noise-generated corrections to the annealed noise can be safely ignored.

Generalizing (B5) to d dimensions via the "hard" continuation gives

$$\delta D_A = \alpha^2 D_A^2 \int_> \frac{d^{d-1}k_h}{(2\pi)^{d-1}} k_h^2 \int_{-\infty}^{\infty} \frac{dk_x}{2\pi} \frac{k_x^4}{\left(\alpha k_h^2 + \mu_x k_x^4\right)^3} \times O(1). \tag{B10}$$

As in $d = 2$, we can pull the α, μ_x, and k_y dependence of the integral over k_x out by the simple rescaling of the variable of integration from k_x to Q_x via

$$k_x \equiv \left(\frac{\alpha}{\mu_x}\right)^{\frac{1}{4}} \sqrt{k_h} Q_x, \tag{B11}$$

which gives

$$\delta D_A = \frac{\alpha^{1/4} D_A^2}{\mu_x^{\frac{5}{4}}} \int_> \frac{d^{d-1}k_h}{(2\pi)^{d-1}} k_h^{-\frac{3}{2}} \times O(1) = \left[\alpha^{1/4} D_A / \left(\mu_x^{5/4} \Lambda^{\frac{5}{2}-d}\right)\right] D_A d\ell \times O(1) \equiv g_A^{(\mathrm{hard})} D_A d\ell, \tag{B12}$$

where we have defined, up to $O(1)$ multiplicative factors,

$$g_A^{(\mathrm{hard})} \propto \frac{\alpha^{1/4} D_A}{\mu_x^{5/4} \Lambda^{\frac{5}{2}-d}}, \tag{B13}$$

which again is the expression for $g_A^{(\mathrm{hard})}$ quoted in the main text.

Generalizing (B5) to higher dimensions via the "soft" continuation gives

$$\delta D_A = \alpha^2 D_A^2 \int_> \frac{dk_y}{2\pi} k_y^2 \int_{-\infty}^{\infty} \frac{d^{d-1}k_s}{(2\pi)^{d-1}} \frac{k_s^4}{\left(\alpha k_y^2 + \mu_x k_s^4\right)^3} \times O(1). \tag{B14}$$

As in $d = 2$, we can pull the α, μ_x, and k_y dependence of the integral over $\mathbf{k}_s$ out by the simple rescaling of the variables

of integration from $\mathbf{k}_s$ to $\mathbf{Q}_s$ via

$$\mathbf{k}_s \equiv \left(\frac{\alpha}{\mu_x}\right)^{\frac{1}{4}} \sqrt{k_y}\mathbf{Q}_s, \tag{B15}$$

which gives

$$\begin{aligned}\delta D_A &= \frac{\alpha^{\frac{d-1}{4}} D_A^2}{\mu_x^{\frac{d+3}{4}}} \int_> \frac{dk_y}{2\pi} k_y^{\frac{d-5}{2}} \times O(1) \\ &= \left[D_A \alpha^{\frac{(d-1)}{4}} \mu_x^{-\frac{(d+3)}{4}} \Lambda^{\frac{d-3}{2}}\right] D_A d\ell \times O(1) \equiv g_A^{(\mathrm{soft})} D_A d\ell,\end{aligned} \tag{B16}$$

where we have defined, up to $O(1)$ multiplicative factors,

$$g_A^{(\mathrm{soft})} \propto D_A \alpha^{\frac{(d-1)}{4}} \mu_x^{-\frac{(d+3)}{4}} \Lambda^{\frac{d-3}{2}}, \tag{B17}$$

which again is the expression for $g_A^{(\mathrm{soft})}$ quoted in the main text.

APPENDIX C: EVALUATION OF THE INTEGRALS I_1, I_2, I_3, I_4

In this section, we will calculate the integrals I_1, I_2, I_3, and I_4 for the uncontrolled calculation in $d = 2$, the hard continuation, and the soft continuation.

1. The Integral I_1

a. Uncontrolled calculation in exactly $d = 2$

We now calculate the integral I_1 in exactly $d = 2$, integrating over $\Lambda e^{-d\ell} < |k_y| < \Lambda$, $-\infty < k_x < \infty$:

$$\begin{aligned}I_1 &\equiv \int_> \frac{d^2k}{(2\pi)^2} \frac{k_y^2 k_x^6}{\left(\gamma^2 k_x^6 + \alpha^2 k_y^4\right)^2} \\ &= \frac{1}{\pi^2} \int_{\Lambda e^{-d\ell}}^{\Lambda} dk_y \int_0^{\infty} dk_x \frac{k_y^2 k_x^6}{\left(\gamma^2 k_x^6 + \alpha^2 k_y^4\right)^2}.\end{aligned} \tag{C1}$$

Making the change of variable of integration

$$k_x \equiv \left(\frac{\alpha}{|\gamma|}\right)^{\frac{1}{3}} k_y^{\frac{2}{3}} (\tan\theta)^{\frac{1}{3}} \tag{C2}$$

in the k_x integral in (C1) gives

$$\begin{aligned}I_1 &= \frac{1}{3\pi^2}\left(\frac{\alpha}{|\gamma|}\right)^{\frac{11}{3}} \frac{1}{\alpha^4} \int_{\Lambda e^{-d\ell}}^{\Lambda} dk_y k_y^{-\frac{4}{3}} \int_0^{\frac{\pi}{2}} d\theta\ \cos^2\theta (\tan\theta)^{\frac{4}{3}} \\ &= \frac{1}{3\pi^2}\left(\frac{\alpha}{|\gamma|}\right)^{\frac{7}{3}} \frac{\Lambda^{-\frac{1}{3}}}{\alpha^4} d\ell \int_0^{\frac{\pi}{2}} d\theta\ \cos^2\theta (\tan\theta)^{\frac{4}{3}} \\ &= \frac{1}{3\pi^2} |\gamma|^{-\frac{7}{3}} \alpha^{-\frac{5}{3}} \Lambda^{-\frac{1}{3}} d\ell \int_0^{\frac{\pi}{2}} d\theta\ (\cos\theta)^{\frac{2}{3}} (\sin\theta)^{\frac{4}{3}} \\ &= \frac{1}{18\pi} |\gamma|^{-\frac{7}{3}} \alpha^{-\frac{5}{3}} \Lambda^{-\frac{1}{3}} d\ell \\ &= \frac{1}{18} \frac{g^{(\mathrm{unc})}}{\alpha^2 D_Q} d\ell,\end{aligned} \tag{C3}$$

where we have defined

$$g^{(\mathrm{unc})} \equiv \frac{D_Q}{\pi} |\gamma|^{-\frac{7}{3}} \alpha^{\frac{1}{3}} \Lambda^{-\frac{1}{3}}. \tag{C4}$$

Note that, unsurprisingly, both our expression for $g^{(\mathrm{unc})}$ and our result for I_1 agree with the results (C8) and (C7) of the hard continuation, to be discussed next, if we set $d = 2$ in those expressions.

b. Hard continuation

In the "hard" continuation, which we will now present, we treat the "soft" direction x as one-dimensional, while the "hard" direction y is extended to $d - 1$ dimensions. In practice, this means we will simply replace k_y in Fourier space with a $(d - 1)$-dimensional vector $\mathbf{k}_h$ orthogonal to the x direction. This gives

$$\begin{aligned}I_1 &\equiv \int_> \frac{d^dk}{(2\pi)^d} \frac{k_h^2 k_x^6}{\left(\gamma^2 k_x^6 + \alpha^2 k_h^4\right)^2} \\ &= \frac{2}{(2\pi)^d} \int_{\Lambda e^{-d\ell} |\mathbf{k}_h| < \Lambda} d^{d-1}k_h \int_0^{\infty} dk_x \frac{k_h^2 k_x^6}{\left(\gamma^2 k_x^6 + \alpha^2 k_h^4\right)^2}.\end{aligned} \tag{C5}$$

Making the change of variable of integration

$$k_x \equiv \left(\frac{\alpha}{|\gamma|}\right)^{\frac{1}{3}} k_h^{\frac{2}{3}} (\tan\theta)^{\frac{1}{3}} \tag{C6}$$

in the k_x integral in (C5) gives

$$\begin{aligned}I_1 &= \frac{2S_{d-1}}{3(2\pi)^d}\left(\frac{\alpha}{|\gamma|}\right)^{\frac{7}{3}} \frac{1}{\alpha^4} \int_{\Lambda e^{-d\ell}}^{\Lambda} dk_h k_h^{d-\frac{10}{3}} \int_0^{\frac{\pi}{2}} d\theta\ \sin^{\frac{4}{3}}\theta \cos^{\frac{2}{3}}\theta \\ &= \frac{2S_{d-1}}{3(2\pi)^d}\left(\frac{1}{|\gamma|^7\alpha^5}\right)^{\frac{1}{3}} \Lambda^{\frac{3d-7}{3}} d\ell \int_0^{\frac{\pi}{2}} d\theta\ \sin^{\frac{4}{3}}\theta \cos^{\frac{2}{3}}\theta \\ &= \frac{S_{d-1}}{18(2\pi)^{d-1}}\left(\frac{1}{|\gamma|^7\alpha^5}\right)^{\frac{1}{3}} \Lambda^{\frac{3d-7}{3}} d\ell \\ &= \frac{g^{(\mathrm{hard})}}{18\alpha^2 D_Q} d\ell,\end{aligned} \tag{C7}$$

where

$$g^{(\mathrm{hard})} \equiv \frac{S_{d-1}}{(2\pi)^{d-1}} |\gamma|^{-\frac{7}{3}} \alpha^{\frac{1}{3}} D_Q \Lambda^{\frac{3d-7}{3}}. \tag{C8}$$

c. Soft continuation

In the "soft" continuation, we treat the "soft" direction x as $(d - 1)$-dimensional, while the "hard" direction y is taken to be one-dimensional. In practice, this means we will simply replace k_x in Fourier space with a $(d - 1)$-dimensional vector $\mathbf{k}_s$ orthogonal to the y direction. This gives

$$\begin{aligned}I_1 &\equiv \int_> \frac{d^dk}{(2\pi)^d} \frac{k_y^2 k_s^6}{\left(\gamma^2 k_s^6 + \alpha^2 k_y^4\right)^2} \\ &= \frac{2S_{d-1}}{(2\pi)^d} \int_{\Lambda e^{-d\ell}}^{\Lambda} dk_y \int_0^{\infty} dk_s \frac{k_y^2 k_s^{d+4}}{\left(\gamma^2 k_s^6 + \alpha^2 k_y^4\right)^2}.\end{aligned} \tag{C9}$$

Making the change of variable of integration

$$k_s \equiv \left(\frac{\alpha}{|\gamma|}\right)^{\frac{1}{3}} k_y^{\frac{2}{3}} (\tan\theta)^{\frac{1}{3}} \tag{C10}$$

in the k_s integral in (C9) gives

$$\begin{aligned} I_1 &= \frac{2S_{d-1}}{3(2\pi)^d}\left(\frac{\alpha}{|\gamma|}\right)^{\left(\frac{d+5}{3}\right)}\frac{1}{\alpha^4}\int_{\Lambda e^{-d\ell}}^{\Lambda} dk_y k_y^{\left(\frac{2d-8}{3}\right)} \\ &\quad\times\int_0^{\frac{\pi}{2}} d\theta\ \cos^2\theta(\tan\theta)^{\left(\frac{d+2}{3}\right)} \\ &= \frac{2S_{d-1}}{3(2\pi)^d}\left(\frac{\alpha}{|\gamma|}\right)^{\left(\frac{d+5}{3}\right)}\frac{\Lambda^{\left(\frac{2d-5}{3}\right)}}{\alpha^4}d\ell \\ &\quad\times\int_0^{\frac{\pi}{2}} d\theta\ \cos^2\theta(\tan\theta)^{\left(\frac{d+2}{3}\right)} \\ &= \frac{2S_{d-1}}{3(2\pi)^d}|\gamma|^{-\left(\frac{d+5}{3}\right)}\alpha^{\left(\frac{d-7}{3}\right)}\Lambda^{\left(\frac{2d-5}{3}\right)}d\ell \\ &\quad\times\int_0^{\frac{\pi}{2}} d\theta\,(\cos\theta)^{\frac{4-d}{3}}(\sin\theta)^{\frac{d+2}{3}} \\ &= \frac{S_{d-1}}{12\sqrt{2}(2\pi)^{d-1}}|\gamma|^{-\left(\frac{d+5}{3}\right)}\alpha^{\left(\frac{d-7}{3}\right)}\Lambda^{\left(\frac{2d-5}{3}\right)}d\ell \\ &= \frac{1}{12}\frac{g^{(\mathrm{soft})}}{\alpha^2 D_\varrho}d\ell, \end{aligned} \tag{C11}$$

where in the penultimate equality we have set $d=\frac{5}{2}$ in the integrand of the integral over θ, and in the final equality we have defined

$$g^{(\mathrm{soft})} \equiv \frac{S_{d-1}D_\varrho}{\sqrt{2}(2\pi)^{d-1}}|\gamma|^{-\left(\frac{d+5}{3}\right)}\alpha^{\left(\frac{d-1}{3}\right)}\Lambda^{\left(\frac{2d-5}{3}\right)}. \tag{C12}$$

2. Integral I_2

a. Uncontrolled calculation in exactly $d=2$

In exactly $d=2$,

$$\begin{aligned} I_2 &\equiv \int_> \frac{d^2k}{(2\pi)^2}\frac{k_y^2k_x^{12}}{\left(\gamma^2k_x^6+\alpha^2k_y^4\right)^3} \\ &= \frac{1}{\pi^2}\int_{\Lambda e^{-d\ell}}^{\Lambda} dk_y\int_0^\infty dk_x\,\frac{k_y^2k_x^{12}}{\left(\gamma^2k_x^6+\alpha^2k_y^4\right)^3}. \end{aligned} \tag{C13}$$

Inserting (C2) into (C13) we get

$$\begin{aligned} I_2 &= \frac{1}{3\pi^2}\left(\frac{\alpha}{|\gamma|}\right)^{\frac{13}{3}}\frac{1}{\alpha^6}\int_{\Lambda e^{-d\ell}}^{\Lambda} dk_y k_y^{-\frac{4}{3}}\int_0^{\frac{\pi}{2}} d\theta\ \cos^4\theta(\tan\theta)^{\frac{10}{3}} \\ &= \frac{1}{3\pi^2}|\gamma|^{-\frac{13}{3}}\alpha^{-\frac{5}{3}}\Lambda^{-\frac{1}{3}}d\ell\int_0^{\frac{\pi}{2}} d\theta\ \cos^{\frac{2}{3}}\theta\sin^{\frac{10}{3}}\theta \\ &= \frac{7}{216}\frac{g^{(\mathrm{unc})}}{\gamma^2\alpha^2D_\varrho}d\ell. \end{aligned} \tag{C14}$$

b. Hard continuation

Continuing to higher dimensions using the hard continuation described above gives

$$\begin{aligned} I_2 &\equiv \int_> \frac{d^dk}{(2\pi)^d}\frac{k_h^2k_x^{12}}{\left(\gamma^2k_x^6+\alpha^2k_h^4\right)^3} \\ &= \frac{2}{(2\pi)^d}\int_{\Lambda e^{-d\ell}}^{\Lambda} d^{d-1}k_h\int_0^\infty dk_x\,\frac{k_h^2k_x^{12}}{\left(\gamma^2k_x^6+\alpha^2k_h^4\right)^3}. \end{aligned} \tag{C15}$$

Changing variables and inserting (C6) into (C15) we get

$$\begin{aligned} I_2 &= \frac{2S_{d-1}}{3(2\pi)^d}\left(\frac{\alpha}{|\gamma|}\right)^{\frac{13}{3}}\frac{1}{\alpha^6} \\ &\quad\times\int_{\Lambda e^{-d\ell}}^{\Lambda} dk_h k_h^{d-\frac{10}{3}}\int_0^{\frac{\pi}{2}} d\theta\ \sin^{\frac{10}{3}}\theta\cos^{\frac{2}{3}}\theta \\ &= \frac{7S_{d-1}}{216(2\pi)^{d-1}}|\gamma|^{-\frac{13}{3}}\alpha^{-\frac{5}{3}}\Lambda^{\frac{3d-7}{3}}d\ell \\ &= \frac{7g^{(\mathrm{hard})}}{216\gamma^2\alpha^2D_\varrho}d\ell. \end{aligned} \tag{C16}$$

c. Soft continuation

Continuing to higher dimensions using the soft continuation defined above yields

$$\begin{aligned} I_2 &\equiv \int_> \frac{d^dk}{(2\pi)^d}\frac{k_y^2k_s^{12}}{\left(\gamma^2k_s^6+\alpha^2k_y^4\right)^3} \\ &= \frac{2S_{d-1}}{(2\pi)^d}\int_{\Lambda e^{-d\ell}}^{\Lambda} dk_y\int_0^\infty dk_s\,\frac{k_y^2k_s^{d+10}}{\left(\gamma^2k_s^6+\alpha^2k_y^4\right)^3}. \end{aligned} \tag{C17}$$

Inserting (C10) into (C17) we obtain

$$\begin{aligned} I_2 &= \frac{2S_{d-1}}{3(2\pi)^d}\left(\frac{\alpha}{|\gamma|}\right)^{\frac{d+11}{3}}\frac{1}{\alpha^6}\int_{\Lambda e^{-d\ell}}^{\Lambda} dk_y k_y^{\frac{2d-8}{3}} \\ &\quad\times\int_0^{\frac{\pi}{2}} d\theta\ \cos^4\theta(\tan\theta)^{\frac{d+8}{3}} \\ &= \frac{2S_{d-1}}{3(2\pi)^d}|\gamma|^{-\left(\frac{d+11}{3}\right)}\alpha^{\left(\frac{d-7}{3}\right)}\Lambda^{\left(\frac{2d-5}{3}\right)}d\ell\int_0^{\frac{\pi}{2}} d\theta\ \cos^{\frac{1}{2}}\theta\sin^{\frac{7}{2}}\theta \\ &= \frac{5}{96}\frac{g^{(\mathrm{soft})}}{\gamma^2\alpha^2D_\varrho}d\ell, \end{aligned} \tag{C18}$$

where in the integrals over θ we have set $d=5/2$.

3. integral I_3

a. Uncontrolled calculation in exactly $d=2$

In exactly $d=2$,

$$\begin{aligned} I_3 &\equiv \int_> \frac{d^2k}{(2\pi)^2}\frac{k_x^6k_y^6}{\left(\gamma^2k_x^6+\alpha^2k_y^4\right)^3} \\ &= \frac{1}{\pi^2}\int_{\Lambda e^{-d\ell}}^{\Lambda} dk_y\int_0^\infty dk_x\,\frac{k_y^6k_x^6}{\left(\gamma^2k_x^6+\alpha^2k_y^4\right)^3}. \end{aligned} \tag{C19}$$

Inserting (C2) into (C19) we get

$$\begin{aligned} I_3 &= \frac{1}{3\pi^2}\left(\frac{\alpha}{|\gamma|}\right)^{\frac{7}{3}}\frac{1}{\alpha^6}\int_{\Lambda e^{-d\ell}}^{\Lambda} dk_y k_y^{-\frac{4}{3}}\int_0^{\frac{\pi}{2}} d\theta\ \cos^4\theta(\tan\theta)^{\frac{4}{3}} \\ &= \frac{1}{3\pi^2}|\gamma|^{-\frac{7}{3}}\alpha^{-\frac{11}{3}}\Lambda^{-\frac{1}{3}}d\ell\int_0^{\frac{\pi}{2}} d\theta\ \cos^{\frac{8}{3}}\theta\sin^{\frac{4}{3}}\theta \\ &= \frac{5}{216}\frac{g^{(\mathrm{unc})}}{\alpha^4D_\varrho}d\ell. \end{aligned} \tag{C20}$$

b. Hard continuation

Continuing to higher dimensions using the hard continuation gives

$$I_3 \equiv \int_> \frac{d^d k}{(2\pi)^d} \frac{k_x^6 k_h^6}{\left(\gamma^2 k_x^6 + \alpha^2 k_h^4\right)^3} = \frac{2}{(2\pi)^d} \int_{\Lambda e^{-d\ell}}^{\Lambda} d^{d-1}k_h \int_0^\infty dk_x \frac{k_x^6 k_h^6}{\left(\gamma^2 k_x^6 + \alpha^2 k_h^4\right)^3}. \quad \text{(C21)}$$

Changing variables and inserting (C6) into (C21) we get

$$\begin{aligned} I_3 &= \frac{2S_{d-1}}{3(2\pi)^d}\left(\frac{\alpha}{|\gamma|}\right)^{\frac{7}{3}} \frac{1}{\alpha^6} \int_{\Lambda e^{-d\ell}}^{\Lambda} dk_h k_h^{d-\frac{10}{3}} \int_0^{\frac{\pi}{2}} d\theta \, \sin^{\frac{4}{3}}\theta \cos^{\frac{8}{3}}\theta \\ &= \frac{5S_{d-1}}{216(2\pi)^{d-1}} |\gamma|^{-\frac{7}{3}} \alpha^{-\frac{11}{3}} \Lambda^{\frac{3d-7}{3}} d\ell \\ &= \frac{5g^{(\text{hard})}}{216\alpha^4 D_\varrho} d\ell. \end{aligned} \quad \text{(C22)}$$

c. Soft continuation

Continuing to higher dimensions using the soft continuation gives

$$I_3 \equiv \int_> \frac{d^d k}{(2\pi)^d} \frac{k_s^6 k_y^6}{\left(\gamma^2 k_s^6 + \alpha^2 k_y^4\right)^3} = \frac{2S_{d-1}}{(2\pi)^d} \int_{\Lambda e^{-d\ell}}^{\Lambda} dk_y \int_0^\infty dk_s \frac{k_y^6 k_s^{d+4}}{\left(\gamma^2 k_s^6 + \alpha^2 k_y^4\right)^3}. \quad \text{(C23)}$$

Inserting (C10) into (C23) gives

$$\begin{aligned} &= \frac{2S_{d-1}}{3(2\pi)^d}\left(\frac{\alpha}{|\gamma|}\right)^{\left(\frac{d+5}{3}\right)} \frac{1}{\alpha^6} \int_{\Lambda e^{-d\ell}}^{\Lambda} dk_y k_y^{\frac{2d-8}{3}} \\ &\quad \times \int_0^{\frac{\pi}{2}} d\theta \, \cos^4\theta (\tan\theta)^{\frac{d+2}{3}} \\ &= \frac{2S_{d-1}}{3(2\pi)^d} |\gamma|^{-\left(\frac{d+5}{3}\right)} \alpha^{\frac{d-13}{3}} \Lambda^{\frac{2d-5}{3}} d\ell \int_0^{\frac{\pi}{2}} d\theta \, \cos^{\frac{5}{2}}\theta \sin^{\frac{3}{2}}\theta \\ &= \frac{1}{32} \frac{g^{(\text{soft})}}{\alpha^4 D_\varrho} d\ell, \end{aligned} \quad \text{(C24)}$$

where in the integrals over θ we have set $d = 5/2$.

4. Integral I_4

a. Uncontrolled calculation in exactly d = 2

In exactly $d = 2$,

$$I_4 \equiv \int_> \frac{d^2 k}{(2\pi)^2} \frac{k_x^2 k_y^4}{\left(\gamma^2 k_x^6 + \alpha^2 k_y^4\right)^2} = \frac{1}{\pi^2} \int_{\Lambda e^{-d\ell}}^{\Lambda} dk_y \int_0^\infty dk_x \frac{k_x^2 k_y^4}{\left(\gamma^2 k_x^6 + \alpha^2 k_y^4\right)^2}. \quad \text{(C25)}$$

Inserting (C2) into (C25) we get

$$\begin{aligned} I_4 &= \frac{1}{3\pi^2} \frac{1}{\alpha^3|\gamma|} \int_{\Lambda e^{-d\ell}}^{\Lambda} dk_y \, k_y^{-2} \int_0^{\frac{\pi}{2}} d\theta \, \cos^2\theta \\ &= \frac{1}{6\pi} \frac{1}{\alpha^3|\gamma|} \int_{\Lambda e^{-d\ell}}^{\Lambda} dk_y \, k_y^{-2} = \frac{1}{6\pi} \frac{1}{\alpha^3|\gamma|} \Lambda^{-1} d\ell. \end{aligned} \quad \text{(C26)}$$

b. Hard continuation

Continuing to higher dimensions using the hard continuation gives

$$I_4 \equiv \int_> \frac{d^d k}{(2\pi)^d} \frac{k_x^2 k_h^4}{\left(\gamma^2 k_x^6 + \alpha^2 k_h^4\right)^2} = \frac{2}{(2\pi)^d} \int_{\Lambda e^{-d\ell}}^{\Lambda} d^{d-1}k_h \int_0^\infty dk_x \frac{k_x^2 k_h^4}{\left(\gamma^2 k_x^6 + \alpha^2 k_h^4\right)^2}. \quad \text{(C27)}$$

Changing variables and inserting (C6) into (C27) we get

$$\begin{aligned} I_4 &= \frac{2S_{d-1}}{3(2\pi)^d} \frac{1}{\alpha^3|\gamma|} \int_{\Lambda e^{-d\ell}}^{\Lambda} dk_h \, k_h^{d-4} \int_0^{\frac{\pi}{2}} d\theta \, \cos^2\theta \\ &= \frac{S_{d-1}}{12(2\pi)^{d-1}} \frac{1}{\alpha^3|\gamma|} \int_{\Lambda e^{-d\ell}}^{\Lambda} dk_h \, k_h^{d-4} \\ &= \frac{S_{d-1}}{12(2\pi)^{d-1}} \frac{1}{\alpha^3|\gamma|} \Lambda^{d-3} d\ell. \end{aligned} \quad \text{(C28)}$$

c. Soft continuation

Continuing to higher dimensions using the soft continuation gives

$$I_4 \equiv \int_> \frac{d^d k}{(2\pi)^d} \frac{k_s^2 k_y^4}{\left(\gamma^2 k_s^6 + \alpha^2 k_y^4\right)^2} = \frac{2S_{d-1}}{(2\pi)^d} \int_{\Lambda e^{-d\ell}}^{\Lambda} dk_y \int_0^\infty dk_s \frac{k_s^d k_y^4}{\left(\gamma^2 k_s^6 + \alpha^2 k_y^4\right)^2}. \quad \text{(C29)}$$

Inserting (C10) into (C29) we get

$$\begin{aligned} I_4 &= \frac{2S_{d-1}}{3(2\pi)^d} \alpha^{\frac{d-11}{3}} |\gamma|^{-\frac{d+1}{3}} d\ell \int_0^{\frac{\pi}{2}} d\theta \, (\cos\theta)^{\frac{8-d}{3}} (\sin\theta)^{\frac{d-2}{3}} \\ &= \frac{2S_{d-1}}{3(2\pi)^d} \alpha^{\frac{d-11}{3}} |\gamma|^{-\frac{d+1}{3}} d\ell \int_0^{\frac{\pi}{2}} d\theta \, \cos^{\frac{11}{6}}\theta \sin^{\frac{1}{6}}\theta \\ &= \frac{5\pi}{36 \sin\left(\frac{5\pi}{12}\right)} \frac{S_{d-1}}{(2\pi)^d} \alpha^{\frac{d-11}{3}} |\gamma|^{-\frac{d+1}{3}} d\ell, \end{aligned} \quad \text{(C30)}$$

where in the integrals over θ we have set $d = 5/2$.

[1] N. D. Mermin and H. Wagner, Absence of Ferromagnetism or Antiferromagnetism in One- or Two-Dimensional Isotropic Heisenberg Models, Phys. Rev. Lett. **17**, 1133 (1966); P. C. Hohenberg, Existence of long-range order in one and two dimensions, Phys. Rev. **158**, 383 (1967).

[2] T. Vicsek, A. Czirók, E. Ben-Jacob, I. Cohen, and O. Shochet, Novel Type of Phase Transition in a System of Self-Driven Particles, Phys. Rev. Lett. **75**, 1226 (1995).

[3] J. Toner and Y. Tu, Long-Range Order in a Two-Dimensional Dynamical *XY* Model: How Birds Fly Together, Phys. Rev. Lett. **75**, 4326 (1995).

[4] J. Toner and Y. Tu, Flocks, herds, and schools: A quantitative theory of flocking, Phys. Rev. E **58**, 4828 (1998).

[5] A. B. Harris, Effect of random defects on the critical behavior of Ising models, J. Phys. C **7**, 1671 (1974).

[6] G. Grinstein and A. H. Luther, Application of the renormalization group to phase transitions in disordered systems, Phys. Rev. B **13**, 1329 (1976).

[7] A. Aharony, in *Multicritical Phenomena*, edited by R. Pynn and A. Skjeltorp (Plenum, New York, 1984), p. 309.

[8] D. S. Fisher, Stability of Elastic Glass Phases in Random Field XY Magnets and Vortex Lattices in Type-II Superconductors, Phys. Rev. Lett. **78**, 1964 (1997).

[9] J. Toner, N. Guttenberg, and Y. Tu, Swarming in the Dirt: Ordered Flocks with Quenched Disorder, Phys. Rev. Lett. **121**, 248002 (2018).

[10] J. Toner, N. Guttenberg, and Y. Tu, Hydrodynamic theory of flocking in the presence of quenched disorder, Phys. Rev. E **98**, 062604 (2018).

[11] Y. Duan, B. Mahault, Y. Q. Ma, X. Q. Shi, and H. Chaté, Breakdown of Ergodicity and Self-Averaging in Polar Flocks with Quenched Disorder, Phys. Rev. Lett. **126**, 178001 (2021).

[12] A. Morin, N. Desreumaux, J.-B. Caussin, and D. Bartolo, Distortion and destruction of colloidal flocks in disordered environments, Nat. Phys. **13**, 63 (2017).

[13] A. Chardac, S. Shankar, M. C. Marchetti, and D. Bartolo, Emergence of dynamic vortex glasses in disordered polar active fluids, Proc. Natl. Acad. Sci. USA **118**, e2018218118 (2021).

[14] S. Ro, Y. Kafri, M. Kardar, and J. Tailleur, Disorder-Induced Long-Ranged Correlations in Scalar Active Matter, Phys. Rev. Lett. **126**, 048003 (2021).

[15] E. Pinçe, S. K. P. Velu, A. Callegari, P. Elahi, S. Gigan, G. Volpe, and G. Volpe, Disorder-mediated crowd control in an active matter system, Nat. Commun. **7**, 10907 (2016).

[16] R. Das, M. Kumar, and S. Mishra, Polar flock in the presence of random quenched rotators, Phys. Rev. E **98**, 060602(R) (2018).

[17] S. Kumar and S. Mishra, Active nematics with quenched disorder, Phys. Rev. E **102**, 052609 (2020).

[18] O. Chepizhko, E. G. Altmann, and F. Peruani, Optimal Noise Maximizes Collective Motion in Heterogeneous Media, Phys. Rev. Lett. **110**, 238101 (2013).

[19] A. Maitra, Active uniaxially ordered suspensions on disordered substrates, Phys. Rev. E **101**, 012605 (2020).

[20] L. Chen, C. F. Lee, A. Maitra, and J. Toner, Packed Swarms on Dirt: Two-Dimensional Incompressible Flocks with Quenched and Annealed Disorder, Phys. Rev. Lett. **129**, 188004 (2022).

[21] L. Chen, C. F. Lee, and J. Toner, Mapping two-dimensional polar active fluids to two-dimensional soap and one-dimensional sandblasting, Nat. Commun. **7**, 12215 (2016).

[22] L. Chen, C. F. Lee, and J. Toner, Incompressible polar active fluids in the moving phase in dimensions $d > 2$, New J. Phys. **20**, 113035 (2018).

[23] L. Chen, J. Toner, and C. F. Lee, Critical phenomenon of the order-disorder transition in incompressible active fluids, New J. Phys. **17**, 042002 (2015).

[24] D. Forster, D. R. Nelson, and M. R. Stephen, Long-Time Tails and the Large-Eddy Behavior of a Randomly Stirred Fluid, Phys. Rev. Lett. **36**, 867 (1976).

[25] D. Forster, D. R. Nelson, and M. J. Stephen, Large-distance and long-time properties of a randomly stirred fluid, Phys. Rev. A **16**, 732 (1977).

[26] H. H. Wensink, J. Dunkel, S. Heidenreich, K. Drescher, R. E. Goldstein, H. Löwen, and J. M. Yeomans, Meso-scale turbulence in living fluids, Proc. Natl. Acad. Sci. USA **109**, 14308 (2012).

[27] D. R. Nelson, Crossover scaling functions and renormalization group trajectory integrals, Phys. Rev. B **11**, 3504 (1975).

[28] P. C. Martin, O. Parodi, and P. S. Pershan, Unified hydrodynamic theory for crystals, liquid crystals, and normal fluids, Phys. Rev. A **6**, 2401 (1972).

[29] G. F. Mazenko, S. Ramaswamy, and J. Toner, Viscosities Diverge as $1/\omega$ in Smectic-*A* Liquid Crystals, Phys. Rev. Lett. **49**, 51 (1982); Breakdown of conventional hydrodynamics for smectic-*A*, hexatic-*B*, and cholesteric liquid crystals, Phys. Rev. A **28**, 1618 (1983).

[30] G. Grinstein and R. A. Pelcovits, Anharmonic Effects in Bulk Smectic Liquid Crystals and Other "One-Dimensional Solids", Phys. Rev. Lett. **47**, 856 (1981).